R & M No. 3846

R & M No. 3846

PROCUREMENT EXECUTIVE, MINISTRY OF DEFENCE

Aeronautical Research Council
Reports and Memoranda

THE DESIGN OF AXISYMMETRIC COWLS FOR PODDED NACELLES FOR HIGH BY-PASS RATIO TURBOFAN ENGINES

by

M.J. Langley

Aircraft Research Association Limited, Bedford

London: Her Majesty's Stationery Office
£14 NET

THE DESIGN OF AXISYMMETRIC COWLS FOR PODDED NACELLES FOR HIGH BY-PASS RATIO TURBOFAN ENGINES

By M. J. Langley

Aircraft Research Association Ltd, Bedford

REPORTS AND MEMORANDA No.3846*

May 1979

SUMMARY

The Report describes a research programme undertaken at ARA in 1968-73. It represents the first attempt in the UK to design forecowl profiles for a podded engine nacelle of modern proportions, with the specific aim of obtaining favourable supercritical flow development over the cowl exterior.

Six cowl shapes were tested, of empirical design but exploiting the 'peaky' pressure distribution principle previously evolved for high speed aerofoils. Earlier results for NACA 1-series cowls were used as a basis of comparison though all the present cowls had larger lip radii than NACA 1-series cowls in order to improve the low speed performance in conditions that might correspond to a windmilling engine in single-engine flight of a twin-engined transport. The essential measurements were of mass flow, drag (by wake traverse) and surface pressure distributions.

The detailed pressure plotting throws light on the nature of the principal flow characteristics - peak suction, lip separation, recompression and reattachment, shock wave progression etc - and enables these to be related to the occurrence of drag rise, from either increase of Mach number or decrease of flow ratio (spillage). The level of high speed drag performance reached by the best cowl designs tested was equivalent to or slightly better than the corresponding optimum NACA 1-series cowl, superiority at low speed being retained throughout.

The analysis provides some guidance on what pressure distributions to choose as targets for design calculations by modern theoretical methods. This approach is likely to produce better cowls than the NACA 1-series particularly for applications where non-aerodynamic factors dictate the use of non optimum geometric proportions. Overall, the aim of producing favourable supercritical pressure distributions by constructive design was reasonably well fulfilled.

* Replaces ARA Report No.54 - ARC 38204

CONTENTS

1. INTRODUCTION

This report describes the aims and achievements of a research programme undertaken at ARA in 1968-73 under a contract from MOD(PE). The programme represented the first serious attempt in the UK to design the forecowl of a podded nacelle for a subsonic transport aircraft with the specific aim of obtaining a favourable supercritical flow development over the outside of the cowl in the design condition. Previously, cowl shapes for a given choice of various geometric parameters had been selected from a standard family, usually the NACA 1-series which is a series of shapes designed essentially for subcritical flow. Now, in this programme, the emphasis was on finding a shape that would give a desired type of pressure distribution in subcritical flow. In 1968-73, there were no methods for calculating the supercritical flow over a ducted body or cowl and so the design approach had to be empirical in nature, being guided by an analysis of earlier data for NACA 1-series cowls and by relevant experience in the design of advanced two-dimensional aerofoils.

If the programme were repeated now in 1979, use would be made of new methods[1] for calculating the supercritical flow over a complete cowl. The existence of these methods does not detract however from the value of the earlier programme or the usefulness of this report. In future, one will certainly make use of the new theoretical methods but one will still need some idea of a suitable shape and/or target pressure distribution to serve as a starting point for design calculations.

Somewhat by chance, the performance of the best cowl of the six tested in this programme was only slightly better than that of the corresponding NACA 1-series cowl. This does not imply that the design approach was unsuccessful but rather reflects the fact that coincidentally the particular NACA 1-series cowl gave a favourable form of supercritical pressure distribution at an appropriate cruise Mach number over a fairly wide range of intake flow ratio. The value of the design approach coupled with the new theoretical methods is that such favourable pressure distributions will eventually be obtained by constructive design rather than by accident and will permit the use of a wider range of overall geometry, thereby easing the difficulties of meeting ever more severe practical constraints.

The programme is concerned with the design of the forward part of the cowl. Strictly, one should consider the design of a complete cowl since, with present-day typical geometries, it cannot be categorically assumed that there is no interaction from the rear cowl on the flow over the forecowl. However, the nature of the programme was conditioned by the rig available at the time; furthermore, the absence of significant interference from the rear in present tests does not affect conclusions as to what are desirable pressure distributions for the forecowl; it may however affect the geometry needed to achieve those distributions.

2. DESIGN OF PODDED INTAKES

2.1. General Principles

The function of an intake/cowl combination is to present the required airflow to the engine with the minimum loss, distortion and fluctuation and to house the engine in a nacelle with the smallest possible external drag. Ideally, low drag implies small frontal area, small wetted surface area, no excess viscous drag due to boundary layer thickening and/or separation and no wave drag. The good internal and external characteristics should be maintained over the operational range of incidence, Mach number and intake mass flow. The aerodynamic design process is essentially an attempt to find the best compromise between the different requirements.

Neale[2] has described the problems faced in finding a suitable nacelle shape for the modern turbofan engine of high by-pass ratio. On the one hand, because of the low specific thrust of such engines, it is more important than in the past to obtain low external drag and good intake pressure recovery while, on the other hand, the shape and size of the engine has added to the difficulties of reconciling internal and external flow requirements within the overall geometric constraints. A typical nacelle shape is shown in Fig.1; terms describing the geometry of the forecowl are defined in Fig.2. Clearly, the nacelle has to wrap round the engine and its accessories; the required standard of flow being offered to the engine and noise considerations applied to its operation tend to control the inlet area and duct length; for the external cowl shape, one is left with refinement of the choice of length and maximum diameter and with the problem of determining the actual cowl profile as a means of obtaining the lowest possible drag. Considering the influence of internal flow requirements, the inlet has to operate with low losses at high mass flow ratio under zero and low forward speed conditions; for this, an internal contraction (or 'bellmouth') is required. The thickness of the cowl is kept to a minimum by using a throat (Fig.2) followed by a diffuser. The minimum possible throat size is determined by the maximum mass flow required by the engine under other flight conditions. The most demanding condition in this respect depends on the type of engine and its application but usually, it is either the climb or the start of cruise. Most of the internal duct length is required by the diffuser in which the mean internal stream velocity is reduced from a near-sonic value at the throat, to the value, usually about $M = 0.5$, required by the compressor or fan. Estimates based on the required bellmouth area and acceptable diffuser angles determine the minimum diameter required for the highlight and its axial position relative to the engine face. Then, the internal requirements having largely dictated the highlight diameter and length of the nacelle, one chooses the thinnest cowl that can be fitted around the engine and

its accessories as a means of minimising the nacelle maximum diameter, D_{max}, Fig.2. The need to minimise D_{max} is much greater than it was, say 25 years ago; if D_{max} is not kept to a minimum, basic profile drag level will tend to be unacceptable and practical constraints such as ground clearance for an underwing nacelle are likely to be violated. Essentially, this is the source of the added design difficulty; a typical value for the intake highlight diameter ratio, D_i/D_{max}, is now 0.85 whereas formerly it would have been about 0.5 - 0.6. This means that relatively speaking, there is much less frontal area for the cowl surface between highlight and maximum diameter. The function of this cowl forebody is to produce sufficient suction on the forward-facing surface to balance the change in momentum of the entering streamtube between freestream conditions and the entry plane, i.e. to compensate for the 'pre-entry drag'. Any failure to do this is normally described as spillage drag and is ascribable to excess profile drag, wave drag or a flow separation. A smaller frontal area for this surface implies a higher mean suction and hence more risk of wave drag for a given freestream Mach number, or steeper adverse pressure gradients for a given mass flow ratio. It follows that one normally has to refine the choice of forecowl length and maximum diameter and search for a shape for the cowl that will minimise the wave drag at cruise mass flow and high Mach number, will reduce the spillage drag at lower flow ratio and Mach number (in for example, an engine-windmilling condition) and finally, will give a satisfactory flow under high incidence conditions at low speeds typical of aircraft take-off and landing.

2.2. NACA 1-series Cowls

Up to 1968, it had been general practice to select a basic axisymmetric cowl for any new nacelle application for a subsonic transport from a standard family, e.g. in the UK, the NACA 1-series, and then to modify it as required to cope with any asymmetric accessories and installation problems. The ordinates of the NACA 1-series were defined in 1945 and extensive pressure plotting data were given in two NACA reports[3,4] dating from 1945 and 1949. Later, in the period 1960-8, many forecowls of this family were tested in the ARA 9ft x 8ft transonic tunnel for Rolls Royce Ltd, primarily to obtain drag data by the wake traverse technique, using the rig to be described in 3.2, and partly to extend the data to larger highlight diameter ratios up to $D_i/D_{max} = 0.90$. Correlations of the data from which the designer can select a suitable cowl for his particular requirements have since been published, e.g. Refs.5,6. For any given highlight diameter/maximum diameter ratio, one can select a forecowl length/diameter ratio to give the best compromise between a high drag-rise boundary at cruise mass flow and a good spillage drag boundary at reduced mass flow and Mach number. A shorter cowl will tend to be in trouble at high Mach number because the suctions will be too high near the maximum diameter or crest (Fig.2); a longer cowl will tend to have premature spillage drag because the lip will be too sharp and the peak suction

too high, thus leading to a premature flow separation in the adverse pressure gradient aft of this peak. These general trends were first described in Ref.7 (1952). At modest D_i/D_{max}, the 'optimum' is in fact, a range of possible lengths and so there is considerable freedom to choose a cowl geometry that will meet the other requirements and constraints; but with increase in D_i/D_{max}, the optimum becomes more sharply tuned, e.g. at $D_i/D_{max} = 0.85$, $(L_F/D_{max})_{opt} = 0.45 \pm 0.05$ while for $D_i/D_{max} = 0.90$, it appears virtually impossible to find a satisfactory cowl within the NACA 1-series. It should be noted that the change from $D_i/D_{max} = 0.85$ to $D_i/D_{max} = 0.90$ is not trivial; it implies a reduction of more than 30% in the thickness of the cowl.

The original aim with the NACA 1-series was to obtain the highest possible values of M_{crit}, the Mach number at which the local flow over the cowl first becomes supersonic. The design pressure distribution for a cruise mass flow condition therefore was of the rooftop type, i.e. constant C_p over as much as possible of the length of the forecowl. However, an analysis[8] of the surface pressures and drag data for the NACA 1-series cowls tested at ARA showed that the Mach number (M_d) for the start of the rapid increase in drag with Mach number was close to M_{crit} only for cases where the flow first became supersonic at the rear of the forecowl, i.e. near the crest. For cases where the low speed pressure distribution contained a peak suction near the lip of the cowl followed by a steady recompression, M_d could be as much as 0.2 higher than M_{crit}. This result had been noted much earlier from tests in Germany in about 1943 (see Ref.9, page 82). The more recent analysis[8] of data for NACA 1-series cowls suggested that there was a significantly better correlation (though still not perfect) between M_d and M_{crest}, the Mach number at which the shock first moved back to the crest. The best drag characteristics, i.e. M_d up to within 0.02 of M_{crest}, were obtained for cases where the pressure distributions near M_{crest} and M_d still contained a rapid expansion around the lip to a peak supersonic local Mach number followed by a largely isentropic recompression with only weak shocks situated at or near the crest. The NACA 1-series 0.85/0.45 cowl, where $D_i/D_{max} = 0.85$, $L_F/D_{max} = 0.45$ gives pressure distributions of this type over a wide range of intake mass flow and this accounts for its superiority over other NACA 1-series cowls of the same highlight diameter ratio. Coincidentally, this 0.85/0.45 geometry has proved to be very suitable for various practical applications but in general it had been realised by 1968 that continued use of the NACA 1-series for all applications would mean that in some cases, increases in external drag would have to be accepted for the sake of meeting other requirements and constraints.

2.3. Approach to Supercritical Cowl Design

As noted above, the problem of external cowl design becomes one of designing a surface with a pressure distribution which develops, with change of inlet flow ratio and Mach number, in a manner likely to delay serious boundary

separation and the appearance of strong shock waves near or aft of the crest. Analysis[6] of the data for NACA 1-series cowls showed qualitatively what type of incompressible pressure distribution and nacelle shape would be expected to show a favourable supercritical flow development; the aim of the research described in this report was to demonstrate the achievement of good supercritical flow as the result of deliberate design and to quantify the desirable target design pressure distributions.

Clearly, up to a point, there is an analogy here with the high speed design aims for a two-dimensional aerofoil. In both cases, one is interested in what Pearcey was the first[10] to describe as a 'peaky' pressure distribution. Much had already been learnt by 1968 about how to design the nose of a two-dimensional aerofoil to obtain favourable pressure distributions of this type and this experience served as a starting point for the design of the first two cowls of the present programme. It was realised from the outset that the analogy could not be pushed too far. The design aims, while broadly similar, are nevertheless different in detail; with an aerofoil, one wants to carry as much lift as possible for a given shock strength, so the trend with some advanced supercritical sections[11] is towards achieving an extended supersonic region containing a peak suction not necessarily very close to the leading edge; with a cowl, however, the primary aim is to recover as much as possible of the pre-entry drag and thus, there is a need to expand the flow quickly to a peak suction close to the lip so that high suctions are generated on the forward facing part of the surface near the lip highlight. Recognising this difference, experience in the design of 'peaky' two-dimensional sections was nevertheless useful in approaching the cowl design problem. The concept adopted was firstly that the lip profile should be circular for some distance on either side of the highlight point: this avoids the discontinuity in curvature which occurs with a strict application of NACA 1-series profiles. Then for the external profile, this initial region of constant curvature was to be followed by a rapid, though not discontinuous, reduction in curvature following 'peaky aerofoil' practice. The peak suction would occur near the position of abrupt curvature change and the art of the exercise lay in finding a distribution of curvature from lip to crest that would produce well-conditioned, near optimum recompressions (i.e. avoiding strong shock waves) over a range of flow conditions embracing both high free stream Mach number at moderate mass flow ratio and low flow ratios at low free stream Mach number. As with two-dimensional aerofoils, it was felt that one should not strive for literally shock-free recompression which, if it could be obtained at all, was likely to persist only over a very limited range of intake flow conditions.

Further details of the profile design process adopted are given in section 4.

3. DETAILS OF EXPERIMENT

3.1. Choice of Cowls

Six cowls in three pairs were designed and tested in the present experiment. The parameters initially defining the external cowl geometry are the highlight diameter ratio D_i/D_{max} and the forecowl length to diameter ratio L_F/D_{max} (Fig.2). Cowls 1, 3, 4 and 6 had $D_i/D_{max} = 0.85$ and cowls 2 and 5, $D_i/D_{max} = 0.90$, these values being selected on the grounds that the former was typical of nacelles being designed for subsonic transports at the time of this programme, while the latter prescribed what was expected to be the thinnest possible cowl for a cruise Mach number near M = 0.85. Another reason for choosing these values was that several NACA 1-series cowls with $D_i/D_{max} = 0.85$ and 0.90 had been tested previously on the same B.5 rig, although unfortunately the drag data for the 0.90 cowls are suspect and are not therefore included in the comparisons of this report. The values of L_F/D_{max} were 0.45 for cowls 1, 3 and 4, 0.499 for cowl 6 (due to a special circumstance which emerges in the discussion of section 4) and 0.35 for cowls 2 and 5. Thus, in the broad the cowls combined the proportions either 0.85/0.45 (cowls 1, 3, 4 and 6) or 0.90/0.35 (cowls 2 and 5): combinations which the NACA 1-series data suggested were near-optimum and which also were considered realistic values for practical nacelles.

The selected design conditions, against which the characteristics of the cowls were to be judged, were:

(a) high Mach number : $M_o = 0.85$, A_o/A_i* = 0.6 - 0.7

(b) low Mach number : $M_o = 0.4$, A_o/A_i = 0.35 - 0.4

These conditions would be appropriate for a twin-engined airbus cruising in the Mach number range $M_o = 0.80$ to 0.85. Condition (a) relates to cruising flight, the most critical case being in general the end of the cruise, this giving the lowest A_o/A_i. Condition (b) corresponds to a windmilling engine during single-engined operation, an important design condition for a twin-engined aircraft, though of less significance for an aircraft with three or more engines. The choice of these two conditions for special attention does not mean that the cowl performance at other Mach numbers and flow ratios is not of interest: obviously, for example, a cowl having poor performance for high flow ratio at any Mach number between 0.4 and 0.85 is undesirable.

Characteristics of the test rig necessitated that all the model cowls had long parallel cylindrical centre sections, unrepresentative of true engine

---

* Intake mass flow ratio is presented as A_o/A_i where A_o is the cross-section area of the entering streamtube under free stream conditions, and A_i is the highlight area. A_o/A_i is related to the inlet mean velocity ratio V_i/V_o by the expression

$$\frac{(\gamma - 1)}{2} M_o^2 \left(\frac{V_i}{V_o}\right)^{\gamma+1} - \left(1 + \frac{\gamma-1}{2} M_o^2\right) \left(\frac{V_i}{V_o}\right)^{\gamma-1} + \left(\frac{A_o}{A_i}\right)^{\gamma-1} = 0 .$$

nacelle shapes. Thus, the maximum diameter of the models was 7 inches (17.78 cm): the parallel section extended from the crest of the forecowl back to 2.07 D_{max} aft of the highlight and this was followed by a conically tapered afterbody of 5^{o} semi-angle and length 0.79 D_{max}. This situation was similar to that in which, as mentioned in section 2.2, data for NACA 1-series cowls had been derived by earlier tests using the same basic rig.

Details of the internal geometry are shown in Fig.3. All cowls had a 1.25 contraction ratio from highlight area to throat area, followed by a low-angle conical diffuser to blend to the duct diameter on the rig. A full set of ordinates, surface slopes and curvatures for the cowl external profiles is contained in Tables 1-6. Details of the derivation of these profiles, for the basic proportions as already defined, are discussed in section 4.

3.2. Experimental Rig

3.2.1. General arrangement

The cowls were tested on the Rolls Royce B.5 rig, details of which are shown in Figs.4, 5 and 6. As indicated in Figs.4 and 5, the model cowl is in three sections, the first comprising the design forecowl and part of the parallel mid-section, the second being a standard parallel piece and the third being the tapered conical afterbody. There is then a short parallel support tube of diameter 0.875 D_{max} ahead of the sting which has a conical expanding taper again of 5^{o} semi-angle. The internal flow is exhausted around the sting at the rear of the model. The inlet mass flow can be continuously varied using an electrically driven plug mounted on the front of the sting. The four wake traverse rakes are positioned on the parallel portion of the support tube.

Each cowl had approximately 40 static pressure tappings. On cowls 1 and 2 these were arranged in two runs, one at the top of the cowl and the other at the bottom. On cowls 3-6, all the holes were in a single run at the top of the cowl. In order to avoid having the pressure tappings too close to one another near the highlight, they were spread to either side of the vertical centre line, the maximum deviation in azimuth from the vertical being less than 4^{o}.

3.2.2. Inlet mass flow

Measurements were made according to standard procedure for the B.5 rig. Thus, internal mass flow is determined from measurements of the static and total pressure in a parallel portion of the duct (Fig.4). The static pressure is measured at 5 positions, one near the centre of the duct and four around the circumference. Total pressure is measured with two tubes, one near the centre of the duct and the other at the bottom. These measurements and the associated calculations are made on the assumption that the flow at the measurement station consists of a largely isentropic core, of constant total and static pressure,

together with a thin boundary layer on the wall of the duct. Thus, the single pitot and static tubes at the centre of the duct determine conditions in the major portion of the flow and the remaining instrumentation is used to determine the mass flow in the boundary layer. When there are strong shock waves or major flow separations in the internal flow, it is not possible to obtain an accurate measurement of the internal flow rate in this way but this should not affect the main conclusions from the results in the present report.

3.2.3. Drag

Again following standard practice for the B.5 rig, the values of external drag were determined by the wake traverse technique using pressure measurements from four rakes mounted 90° apart around the model in vertical and horizontal planes. Details of these rakes are shown in Fig.4. The uppermost rake has 26 total pressure tubes, the other three rakes have 24. The tubes are mounted at identical radii on each rake, the extra two tubes on the upper side being at greater radii to cover the increased wake height in the lee of the model at positive incidence. The static pressure is measured at three positions on each rake, the innermost one being a surface static pressure tapping. All the pressures were recorded using scanivalves and all connections for the total pressures were arranged to have the same lag characteristics with a time constant long enough to ensure that small disturbances within the wake could be damped out.

The values of drag were computed from the rake total and static pressures using a compressible flow version of the original Jones method[12]. The external drag, D is calculated by evaluation at the traverse station of the integral

$$D = \int \dot{m} \, (V_o - v) dA$$

where $\dot{m}$ is the mass flow rate through an element of wake area dA, V_o is the freestream velocity and v is the velocity in the streamtube at downstream infinity calculated on the assumption that no further total head losses occur after the traverse station. The integrand becomes zero when there are no total head losses irrespective of the local static pressure. Thus, the integral could in theory be evaluated over the whole area covered by the rakes irrespective of the extent of the cowl wake. However, experience has shown that this approach gives large scatter in the final results, and with this particular experimental set-up it led to drags which appeared to be somewhat too high. These troubles were traced to minor spurious total head losses far outside the wake due to either failings in the instrumentation or slight imperfections in the tunnel flow. The losses in total pressure were trivial but had a significant effect on the integrated drag because of the large area weighting of the outermost tubes. The integration was therefore confined to the wake only, the outer edge of the wake being found by

asking the computer to search along the rake measurements (from the outermost tube inwards) until a significant total head loss (ΔH = 0.004" Hg, i.e. 0.013% H_o) was found. The reference freestream total pressure, used for calculating V_o for each rake, was then taken to be the average of all good pitot readings outside the wake. By the application of standard compressible flow relationships, the drag was then calculated.

Earlier in the report, it was stressed that the present research is concerned with the design of a forecowl. The long parallel mid-section ensures that there is little interference from the truncated aft cowl. Nevertheless, it should be noted that the drag measurements are for the complete cowl and even include the skin friction on the support tube ahead of the rakes. It follows that absolute values of C_D are to be disregarded. The purpose of the tests is to show how the drag varies with Mach number and intake flow ratio and to provide a comparison between the different forecowl designs.

3.3. Range of Tests

The tests were made in the ARA 9ft x 8ft transonic tunnel at Mach numbers from M = 0.4 to M = 0.95 at a tunnel total pressure of 1 atmosphere giving a test Reynolds number based on the cowl maximum diameter varying from R = 1.5 x 10^6 at M = 0.4 to R = 2.4 x 10^6 at M = 0.95. Tests were made at 0^o, 3^o and occasionally 6^o incidence but the discussion in this report concentrates on the results for 0^o incidence; it is known however that if the results for 3^o had been included, this would not have affected the conclusions from the analysis to any appreciable extent.

Boundary layer transition was fixed using roughness bands of Ballotini of 0.0035 - 0.0041 inches diameter extending from 0.4 inches to 0.6 inches (x/D_{max} : 0.057 - 0.086) aft of highlight.

The tests were made between April 1968 and November 1970.

3.4. Presentation of Results

The actual test data have been fully recorded graphically in Ref.12. The present report concentrates on analytical discussion and to that end recalls a wide selection but not the whole body of results for presentation in this document.

The presentation of results is twofold. In section 4, which is concerned to describe the evolution of the cowl profile shapes, the drag results in terms of Mach number and flow ratio are given in order to explain the step-by-step process. In section 5, detailed pressure distributions are shown and analysed with the aim of explaining the nature of flow breakdown as and when it occurs.

4. COWL PROFILES AND DRAG RESULTS

4.1. Cowls 1 and 2

The broad principles adopted in deriving the cowl profiles, for given overall proportions, have already been stated (section 2.3). Cowls 1 and 2 represent the initial attempts to apply these principles, for proportions 0.85/0.45 and 0.90/0.35 respectively.

The only data available to assist in the design of these first two cowls were those for the corresponding NACA 1-series cowls. These were analysed to give estimates of stagnation point position and its variation with Mach number and mass flow, coupled with angular expansion rates from the stagnation point and around the cowl lip. The data supported a suggestion that a peak local Mach number of about 1.2 at $M_o = 0.85$, $A_o/A_i = 0.7$, if combined with a suitable recompression aft of the peak, would probably give good reduced mass flow performance at this Mach number. In order to meet the low Mach number design target, larger values of leading edge radii were used than those applicable to NACA 1-series cowl shapes. The actual values, expressed as ρ/D_{max} with NACA 1-series values in parentheses, were for cowl 1, 0.0224 (.0077) and for cowl 2, 0.0179 (.0045). A crude estimate was made of the local slope on the external surface where the rapid decrease in curvature should start. Appropriate values for this slope seemed to be about 45^o for cowl 1 (85/45) and about 50^o for cowl 2 (90/35). The remainder of the profile was filled in by eye to give what appeared to be an acceptable distribution of curvature, according to the principles being followed. The curvature distributions which emerged are shown in Figs.7 and 8 (together with those of later cowls of the series). Surface slopes are plotted in Figs.9 and 10.

Some considerable time was spent in the determination of convenient analytical expressions for defining the shape of that part of the cowl profile between the end of the circular arc leading edge and the crest; the aims of such expressions were to give continuity of first and second derivatives at the fairing point, and adequate control of the curvature distribution downstream. Various forms of expression were tried and the one finally selected as being the most useful was:

$$x^2 + axy + bx^2y + cy^2 + dx + ey + f = 0$$

This form of expression (the equation of a general conic section with an extra term in x^2y) allows the imposition of six constraints, three of which are needed at the forward fairing point and two at the crest. The sixth parameter is available for varying the profile; the way it was used in practice was to define the degree of curvature at the crest. Profiles generated from this expression were used for the basic shapes of all six cowls. The last two cowls (5 and 6),

however, required some numerical modification to produce effects not obtainable with the basic equation; these modifications are described later. With cowls 1 and 2 a low value of curvature at the crest was used in order to restrict supersonic expansion near the crest at high Mach number. The external lip shapes of these first two cowls are compared with the equivalent NACA 1-series shapes in Fig.11.

The internal profile from highlight to throat was obtained by carrying the nose radius internally through about 20° angle and then fairing back to the throat by a similar process to that used externally. A representative contraction ratio, $A_i/A_t = 1.25$ (Fig.2), was used throughout and the axial distance from highlight to throat was made equal to the difference in diameters, $x_{throat} = D_i - D_t$. No attempt was made with any of the cowls to optimise the internal shape with respect to internal performance.

The tests of cowls 1 and 2 showed that the performance at low Mach number ($M = 0.4$) was excellent, better, in fact, than the target of retaining low drag down to flow ratios $A_o/A_i = 0.35 - 0.4$ (section 3.1). At high Mach number however the performance was not as good as had been hoped. This can be seen in Figs.12 to 17, where the principal zero-incidence drag data for the various cowls are shown. Figs.12 and 15 give external drag coefficient versus flow ratio, Figs.13 and 16 give external drag coefficient versus Mach number and in Figs.14 and 17 the flow ratio for drag divergence is plotted against Mach number. Comparative data for the NACA 85/45 cowl have been included in Figs.12 to 14. Divergence here refers to the rapid increase of drag occurring below a certain level of flow ratio for a given cowl at a given Mach number M_o. The basic drag level can be approximated by the expression* $C_{Db} = 0.044 - 0.01\ M_o$ and a divergence flow ratio $(A_o/A_i)_d$ is defined as the flow ratio for which $C_D = C_{Db} + 0.01$.

It can be seen from Figs.12(a) and 15(a) that at $M = 0.4$, neither cowl 1 nor cowl 2 gives any major increase in drag down to the lowest mass flow ratio of the tests (i.e. just over 0.3), although there is a marked creep on cowl 2 which results in a nominal divergence ratio $(A_o/A_i)_d = 0.38$. It seems clear that the philosophy of using a large leading edge radius with no discontinuity in curvature at the lip has been successful at this low Mach number in keeping down the peak velocities near the lip and hence in avoiding premature drag divergence. This will be discussed more fully in section 5.

Fig.14 shows that in terms of $(A_o/A_i)_d$, the divergence flow ratio at constant Mach number, the performance of cowl 1 is superior to the NACA 1-series

---

*The level decreases with increasing Mach number because of the variation of test Reynolds number with Mach number.

cowl up to M = 0.8. Above this Mach number, however, the NACA cowl is markedly better, for example 0.07 in divergence flow ratio at M = 0.85. The corresponding superiority in drag rise Mach number at constant flow ratio can be seen in Fig.13. This behaviour is considered at greater length in section 5: suffice it to say at this point that, compared with the appropriate NACA cowl, cowls 1 and 2 have lower peak suctions, further from the lip, but also have stronger terminating shocks, again further from the lip. The differences stem from the larger leading edge radius used for the present cowls and it was concluded that it would not be possible to improve the high Mach number performance solely by changing the profile shape downstream of the lip radius. In other words, it was felt it would be necessary to sacrifice some of the excellent low Mach number performance in order to improve the performance at high speeds.

4.2. Cowls 3 and 4

Cowls 3 and 4 were designed with the same overall proportions as cowl 1 (D_i/D_{max} = 0.85, L_F/D_{max} = 0.45), with the aim of investigating the effect of reducing leading edge radius. The values of ρ/D_{max} chosen were 0.0143 for cowl 3 and 0.0186 for cowl 4 (cf. 0.0224 for cowl 1 and 0.0077 for the equivalent NACA cowl). In the hope of maintaining low peak suction levels similar to that of cowl 1, a change was made to the point of departure from the leading edge circular arc. Using available calculation methods for incompressible flow[14,15] the stagnation point position on the lip was estimated as a function of lip radius. It was found that for cowls 3 and 4, the stagnation point was 5^o and $2\frac{1}{2}^o$ respectively further round towards the inside of the cowl than for cowl 1: these angles were therefore added to the angle of slope at departure of the outer profile from circular, thereby keeping constant the total circular sector angle from the stagnation point to the point of departure. Thus, as shown in Fig.7, cowl 3 starts to flatten out at 50^o slope and cowl 4 at 47.5^o.

Somewhat different philosophies were applied to determining the two profiles aft of the circular leading edge. Cowl 3 was given a rapid flattening aft of the lip, followed by relatively more curvature than cowl 1 aft of x/D_{max} = 0.1: the aim was to obtain a quick recompression after the peak suction, which it was hoped would weaken the subsequent shock wave over a wide range of Mach number. In the case of cowl 4 the area of low curvature was spread over a larger part of the cowl surface but finally near the crest the curvature was increased relative to cowl 1: this was because it was considered that the low crest region curvature of cowl 1 (and cowl 2) had indirectly contributed to the inferior performance at high M_o by strengthening the shock wave (since lower curvature at the crest implies higher curvature further forward in the supersonic flow region). These curvature distributions for cowls 3 and 4 are plotted in Fig.18 using cowl 1 as

a basis and against slope in Fig.19.

The effect of these changes from cowl 1 on the theoretical incompressible flow can be seen in Fig.20. The changes are consistent with the geometric variation in that the pressure distribution for cowl 3 has a narrow peak followed by low velocities and a region of slight re-acceleration near the mid part of the profile; whilst cowl 4 has a more gradual recompression after the peak, with velocities less than for cowl 1 except for a small region near the crest ($x/D_{max} = 0.45$).

Turning to the experimental results, these show (Figs.12(a) and 14) that the behaviour of both cowls at $M_o = 0.4$ was still very good. The divergence value of A_o/A_i was lower than 0.3 in both cases i.e. significantly better than the design target. At M = 0.5, however, (Fig.14), $(A_o/A_i)_d$ was increased by nearly 0.1 for both cowls as compared with cowl 1. At higher Mach numbers cowl 3 was again particularly good at reduced mass flow (Figs.13(a,b)) but at high flow ratios an early drag rise was exhibited (Fig.13(c)). As compared with the NACA 1-85-45 cowl, cowl 3 was roughly equivalent at $M_o = 0.85$, equivalent (high flow ratio) or superior (low flow ratio) at lower Mach numbers but inferior at higher Mach numbers. In terms of drag rise Mach number cowl 4 also was better than cowl 1 and, unlike cowl 3, the improvement in this case was sustained at the higher flow ratios (Fig.13c).

Broad conclusions are that the design aims of cowls 3 and 4 were achieved in some measure in that the high Mach number performance was improved at the expense of an acceptable deterioration in low Mach number characteristics. It seems that the high Mach number performance of cowl 3 was degraded by the increased curvature in the mid-cowl region, which gives, at high mass flow, a triangular pressure distribution with the flow accelerating up to the shock wave: at reduced Mach number however, with the shock wave lying ahead of this region, the performance was significantly better than that of either cowl 1 and cowl 4. To summarise: as forecast while the cowls were being designed, cowl 4 is the better cowl at high mass flow and high Mach number and cowl 3 the better at reduced mass flow and lower Mach numbers.

4.3. Cowls 5 and 6

Despite the improvements produced by cowls 3 and 4 over the level of performance of cowl 1, the high Mach number performance in particular of the NACA 1-85-45 cowl had not yet been matched (Figs.13b,c). Characteristics at $M_o = 0.4$, however, were still significantly better than the nominal target set; so it was felt that a profile might be devised combining the best features of cowls 3 and 4, which whilst allowing some further sacrifice of low Mach number performance, would be better than the NACA 1-series cowl at high Mach numbers.

Going further, the same principles might be used to derive a successful profile for the higher diameter ratio of 0.9, though here the comparisons would essentially be made with cowl 2 only, the existing drag data for the corresponding NACA 1-series cowl being considered unreliable. Cowls 5 and 6 represent these further design attempts, cowl 5 having the 0.90 diameter ratio and cowl 6 the 0.85 diameter ratio.

The profile for cowl 6 was derived from that of cowl 3 in the following way. Starting with the cowl 3 distribution of curvature as shown in Fig.19, a modified distribution was specified from a point near $x/D_{max} = 0.07$, (somewhat ahead of the higher curvature region of cowl 3) to the crest. This new distribution of curvature was of similar form to that of cowl 4 but running at a lower level (in terms of D_{max}/ρ versus slope angle θ). Integrating the curvature by means of $x = \int \rho \cos\theta \, d\theta$ and $z = \int \rho \sin\theta \, d\theta$ gave the shape ordinates, corresponding at this stage however to changed values of the overall dimensions D_i/D_{max} and L_F/D_{max}. Scaling the ordinates to the required value of D_i/D_{max} (0.85) resulted in a value 0.499 for L_F/D_{max} compared with 0.45 for the earlier cowls. It was deemed unnecessary to make a further correction for this remaining difference.

The final shape had a small reduction in nose radius ($\rho/D_{max} = 0.0122$) compared with cowl 3, higher curvature near the nose and near the crest and less at intermediate stations approaching the crest. The calculated incompressible pressure distribution (Fig.20) shows a general similarity to that of cowl 4 (with lower velocities in general) from which it was hoped that a good degree of shock-free recompression would be provided at high Mach number.

The design of cowl 5 followed similar lines to that of cowl 6 except that there was no counterpart to cowl 3 initially available. An 'intermediate design' was therefore devised, using the geometric forms used for cowls 1 and 4: this had a reduced leading edge radius (0.0129) compared with cowl 2 (0.0179), in order that the profile aft of the lip might be flatter, but at the same time the circular arc was terminated at a slope of 52.5°, as compared with 50°, in order to counter the effect of the reduced leading edge radius on peak suction.

In order to produce a cowl with analogous characteristics to that of cowl 6 the 'intermediate' cowl was then modified so as to reduce the suction level behind the peak. This was accomplished in a similar way to the change from cowl 3 to cowl 6. A new curvature distribution was specified and integrated numerically and the resulting overall shape was scaled to $D_i/D_{max} = 0.90$. The value of L_F/D_{max} came out to be 0.354, only slightly higher than that for cowl 2. The leading edge radius was 0.0109 D_{max} as compared with 0.0045 D_{max} for the NACA 1-90-35 cowl. Curvature distributions involved in this process are plotted in Fig.21 and incompressible pressure distributions in Fig.22. The high concavity of the cowl 5 pressure distribution behind the peak and the increased suctions near the crest may be noted.

The results for cowls 5 and 6 show qualitatively the expected changes in drag characteristics. On cowl 6 the hoped-for shock-free flows seem to have been obtained, so that the drag-rise Mach numbers for flow ratios 0.6 and above (Fig.13c) compare favourably with those of the NACA 1-85-45 cowl. This is despite the higher length ratio of cowl 6 (L_F/D_{max} = 0.499) which is probably away from optimum, so that a comparison at constant length ratio might make cowl 6 look even better. There is a large improvement over the earlier cowls 3 and 4. At lower Mach number (Figs.12a and 13a) the results for cowl 6 remain superior to those for the NACA cowl, whilst showing a deterioration as compared with cowls 1, 3 and 4. The value of $(A_o/A_i)_d$ at M_o = 0.4 is 0.36, i.e. cowl 6 still meets the initial design target.

Cowl 5 shows up to considerable advantage at high Mach number compared with cowl 2 (Fig.16). For example at A_o/A_i = 0.7 the drag-rise Mach number is about 0.045 higher. Examination of the surface pressures (section 5) however suggests that cowl 5 is still only just as good as, or possibly slightly inferior to, the NACA 1-90-35 cowl. The results illustrate the difficulty of combining good characteristics at both high and low Mach numbers. With such a high diameter ratio as 0.90, it would seem to be necessary to concentrate more exclusively on the high Mach number design for significant improvement to be achieved in that respect.

5. ANALYSIS OF PRESSURE DISTRIBUTIONS

5.1. General

In this section the measured cowl pressure distributions are examined with the aim of explaining the features of the flow which cause the rapid increase in drag when they occur and how these are related to cowl geometry and to the calculable characteristics for incompressible inviscid flow. It is convenient to divide the speed range into regions of low, medium and high free stream Mach number as follows:

(i) low Mach number (M_o = 0.4 in the experiment) where the flow is wholly subsonic,

(ii) intermediate Mach number ($0.5 \leq M_o \leq 0.7$) where the flow readily becomes supersonic close to the cowl lip,

(iii) high Mach number ($M_o > 0.7$) where a more extensive supersonic region exists, terminated by a shock wave some distance from the lip.

For each speed range the flow over one of the cowls is discussed in some detail and then the different cowls are compared in order to explain their drag characteristics. The analysis concentrates on the cowls with D_i/D_{max} = 0.85

but reference is made to the 0.90 cowls and the NACA 1-series where this is thought to be helpful.

5.2. Low Mach Number

In Figure 23 pressure distributions are shown for the region close to the lip of cowl 6 at $M_o = 0.4$. For several flow ratios the measured pressure distributions are compared with those calculated for inviscid incompressible flow by the method of Ref.14. At $A_o/A_i = 0.7$, the highest flow ratio, the calculated pressure distribution is a good approximation to the experimental results. At the next lower flow ratio however ($A_o/A_i = 0.6$), there is a distinct deviation of the experimental pressure distribution between $x/D_{max} = 0.01$ and 0.25 and this becomes progressively more pronounced down to $A_o/A_i = 0.4$. The deviation is indicative of a bubble-type flow separation emanating from the point where the experimental pressure distribution departs from the inviscid distribution. The boundary layer is laminar at separation and through the region of roughly constant pressure which follows; transition then occurs and the resulting turbulent layer is able to reattach giving a delayed pressure rise and ultimate return to approximately the pressure distribution for attached flow. As the flow ratio is decreased the peak suction increases, the separation point moves forward ($x/D_{max} = 0.011$ at $A_o/A_i = 0.6$, 0.007 at 0.5, 0.005 at 0.4) and the bubble becomes shorter while the pressure rise across it increases.

At $A_o/A_i = 0.3$ the experimental distribution has changed significantly: the peak suction has collapsed and the separated region has become much more extensive. This change corresponds to the phenomenon of 'bubble bursting', as described by Crabtree[16] and others in the context of flow over an aerofoil: the short bubble present at higher flow ratios has burst and been replaced by a long bubble, originating closer to the leading edge, thus giving a lower suction peak*, a delayed transition and a much gentler pressure rise in the approach to the inviscid pressure distribution.

The limiting pressure rise to reattachment of the short bubble was found empirically by Crabtree to be given by

$$\sigma \equiv \frac{C_{p_r} - C_{p_s}}{1 - C_{p_s}} \doteqdot 0.35$$

where the suffices s and r refer to separation and reattachment respectively. From the measured distribution for $A_o/A_i = 0.4$ in Fig.23, the values of C_{p_s} and

*The second peak shown by the pressure distribution for $A_o/A_i = 0.3$ in Fig.23 is believed to be caused by the staggering of pressure orifices on the model together with some departure of the flow from axial-symmetry in the range of transition from short to long bubble.

C_{p_r} are -2.27 and -1.12, which yield a value of σ in close agreement with Crabtree's.

A close inspection of the C_D - A_o/A_i variation for M = 0.4 (Figs.12a and 15a) reveals that:

(a) a small increase in slope (rate of rise of drag coefficient with decreasing flow ratio) occurs in the mid-flow region ($0.36 \lesssim A_o/A_i \lesssim 0.65$) in association with the occurrence of the short bubble;

(b) the major drag rise at lower flow commences shortly before (note: not at) the change to a long bubble, and thus is probably associated with the turbulent reattachment process approaching its limiting pressure rise.

In broad terms, however, the flow ratio for bubble changeover remains the essential parameter relating to cowl spillage drag at low Mach number and this flow ratio is itself linked with the suction peak in the pressure distribution. In Fig.24 the variations of peak suction ($C_{p_{min}}$) with flow ratio are shown for all the cowls, both as calculated for incompressible flow and also as measured for M_o = 0.4. Bubble bursting is shown by a major departure of the experimental curve from the theoretical, as flow ratio is reduced. Reference to the drag curves (Figs.12a and 15a) shows that with one exception (cowl 2) this corresponds closely to the value of C_D rising above a level 0.05. The values of flow ratio for the departure are broadly paired, highest for cowls 5 and 6 (smallest lip radius), lower for cowls 3 and 5 and not reached (but below 0.3) in the case of cowls 1 and 2. It is of some significance that the values of $C_{p_{min}}$ at departure all lie within a narrow band; in fact a useful design guide may be obtained from the flow ratio for which the theoretical incompressible $C_{p_{min}}$ has the value -3.0, as the following table shows.

Cowl	1	2	3	4	5	6
Value of A_o/A_i for which theoretical $C_{p_{min}} = -3.0$	0.22	0.35	0.30	0.26	0.45	0.36
Experimental value of $(A_o/A_i)_d$	< 0.3	< 0.3	0.28	0.28	0.45	0.35

Agreement is good in all cases save that of cowl 2. It is worth noting that even with cowl 2, the drag and surface pressure results are consistent in the sense that both show no significant divergence in the test range; the mystery is why for the lowest test A_o/A_i, C_D < 0.05 and a short bubble separation is still being maintained despite the fact that $|C_{p_{min}}| > 3.0$. It is possible that the explanation lies in the details of the pressure distributions; on cowl 2, the peak

suction is closer to the lip than on the other cowls and much of the required pressure recovery at low flow ratio apparently occurs immediately downstream of the peak where the boundary layer is relatively thin. However, the number of pressure holes in the cowls is not really sufficient to define the pressure distributions in the detail required and also, there are not enough data points to be able to compare the pressure distributions on different cowls at a given $C_{p_{min}}$.

5.3. Intermediate Mach Number

In the intermediate Mach number range, local supersonic flow appears near the cowl lip. The behaviour is typified by cowl 4 at $M_o = 0.65$ for which pressure distributions are shown in Fig.25. At the highest flow ratio shown ($A_o/A_i = 0.692$) the flow is just supercritical at the peak suction position (note the markings of local Mach number on the various curves). On reducing the flow ratio by 0.1, the peak local Mach number increases to about 1.24. The pressure distribution developing is clearly similar in character to that at low speed (Fig.23) i.e. it again corresponds to a laminar separation, produced by the initial pressure rise, transition in the separated flow (the plateau) and turbulent reattachment involving a further sharp rise in pressure. The difference from the low speed situation is that now supersonic compression is involved in the first pressure rise (and, at sufficiently low flow ratio, in the second pressure rise also). The laminar separation appears to correspond closely to the type of shock-wave/laminar-boundary-layer interaction, with transition following, described by Holder, Pearcey and Gadd.[17] They show pressure distributions of the type shown here (e.g. $A_o/A_i = 0.545$, Fig.25) in which the initial pressure rise and separation correspond to a set of weak compression waves extending forward from the shock.

As the shock wave becomes stronger transition moves forward and the turbulent separated layer has more difficulty in reattaching, thus the length of the separated region rapidly increases. This can be seen in the change from $A_o/A_i = 0.497$ to 0.401 and then 0.353 in Fig.25. The increase in area of the separated region is accompanied by a loss of suction at the lip. This general situation is virtually a repeat of the change from short bubble to long bubble in subcritical flow, occurring however at higher values of flow ratio for the higher free stream Mach number.

Returning to the drag characteristics in Fig.12b, it is seen that while the separated region is of very limited extent the drag has a pronounced creep (greater than at low speed) but no major divergence; this latter occurs when the separated region grows rapidly, e.g. between $A_o/A_i = 0.497$ and 0.401 for cowl 4. It is also noted from Fig.12b that all four cowls 1, 3, 4 and 6 are on the point of flow breakdown near $A_o/A_i = 0.5$. The pressure distributions at this flow ratio

(approximately) for all four are shown in Fig.26. It will be seen that all of the pressure distributions are of the form described for cowl 4 above. In the case of cowl 6 the recompression following the plateau is less steep than for the other cowls, indicating that the separation region has entered the phase of rapid growth. This is reflected in the drag curves, (Fig.12b) by an earlier (i.e. higher A_o/A_i) divergence for cowl 6 (a feature present also at low speed).

The existence of an initial laminar boundary layer and, in particular, of laminar separation raises the question of scale effect between the model results (Reynolds numbers of about 2 million based on cowl diameter) and full scale (typically in the range of 10 to 15 million). The fact that the major drag divergence is related to a spreading of the second recompression phase, where the boundary layer is turbulent even in the model tests, suggests that scale effect will not be overwhelmingly large. However, there are grounds for suggesting that there could be some favourable scale effect. A beneficial feature of the measured pressure distribution that should carry across to full scale is the apparent near-isentropic recompression ahead of the plateau. With a turbulent boundary layer, the pressure-rise to separation would be greater. Experience with aerofoils for conditions when the shock is well ahead of the crest, suggests that with a turbulent boundary layer from near or ahead of the peak suction position, significant separation would not occur until the local Mach number ahead of the shock were about 1.4 and the peak local Mach number perhaps 1.6 or more. By comparison with the measured pressure distributions, it then seems possible that with forward transition at a higher Reynolds number, the drag divergence might be delayed by about 0.1 in A_o/A_i. Another reason for believing that there could be a favourable scale effect is that with a turbulent boundary layer/shock interaction, one would expect the shock to be possibly further forward, i.e. further ahead of the crest. This discussion has necessarily been somewhat hypothetical but the tentative conclusion that at full scale, the drag divergence might be delayed by about 0.1 in A_o/A_i should possibly be regarded as an optimistic assessment applying for free stream Mach numbers up to, say, 0.75.

5.4. High Mach Number

5.4.1. General characteristics

As the freestream Mach number increases, the supersonic region inevitably becomes larger in extent, so the terminating shock wave becomes longer and hence its wave drag (measured in the wake traverse) even for the same shock strength becomes a more important factor. Drag divergence can be obtained even with shock strengths less than that required to separate a turbulent boundary layer and gradually the viscous part of the flow assumes a second order 'displacement surface' effect by comparison with the wave drag. In principle, the displacement surface can modify the wave drag but generally, with an attached

boundary layer, one would expect this effect to be small and certainly, one would expect the changes with Reynolds number to be negligible. Also, it is in this regime that an accurate method* for calculating the inviscid transonic flow over cowls will prove the most useful for speeding up the design process.

Since cowl 6 is the most successful high Mach number design among those for which D_i/D_{max} is 0.85, it is instructive to examine the pressure measurements for this cowl in some detail. Pressure distributions for cowl 6 at two approximately constant mass flows, 0.64 and 0.69, are plotted for various freestream Mach numbers in Fig.27. At the higher of the two flow ratios, supersonic flow ($P/H < 0.528$) first appears at $M_o = 0.65$: there is however no clear indication of the presence of a terminal shock wave until $M_o = 0.84$. Even here, the Mach number ahead of the shock (corresponding to $P/H \doteqdot 0.45$) is only 1.15, signifying a weak shock wave: the same may be said of the distribution at $M_o = 0.85$ so that up to this Mach number the flow is virtually shock free. Beyond $M_o = 0.85$ the shock moves steadily rearward, reaching the crest position at $M_o = 0.89$; the shock strength is then that corresponding to an upstream Mach number of 1.18.

At the slightly lower flow ratio 0.64, the development of this terminal shock follows much the same pattern for Mach numbers M_o from 0.85 upwards. The pressure distribution at $M_o = 0.85$ may be regarded as virtually shock free and it is to be noted that this involves compression from a supersonic Mach number as high as 1.45 (corresponding to a peak suction value $P/H = 0.29$). The result is comparable with those achievable on supercritical aerofoils.

Below $M_o = 0.85$ there is evidence, at this lower flow ratio, of a more forward shock wave forming the termination of a short bubble of separation on the lip. As is the case at lower Mach numbers, little or no drag rise is to be expected from this feature. This conclusion can be confirmed from the drag plots in Fig.13c where the flow ratios of Fig.27 are bracketed and more clearly from Fig.28.

Drag-rise Mach number, according to the definition used earlier (i.e. when $C_D = 0.054 - 0.01\ M_o$) is 0.89. At this Mach number the Mach number upstream of the terminal shock is approximately 1.2.

The above discussion of the results for $A_o/A_i = 0.69$ and 0.64 is summed up by the correlation shown in Fig.28 between the variation of C_D with Mach number and the variation of $C_{p_{min}}$ and C_{p_s} ahead of the shock. It can be noted that the minimum C_D appears to occur at or near the Mach number at which there is the greatest recompression ahead of the shock.

---

* Now available - see Ref.1.

Fig.29 shows the development of pressure distributions on cowl 6, with M_o = 0.85, for flow ratios below 0.64. As the flow ratio is decreased, a terminal shock appears, moving rearwards and increasing in strength. At the lowest mass flow shown, (A_o/A_i = 0.287) the presence of a just supersonic tongue at the foot of the shock wave indicates that the shock is just strong enough to provoke a separation of the boundary layer, (upstream Mach number ≑ 1.38). If the flow ratio were to be reduced still further the flow would eventually separate completely from the lip. This phenomenon can be seen in the case of cowl 5, shown in Fig.30. It would appear that as separation develops at the foot of the terminal shock, the rearward progress of the shock is halted, the separated region grows and eventually becomes incompatible with the remainder of the flow, which then breaks down to that corresponding to the distributions at flow ratios 0.393 and 0.289 where separation has run forward to the lip with almost complete loss of lip suction and virtually constant pressure under the separated flow. Drag results are not available for this last situation, but Fig.15b shows that a major drag rise due to spillage has already taken place, associated with the terminal shock development in the higher range of flow ratio (0.8 to 0.5).

5.4.2. Comparison with other cowls of series

Fig.31 gives a comparison of pressure distributions on cowls 1, 3, 4, 6 at M_o = 0.85 for three flow ratios. Reference to the corresponding drag plot (Fig.12c) shows that at A_o/A_i = 0.7, whilst cowls 1, 4 and 6 are at the 'basic' drag level, cowl 3 has a measurably higher drag. The pressure distributions indicate that the terminal shock on cowl 3 is at an upstream Mach number 1.2 (P/H = 0.41) whereas the shock on cowl 1 is weaker and cowls 4 and 6 have virtually shock free flow. The explanation of these comparisons lies in the higher curvature given to the cowl 3 profile in the mid-forebody region: the reacceleration of flow in this region, ahead of the terminal shock, is clearly featured in the pressure distribution. It is instructive to take this point further by noting (Fig.32) the progressive development of the pressure distribution on cowl 3 at constant flow ratio, from the incompressible (calculated) distribution through the range of experimental Mach numbers. Retrospectively, the undesirability of the region of small reacceleration shown on the incompressible flow distribution is clear.

At the lower flow ratios in Fig.31 the pressure distributions on all the cowls become similar in character though at a given flow ratio the terminal shocks are displaced relative one to another. The spillage drag characteristics (Fig.12c) are also much alike but displaced relatively on the scale of flow ratio. Clearly, the drag rise is associated with the development of the terminal shock, i.e. its position and strength. At a given flow ratio, cowl 1 has the strongest terminal shock (Fig.31) and the highest spillage drag (Fig.12c). For A_o/A_i = 0.6

and 0.5, cowl 6 gave the lowest drag and this is consistent with the indication in Fig.31 that the shock is weaker and further forward than with the other cowls.

The gradual transformation of pressure distribution on cowl 3, from that at high flow ratio, discussed earlier, exhibiting a prominent reacceleration in the mid-profile region, to that at low flow ratio, which is more comparable with those of the other cowls, is shown in Fig.33.

The wave drag associated with a normal shock wave is dependent on its strength (defined say by the Mach number ahead of it) and by its extent. As the extent of the shock wave will primarily be determined by the size of the supersonic region we may expect to find a correlation between shock strength necessary to cause drag divergence (defined at (Ms)d the upstream local Mach number of the shock wave at $(A_o/A_i)d$ as defined previously) and its axial position $(x/D_{max})s$. That this is broadly the case can be seen in Fig.34 which presents data for all the cowls at Mach numbers between 0.70 and 0.95. As expected, the further forward the shock wave position, the greater the shock strength which can be tolerated before drag divergence is reached. If the lateral extent of the shock wave is actually proportional to $(x/D_{max})s$ then since wave drag is also roughly proportional to $(M_s - 1)^3$, we would expect the product $(x/D_{max})s \times (M_s - 1)^3$ at $(A_o/A_i)d$ to be roughly constant. This is also confirmed in Fig.34. The conclusion and the relation shown in Fig.34 should be useful when applying theories which while predicting shock strength and position quite well do not necessarily predict the correct wave drag.

5.4.3. Comparison with NACA 1-series cowls

Detailed comparison with results for NACA 1-series cowls is not easy because of the coarseness of pressure plotting in earlier work and in the case of the 90/35 cowl, a lack of reliable drag data.

In Figs.35a,b, however, the pressure distributions for various mass flows at $M_o = 0.85$ and 0.90 for cowl 6 are compared with those for the NACA 85/45 cowl. In some cases, it is difficult to identify the shock strength and position for the NACA cowl but in general, one can conclude that the shock strengths for the two cowls are fairly similar. However, at M = 0.85 and the higher mass flows, there is a tendency for the pressure distribution on the NACA cowl to re-expand or 'hump' immediately downstream of an isolated peak suction near the lip and at M = 0.90, this has developed into a trend for the pressures to expand ahead of the shock giving a greater shock strength. This presumably correlates with the poorer drag characteristics of the NACA cowl relative to cowl 6 above M = 0.87, as shown in the data plotted in Fig.13c. It is interesting to note that this tendency for a re-expansion ahead of the shock was more pronounced on cowl 3 (see the earlier discussion) and again, the drag data indicate that it is an unfavourable feature.

Comparison of cowl 5 with the NACA 90/35 cowl is restricted to the pressure distributions shown in Fig.36a,b for M_o = 0.85 and 0.90. Again, the distributions are similar, the NACA cowl gives a higher peak suction but the terminating shock wave is on average probably about the same strength as for cowl 5.

The apparent conclusion that the performance of cowl 6 at high Mach number and high mass flow represents an improvement relative to the corresponding cowl of the NACA series may possibly be challenged by some readers on the grounds that strictly, cowl 6 is not an 85/45 but an 85/0.499 cowl and that this change would have improved the high Mach number performance even if one had stayed within the NACA family. However - and this is the important point - one would not generally have been prepared to change to an 85/50 NACA cowl because the high Mach number, high mass flow performance would have been improved at the expense of an unacceptable deterioration in the spillage drag characteristics. This is not the case with cowl 6. Hence, one can fairly claim that use of a design approach such as that described in this report will enable the use of geometric proportions that would otherwise not be favoured. This should ease design problems associated with practical constraints. It should mean that there is still some room for manoeuvre within a range of possible geometries even when designing for a high highlight diameter/maximum diameter ratio such as 0.85 - 0.90. This is in fact, a major advantage of using a design approach in which modern theoretical methods are employed to achieve suitable external pressure distributions in appropriate design conditions.

6. CONCLUSIONS

The main conclusions of the work presented can be stated in broad terms as follows:

1) The use of a larger lip radius than is provided by the NACA 1-series cowls is successful in keeping down peak velocities near the lip and hence restricting the low Mach number drag divergence (spillage drag) to lower values of mass flow ratio (A_o/A_i). The high Mach number performance tends to suffer however (e.g. with cowls 1 and 2) so that for overall gain a restricted increase in lip radius coupled with careful detailed design of the cowl profile from lip to crest is necessary.

2) A flattening of the cowl profile aft of the lip, with an increased curvature near the crest, leads to good performance so long as the terminal shock remains ahead of the region of increased curvature; at sufficiently high Mach number, however, and with high A_o/A_i, local supersonic flow occurs over part of the region of increased curvature

and hence as a result, there is an increase in shock strength and hence in drag. This is the essence of the comparison between cowls 3 and 4.

3) Compromising on the distribution of profile curvature, in accordance with conclusion 2, and compromising further on lip radius in accordance with conclusion 1 led finally to a design (cowl 6) slightly superior to the NACA 1-series profile at high Mach number and still markedly superior at low Mach number. This is for cowls with 0.85 diameter ratio (D_i/D_{max}). At the higher D_i/D_{max} of 0.9 it seems unlikely that any improvement on the 1-series profile could be obtained except by concentrating exclusively on the high Mach number performance, a situation not specifically investigated in the present work.

4) The detailed pressure plotting of the present tests throws light on the nature of the principal flow characteristics - peak suction, lip separation, recompression and reattachment, shock progression etc. It is shown (Fig.34) that the start of the rapid drag rise can be related to a finite shock strength, the value depending on the position of the shock relative to the crest of the cowl, i.e. if the shock is further forward, a greater strength can be tolerated without excessive wave drag. At low flight speeds an interesting correlation emerges between the flow ratio for drag divergence and the calculable incompressible flow characteristic. ($C_{p_{min}}$ near -3.0, see pages 19-20).

5) The overall aim of producing favourable supercritical pressure distributions by constructive design has been reasonably well fulfilled in these experiments. The evidence provided should be helpful in guiding the course of future work in the subject, whether experimental or theoretical/numerical.

6) In particular, the analysis, and specifically the correlation in Fig.34 should be a useful guide to the pressure distributions to choose for design calculations by the modern theoretical methods. This approach should be capable of producing better cowl shapes than the NACA 1-series particularly for applications where non-aerodynamic factors dictate the use of non-optimum geometric proportions.

7. ACKNOWLEDGEMENT

The Aircraft Research Association Ltd wishes to acknowledge the help of Dr J Seddon who completed and edited the text of this report after the author had left the service of the Association.

NOTATION

A	Cross-section area
A_o/A_i	Flow ratio
V	Velocity
M	Mach number
P, C_p	Static pressure and pressure coefficient
H, ΔH	Total head and total head loss
D, C_D	Drag and drag coefficient
$\dot{m}$	Rate of mass flow through element of wake
x, r	Axial and radial coordinates of cowl profile
ρ	Radius of curvature of profile at a point
θ	Angle of slope of profile at a point

Other cowl geometry notation in Fig.2

σ	Crabtree's coefficient (section 5.2)

Suffices

o	Free stream
i	Entry highlight plane
t	Internal throat of inlet
crit	Local flow on cowl first becomes sonic
d	Drag divergence, used with either Mach number, M or flow ratio, A_o/A_i
s	Flow separation
r	Flow reattachment

REFERENCES

1. BAKER, T J — A numerical method to compute inviscid transonic flows around axisymmetric ducted bodies. A.R.A. unpublished. Conference Proceedings of IUTAM Symposium Transsonicum UU, Göttingen, September 1975 Published by Springer Verlag

2. NEALE, M C — Aerodynamic problems of power plant installation. (Part B) - mainly concerning the isolated nacelle. R.Ae.S. Convention on Short Range Transport. May 1969

3. BAALS, D B, SMITH, N F, WRIGHT, J B — The development and application of high critical speed nose inlets. NACA Report 920 1949

4. NICHOLS, M R, KEITH, A L — Investigation of a systematic group of NACA 1-series cowlings with and without spinners. NACA Report 950 1949

5 BUTLER, S F J — Aircraft drag prediction for project appraisal and performance estimation. Paper 6 of AGARD CP No.124 1973

6. STANHOPE, F W — The performance of NACA 1 intakes. Rolls Royce Powerplant Research Report IAR 85002 July 1968

7. SEDDON, J — Air intakes for aircraft gas turbines. J. R.Ae.S., Vol 56, pp 747-781 October 1952

8. HAINES, A B — Some notes on the use of the shock-at-crest criterion for predicting the drag-rise Mach number of nacelle cowls. A.R.A. unpublished January 1970

9. KUCHEMANN, D, WEBER, J — Aerodynamics of propulsion. McGraw-Hill 1953

10. PEARCEY, H H — The aerodynamic design of section shapes for swept wings. Presented at the Second International Congress, ICAS, Zurich September 1960

11. BAUER, F; GARABEDIAN, P R; KORN, D F — Supercritical wing sections. Lecture notes in Economics and Mathematical Systems. Springer-Verlag 1972

12. LANGLEY, M J — Measurements of external drag and surface pressure distribution on six cowls designed for high subsonic Mach number. A.R.A. unpublished 1971

13. CAMBRIDGE UNIVERSITY AERONAUTICS LABORATORY — The measurement of profile drag by the pitot-traverse method. ARC R & M No.1688 1936

14. MASON, J G — Flow synthesis by singularities. Two-dimensional and axisymmetric problems. Rolls Royce Powerplant Research Memo IAM 99801 1968

15. E.S.D.U. — A catalogue of digital computer programs in fluid dynamics. DRIC BR 29590, ARC 36232 1975

16. CRABTREE, L F — The formation of regions of separated flow on wing surfaces. Pt.II Laminar separation bubbles and the mechanism of the leading edge stall. ARC R & M No.3122 July 1957

17. HOLDER, D W; PEARCEY, H H; GADD, G E — The interaction between shock waves and boundary layers. ARC 16077 1953

TABLE 1 COWL 1 EXTERNAL PROFILE

x/D_{Max}	r/D_{Max}	Slope°	ρ/D_{Max}	x/D_{Max}	r/D_{Max}	Slope°	ρ/D_{Max}
0.000	0.4250	90.00	0.0224	0.100	0.4739	11.84	0.7453
0.001	0.43162	72.83	00.0224	0.110	0.4759	11.09	0.8120
0.002	0.43425	65.62	0.0224	0.120	0.4778	10.40	0.8760
0.003	0.43620	60.03	0.0224	0.130	0.4796	9.76	0.9377
0.004	0.43784	55.26	0.0224	0.140	0.4813	9.16	0.9979
0.005	0.4391	51.00	0.0224	0.150	0.4828	8.59	1.0570
0.006	0.4403	47.10	0.0224	0.160	0.4843	8.06	1.1155
0.007	0.4413	43.54	0.0245	0.170	0.4857	7.55	1.1741
0.008	0.4422	40.67	0.0296	0.180	0.4870	7.07	1.2331
0.009	0.4430	38.36	0.0349	0.190	0.4882	6.62	1.2931
0.010	0.4438	36.44	0.0405	0.200	0.4893	6.18	1.3544
0.011	0.4445	34.81	0.0463	0.210	0.4903	5.76	1.4176
0.012	0.4452	33.41	0.0524	0.220	0.4913	5.37	1.4831
0.013	0.4458	32.18	0.0586	0.230	0.4922	4.99	1.5512
0.014	0.4464	31.09	0.0651	0.240	0.4930	4.62	1.6224
0.015	0.4470	30.11	0.0717	0.250	0.4938	4.28	1.6973
0.016	0.4476	29.23	0.0785	0.260	0.4945	3.95	1.7761
0.017	0.4481	28.44	0.0855	0.270	0.4952	3.63	1.8595
0.018	0.4487	27.71	0.0926	0.280	0.4958	3.33	1.9479
0.019	0.4492	27.04	0.0998	0.290	0.4964	3.04	2.0418
0.020	0.4497	26.41	0.1072	0.300	0.4969	2.77	2.1420
0.025	0.4520	23.89	0.1458	0.310	0.4973	2.51	2.2489
0.030	0.4541	22.01	0.1866	0.320	0.4978	2.26	2.3633
0.035	0.4561	20.52	0.2287	0.330	0.4981	2.02	2.4858
0.040	0.4579	19.30	0.2716	0.340	0.4985	1.80	2.6174
0.045	0.4596	18.26	0.3148	0.350	0.4988	1.58	2.7589
0.050	0.4612	17.37	0.3578	0.360	0.4990	1.38	2.9113
0.055	0.4627	16.58	0.4005	0.370	0.4992	1.19	3.0757
0.060	0.4642	15.87	0.4424	0.380	0.4994	1.01	3.2532
0.065	0.4656	15.23	0.4836	0.390	0.4996	0.84	3.4452
0.070	0.4669	14.64	0.5239	0.400	0.4997	0.68	3.6533
0.075	0.4682	14.09	0.5633	0.410	0.4998	0.52	3.8790
0.080	0.4694	13.59	0.6016	0.420	0.4999	0.38	4.1243
0.085	0.4706	13.11	0.6389	0.430	0.5000	0.24	4.3912
0.090	0.4717	12.67	0.6753	0.440	0.5000	0.12	4.6822
0.095	0.4729	12.24	0.7108	0.450	0.5000	0.00	5.0000

TABLE 2 COWL 2 EXTERNAL PROFILE

x/D_{Max}	r/D_{Max}	Slope°	ρ/D_{Max}	x/D_{Max}	r/D_{Max}	Slope°	ρ/D_{Max}
0.000	0.4500	90.00	0.0179	0.075	0.4860	9.51	0.5199
0.001	0.45590	70.73	0.0179	0.080	0.4868	8.98	0.5642
0.002	0.45822	62.62	0.0179	0.085	0.4876	8.48	0.6092
0.003	0.45992	56.30	0.0179	0.090	0.4883	8.02	0.6550
0.004	0.46128	50.90	0.0179	0.095	0.4890	7.60	0.7015
0.005	0.4624	46.33	0.0207	0.100	0.4896	7.20	0.7490
0.006	0.4634	42.76	0.0245	0.110	0.4908	6.47	0.8465
0.007	0.4643	39.87	0.0284	0.120	0.4919	5.83	0.9482
0.008	0.4651	37.46	0.0326	0.130	0.4929	5.25	1.0545
0.009	0.4658	35.41	0.0370	0.140	0.4938	4.74	1.1661
0.010	0.4665	33.64	0.0415	0.150	0.4945	4.27	1.2839
0.011	0.4671	32.08	0.0462	0.160	0.4952	3.84	1.4085
0.012	0.4677	30.70	0.0511	0.170	0.4959	3.45	1.5409
0.013	0.4683	29.46	0.0561	0.180	0.4965	3.09	1.6821
0.014	0.4689	28.35	0.0613	0.190	0.4970	2.77	1.8330
0.015	0.4694	27.33	0.0667	0.200	0.4974	2.47	1.9949
0.016	0.4699	26.41	0.0721	0.210	0.4978	2.19	2.1689
0.017	0.4704	25.56	0.0777	0.220	0.4982	1.94	2.3565
0.018	0.4709	24.77	0.0834	0.230	0.4985	1.70	2.5591
0.019	0.4713	24.04	0.0893	0.240	0.4988	1.49	2.7784
0.020	0.4718	23.36	0.0952	0.250	0.4990	1.29	3.0161
0.025	0.4738	20.55	0.1265	0.260	0.4992	1.11	3.2744
0.030	0.4755	18.42	0.1601	0.270	0.4994	0.94	3.5554
0.035	0.4771	16.72	0.1954	0.280	0.4996	0.79	3.8617
0.040	0.4785	15.32	0.2324	0.290	0.4997	0.64	4.1961
0.045	0.4799	14.14	0.2706	0.300	0.4998	0.51	4.5617
0.050	0.4811	13.13	0.3100	0.310	0.4999	0.39	4.9620
0.055	0.4822	12.23	0.3503	0.320	0.4999	0.28	5.4011
0.060	0.4832	11.44	0.3915	0.330	0.5000	0.18	5.8836
0.065	0.4842	10.74	0.4336	0.340	0.5000	0.09	6.4146
0.070	0.4851	10.10	0.4764	0.350	0.5000	-0.00	7.0000

TABLE 3 COWL 3 EXTERNAL PROFILE

x/D_{Max}	r/D_{Max}	Slope°	ρ/D_{Max}
0.000	0.4250	90.00	0.0143
0.001	0.4303	68.43	0.0143
0.002	0.4323	59.32	0.0143
0.003	0.4338	52.19	0.0143
0.004	0.4349	46.44	0.0177
0.005	0.4359	42.48	0.0232
0.006	0.4368	39.57	0.0292
0.007	0.4376	37.30	0.0356
0.008	0.4383	35.46	0.0423
0.009	0.4390	33.94	0.0494
0.010	0.4396	32.64	0.0567
0.011	0.4403	31.53	0.0644
0.012	0.4409	30.55	0.0723
0.013	0.4414	29.68	0.0805
0.014	0.4420	28.90	0.0889
0.015	0.4426	28.20	0.0975
0.016	0.4431	27.57	0.1063
0.017	0.4436	26.98	0.1152
0.018	0.4441	26.45	0.1243
0.019	0.4446	25.95	0.1335
0.020	0.4451	25.49	0.1429
0.025	0.4474	23.59	0.1908
0.030	0,4495	22.14	0.2395
0.035	0.4514	20.97	0.2879
0.040	0.4533	19.98	0.3351
0.045	0.4551	19.13	0.3803
0.050	0.4568	18.38	0.4234
0.055	0.4584	17.70	0.4640
0.060	0.4600	17.08	0.5023
0.065	0.4615	16.50	0.5381
0.070	0.4629	15.97	0.5718
0.075	0.4643	15.46	0.6033
0.080	0.4657	14.98	0.6330
0.085	0.4670	14.52	0.6610
0.090	0.4683	14.08	0.6875
0.095	0.4695	13.66	0.7128
0.100	0.4707	13.25	0.7368
0.110	0.4730	12.48	0.7822
0.120	0.4751	11.75	0.8250
0.130	0.4772	11.06	0.8660
0.140	0.4791	10.40	0.9061
0.150	0.4808	9.77	0.9461
0.160	0.4825	9.17	0.9866
0.170	0.4841	8.60	1.0281
0.180	0.4855	8.04	1.0710
0.190	0.4869	7.52	1.1159
0.200	0.4882	7.01	1.1632
0.210	0.4894	6.52	1.2132
0.220	0.4905	6.06	1.2664
0.230	0.4915	5.61	1.3232
0.240	0.4924	5.19	1.3841
0.250	0.4933	4.78	1.4495
0.260	0.4941	4.39	1.5200
0.270	0.4948	4.02	1.5959
0.280	0.4955	3.67	1.6780
0.290	0.4961	3.34	1.7668
0.300	0.4967	3.02	1.8631
0.310	0.4972	2.72	1.9675
0.320	0.4976	2.44	2.0810
0.330	0.4980	2.17	2.2044
0.340	0.4984	1.92	2.3387
0.350	0.4987	1.68	2.4852
0.360	0.4990	1.46	2.6451
0.370	0.4992	1.25	2.8198
0.380	0.4994	1.05	3.0110
0.390	0.4996	0.87	3.2204
0.400	0.4997	0.70	3.4503
0.410	0.4998	0.54	3.7028
0.420	0.4999	0.39	3.9808
0.430	0.5000	0.25	4.2872
0.440	0.5000	0.12	4.6256
0.450	0.5000	0.00	5.0000

TABLE 4 COWL 4 EXTERNAL PROFILE

x/D_{Max}	r/D_{Max}	Slope°	ρ/D_{Max}	x/D_{Max}	r/D_{Max}	Slope°	ρ/D_{Max}
0.000	0.4250	90.00	0.0186	0.100	0.4709	11.75	0.8388
0.001	0.4310	71.11	0.0186	0.110	0.4729	11.09	0.9216
0.002	0.4334	63.16	0.0186	0.120	0.4748	10.48	1.0007
0.003	0.4351	56.98	0.0186	0.130	0.4766	9.92	1.0761
0.004	0.4365	51.69	0.0186	0.140	0.4783	9.40	1.1481
0.005	0.4377	46.96	0.0191	0.150	0.4799	8.91	1.2166
0.006	0.4387	43.17	0.0239	0.160	0.4814	8.44	1.2821
0.007	0.4396	40.25	0.0289	0.170	0.4829	8.00	1.3448
0.008	0.4404	37.91	0.0343	0.180	0.4843	7.58	1.4050
0.009	0.4411	35.97	0.0399	0.190	0.4856	7.18	1.4629
0.010	0.4418	34.33	0.0457	0.200	0.4868	6.79	1.5189
0.011	0.4425	32.91	0.0517	0.210	0.4879	6.42	1.5732
0.012	0.4431	31.68	0.0580	0.220	0.4890	6.06	1.6260
0.013	0.4437	30.58	0.0645	0.230	0.4901	5.71	1.6777
0.014	0.4443	29.60	0.0711	0.240	0.4910	5.37	1.7286
0.015	0.4449	28.72	0.0779	0.250	0.4919	5.04	1.7787
0.016	0.4454	27.92	0.0849	0.260	0.4928	4.72	1.8285
0.017	0.4459	27.19	0.0921	0.270	0.4936	4.41	1.8780
0.018	0.4464	26.52	0.0994	0.280	0.4943	4.11	1.9276
0.019	0.4469	25.90	0.1068	0.290	0.4950	3.82	1.9775
0.020	0.4474	25.33	0.1144	0.300	0.4957	3.53	2.0278
0.025	0.4496	22.97	0.1542	0.310	0.4963	3.25	2.0788
0.030	0.4517	21.19	0.1965	0.320	0.4968	2.98	2.1307
0.035	0.4535	19.79	0.2408	0.330	0.4973	2.71	2.1838
0.040	0.4553	18.63	0.2864	0.340	0.4978	2.45	2.2382
0.045	0.4569	17.66	0.3330	0.350	0.4982	2.20	2.2941
0.050	0.4585	16.82	0.3802	0.360	0.4985	1.95	2.3519
0.055	0.4599	16.08	0.4278	0.370	0.4988	1.71	2.4118
0.060	0.4613	15.42	0.4754	0.380	0.4991	1.48	2.4740
0.065	0.4627	14.82	0.5228	0.390	0.4994	1.25	2.5387
0.070	0.4640	14.28	0.5699	0.400	0.4996	1.03	2.6064
0.075	0.4652	13.78	0.6165	0.410	0.4997	0.81	2.6773
0.080	0.4665	13.32	0.6625	0.420	0.4998	0.60	2.7517
0.085	0.4676	12.89	0.7078	0.430	0.4999	0.39	2.8300
0.090	0.4687	12.49	0.7523	0.440	0.5000	0.19	2.9127
0.095	0.4698	12.11	0.7960	0.450	0.5000	0.00	3.0000

TABLE 5 COWL 5 EXTERNAL PROFILE

X/D_{Max}	r/D_{Max}	Slope°	ρ/D_{Max}	x/D_{Max}	r/D_{Max}	Slope°	ρ/D_{Max}
0.000	0.4500	90.00	0.0109	0.080	0.4814	9.73	0.7340
0.001	0.4546	65.23	0.0109	0.085	0.4822	9.35	0.7860
0.002	0.4563	54.69	0.0109	0.090	0.4831	8.99	0.8374
0.003	0.4575	47.06	0.0139	0.095	0 4838	8.66	0.8881
0.004	0.4585	42.00	0.0182	0.100	0.4846	8.34	0.9381
0.005	0.4593	38.33	0.0229	0.110	0.4860	7.75	1.0355
0.006	0.4601	35.49	0.0279	0.120	0.4873	7.22	1.1294
0.007	0.4608	33.21	0.0332	0.130	0.4885	6.73	1.2196
0.008	0.4614	31.32	0.0387	0.140	0.4897	6.27	1.3059
0.009	0.4620	29.71	0.0445	0.150	0.4907	5.84	1.3884
0.010	0.4625	28.33	0.0506	0.160	0.4917	5.44	1.4672
0.011	0.4631	27.13	0.0568	0.170	0.4926	5.06	1.5426
0.012	0.4636	26.06	0.0633	0.180	0.4935	4.69	1.6147
0.013	0.4640	25.10	0.0699	0.190	0.4943	4.34	1.6840
0.014	0.4645	24.24	0.0767	0.200	0.4950	4.01	1.7507
0.015	0.4649	23.46	0.0837	0.210	0.4957	3.69	1.8153
0 016	0.4654	22.75	0.0914	0.220	0.4963	3.38	1.8783
0.017	0.4658	22.10	0.0995	0.230	0.4969	3.07	1.9400
0.018	0.4662	21.50	0.1077	0.240	0.4974	2.78	2.0009
0.019	0.4666	20.95	0.1160	0.250	0.4978	2.50	2.0617
0.020	0.4669	20.44	0.1244	0.260	0.4982	2.23	2.1227
0.025	0.4687	18.35	0.1685	0.270	0.4986	1.96	2.1845
0.030	0.4703	16.77	0.2151	0.280	0.4989	1.70	2.2477
0.035	0.4717	15.52	0.2636	0.290	0.4992	1.45	2.3128
0.040	0.4731	14.49	0.3137	0.300	0.4994	1.21	2.3804
0.045	0.4743	13.62	0.3650	0.310	0.4996	0.97	2.4511
0.050	0.4755	12.86	0.4171	0.320	0.4998	0.74	2.5256
0.055	0.4766	12.20	0.4697	0.330	0.4999	0.51	2.6044
0.060	0.4777	11.61	0.5227	0.340	0.5000	0.30	2.6883
0.065	0.4787	11.08	0.5758	0.350	0.5000	0.09	2.7779
0.070	0.4796	10.59	0.6288	0.354	0.5000	0.00	2.8182
0.075	0.4805	10.15	0.6816				

TABLE 6 COWL 6 EXTERNAL PROFILE

x/D_{Max}	r/D_{Max}	Slope°	ρ/D_{Max}	x/D_{Max}	r/D_{Max}	Slope°	ρ/D_{Max}
0.000	0.4250	90.00	0.0122	0.130	0.4732	10.17	1.0236
0.001	0.4298	66.60	0.0122	0.140	0.4749	9.62	1.1053
0.002	0.4317	56.67	0.0122	0.150	0.4766	9.12	1.1876
0.003	0.4330	48.91	0.0129	0.160	0.4781	8.64	1.2703
0.004	0.4340	43.54	0.0183	0.170	0.4796	8.20	1.3532
0.005	0.4349	39.89	0.0242	0.180	0.4810	7.79	1.4360
0.006	0.4357	37.20	0.0305	0.190	0.4823	7.39	1.5186
0.007	0.4364	35.10	0.0373	0.200	0.4836	7.02	1.6007
0.008	0.4371	33.40	0.0445	0.210	0.4848	6.67	1.6821
0.009	0.4378	31.98	0.0520	0.220	0.4859	6.34	1.7626
0.010	0.4384	30.78	0.0599	0.230	0.4870	6.02	1.8420
0.011	0.4390	29.74	0.0680	0.240	0.4881	5.71	1.9201
0.012	0.4395	28.83	0.0764	0.250	0.4890	5.42	1.9968
0.013	0.4401	28.02	0.0850	0.260	0.4900	5.13	2.0718
0.014	0.4406	27.30	0.0939	0.270	0.4908	4.86	2.1449
0.015	0.4411	26.64	0.1029	0.280	0.4917	4.60	2.2161
0.016	0.4416	26.05	0.1121	0.290	0.4924	4.34	2.2851
0.017	0.4421	25.50	0.1214	0.300	0.4932	4.09	2.3518
0.018	0.4425	25.00	0.1308	0.310	0.4939	3.85	2.4161
0.019	0.4430	24.54	0.1404	0.320	0.4945	3.62	2.4777
0.020	0.4435	24.10	0.1500	0.330	0.4951	3.39	2.5367
0.025	0.4456	22.30	0.1987	0.340	0.4957	3.16	2.5928
0.030	0.4476	20.91	0.2471	0.350	0.4962	2.95	2.6459
0.035	0.4494	19.78	0.2940	0.360	0.4967	2.73	2.6960
0.040	0.4512	18.82	0.3386	0.370	0.4972	2.52	2.7429
0.045	0.4528	17.98	0.3805	0.380	0.4976	2.31	2.7867
0.050	0.4544	17.23	0.4195	0.390	0.4980.	2.11	2.8271
0.055	0.4559	16.55	0.4558	0.400	0.4984	1.91	2.8641
0.060	0.4574	15.91	0.4900	0.410	0.4987	1.71	2.8977
0.065	0.4588	15.33	0.5249	0.420	0.4990	1.51	2.9277
0.070	0.4601	14.78	0.5604	0.430	0.4992	1.32	2.9543
0.075	0.4614	14.27	0.5965	0.440	0.4994	1.12	2.9773
0.080	0.4627	13.79	0.6332	0.450	0.4996	0.93	2.9967
0.085	0.4639	13.34	0.6704	0.460	0.4997	0.74	3.0126
0.090	0.4651	12.91	0.7081	0.470	0.4999	0.55	3.0248
0.095	0.4662	12.50	0.7462	0.480	0.4999	0.36	3.0334
0.100	0.4673	12.12	0.7848	0.490	0.5000	0.17	3.0384
0.110	0.4694	11.41	0.8631	0.499	0.5000	0.00	3.0399
0.120	0.4713	10.76	0.9428				

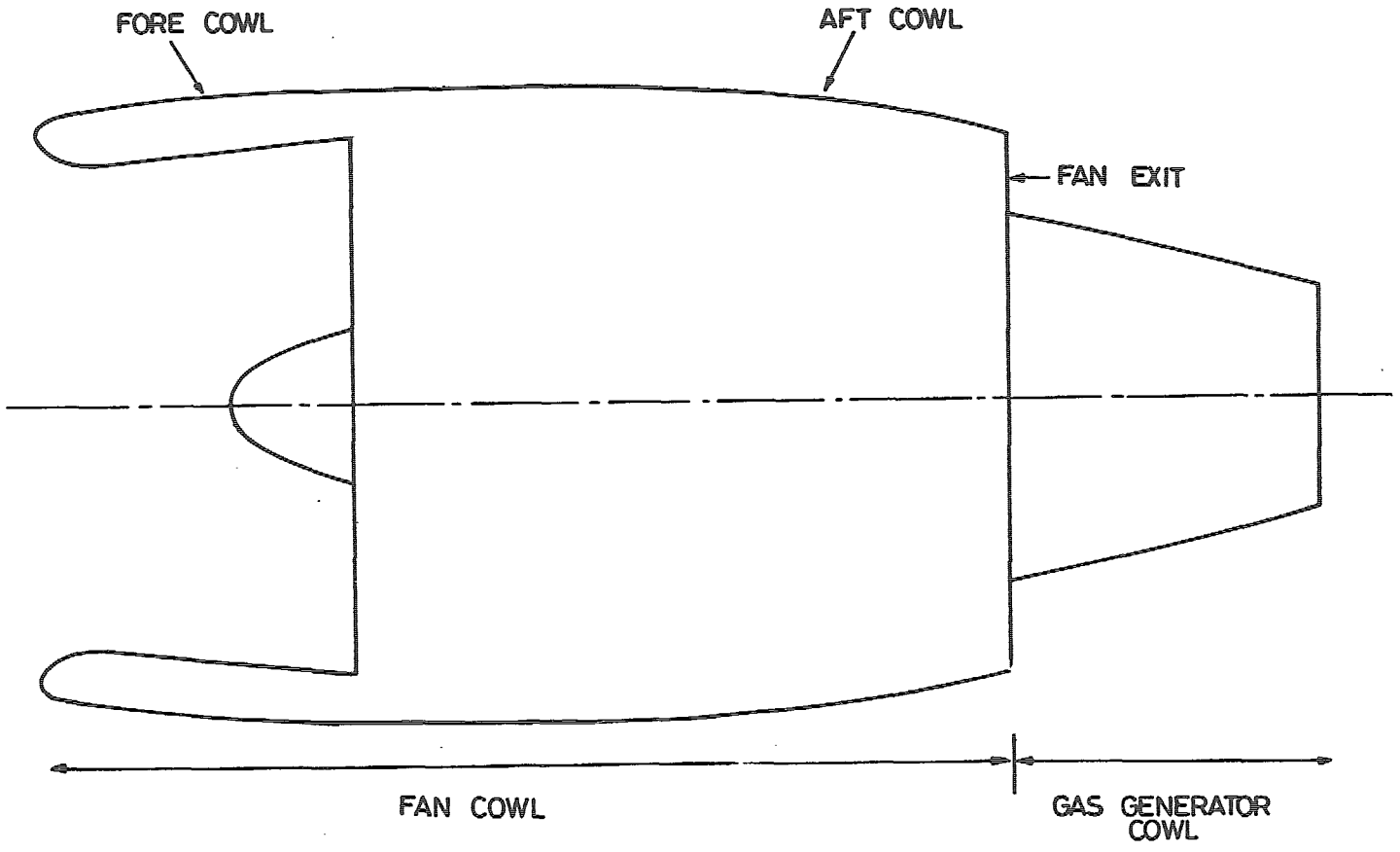

Fig 1 Typical nacelle for high by-pass ratio turbofan engine

Fig 2

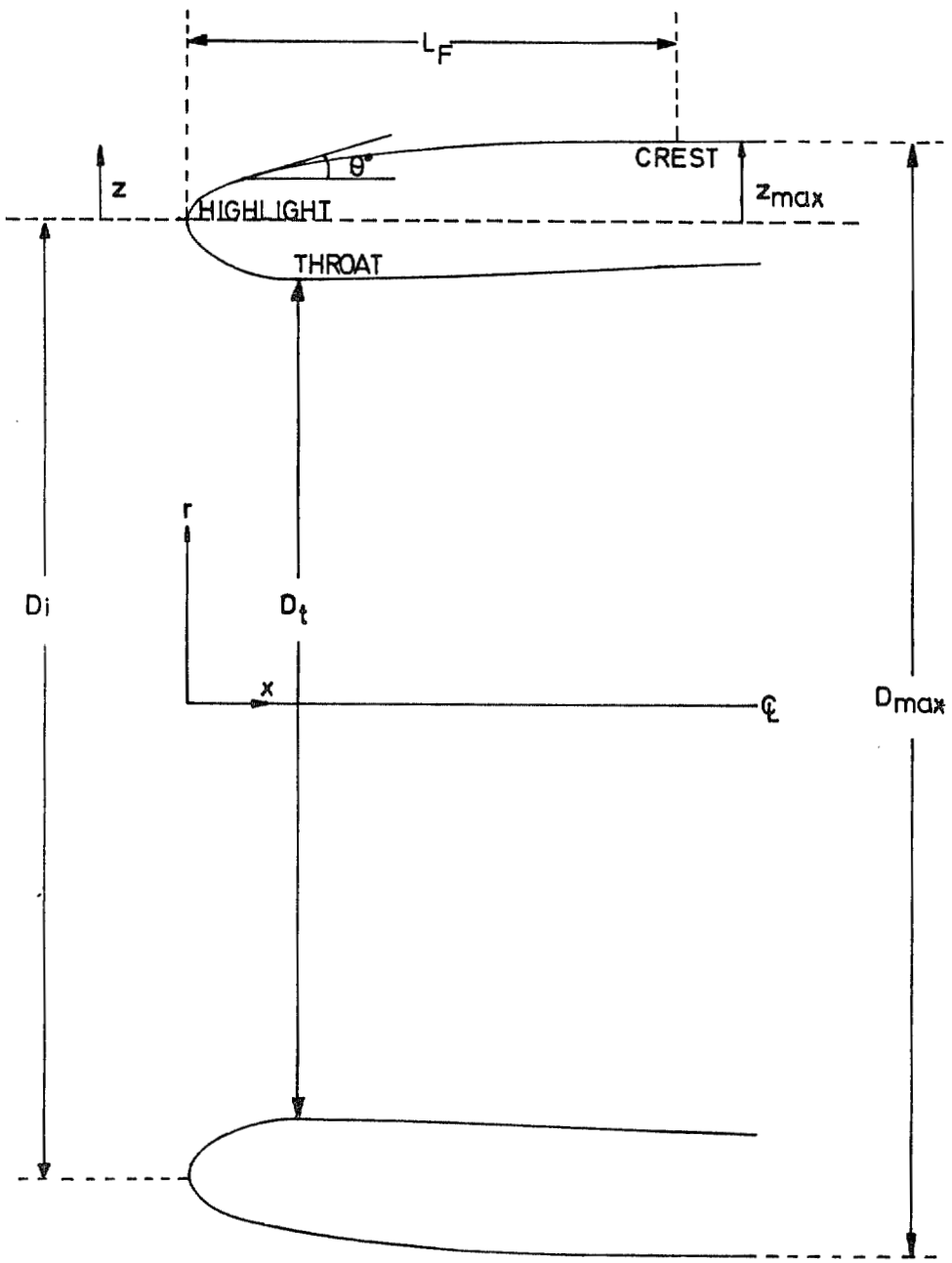

Fig 2 Cowl geometry nomenclature

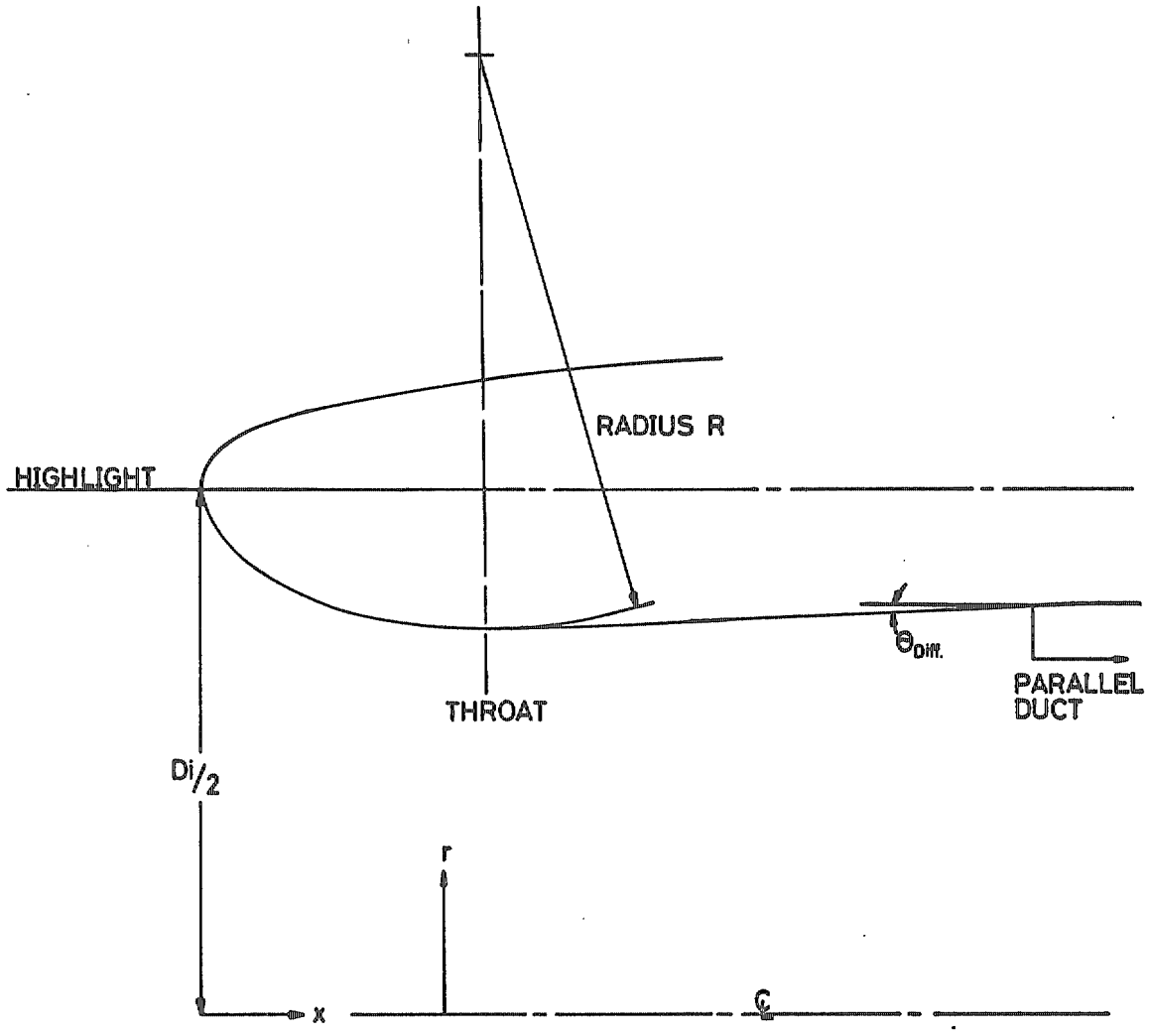

	COWLS 1,3,4,6	COWLS 2,5
THROAT x/Dmax	0.0897	0.0950
r/Dmax	0.3930 ?	0.4025
RADIUS R/Dmax	0.1795	0.1900
DIFFUSER SEMI ANGLE θ_{Diff}	1.871°	0.472°
END OF DIFFUSER x/Dmax	1.0071	1.0071
DUCT RADIUS/Dmax	0.4100	0.4100
CONTRACTION RATIO Ai/At	1.25 ?	1.25

Fig 3 Internal geometry for cowls on B5 rig

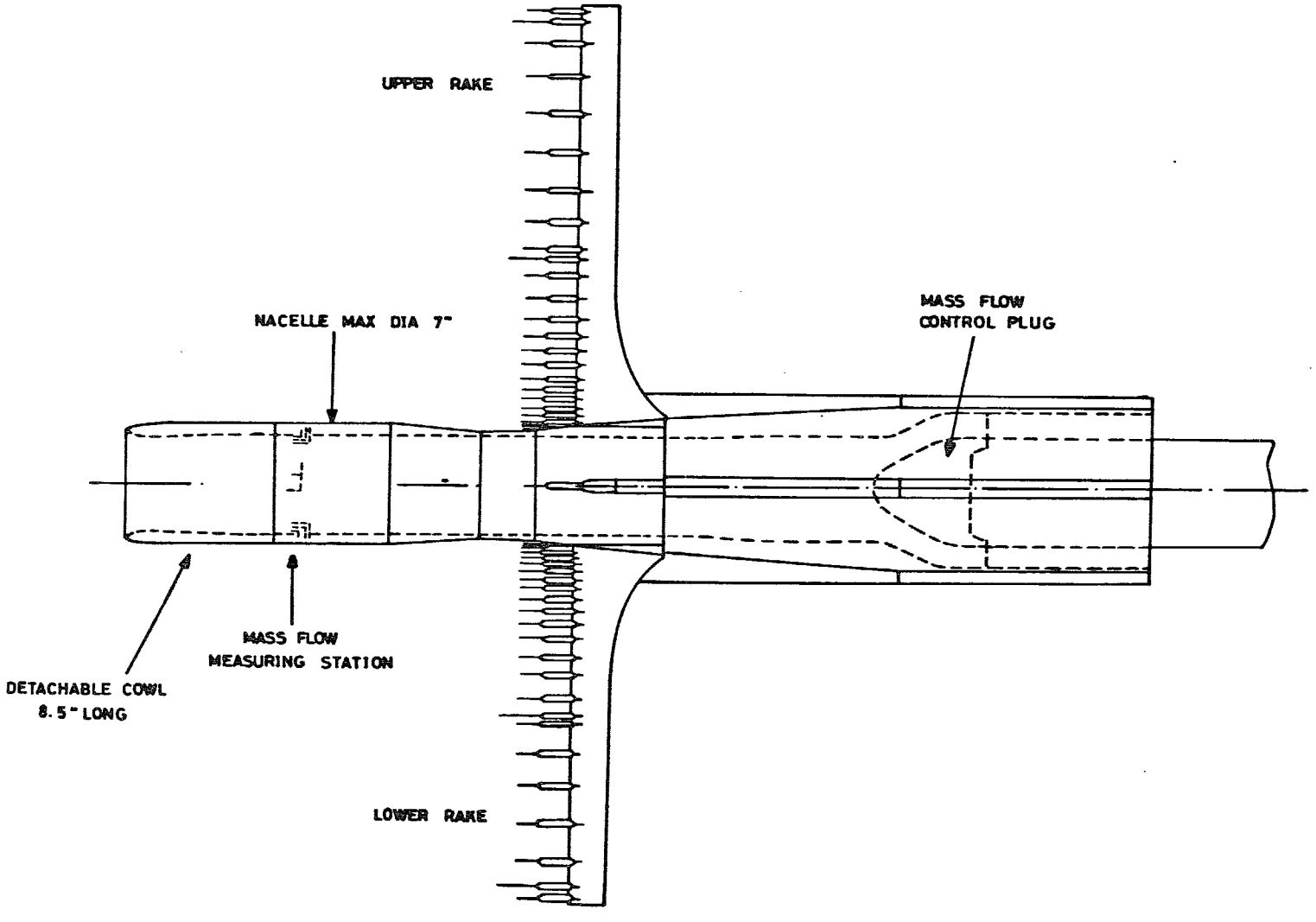

Fig 4 B5 rig general arrangement

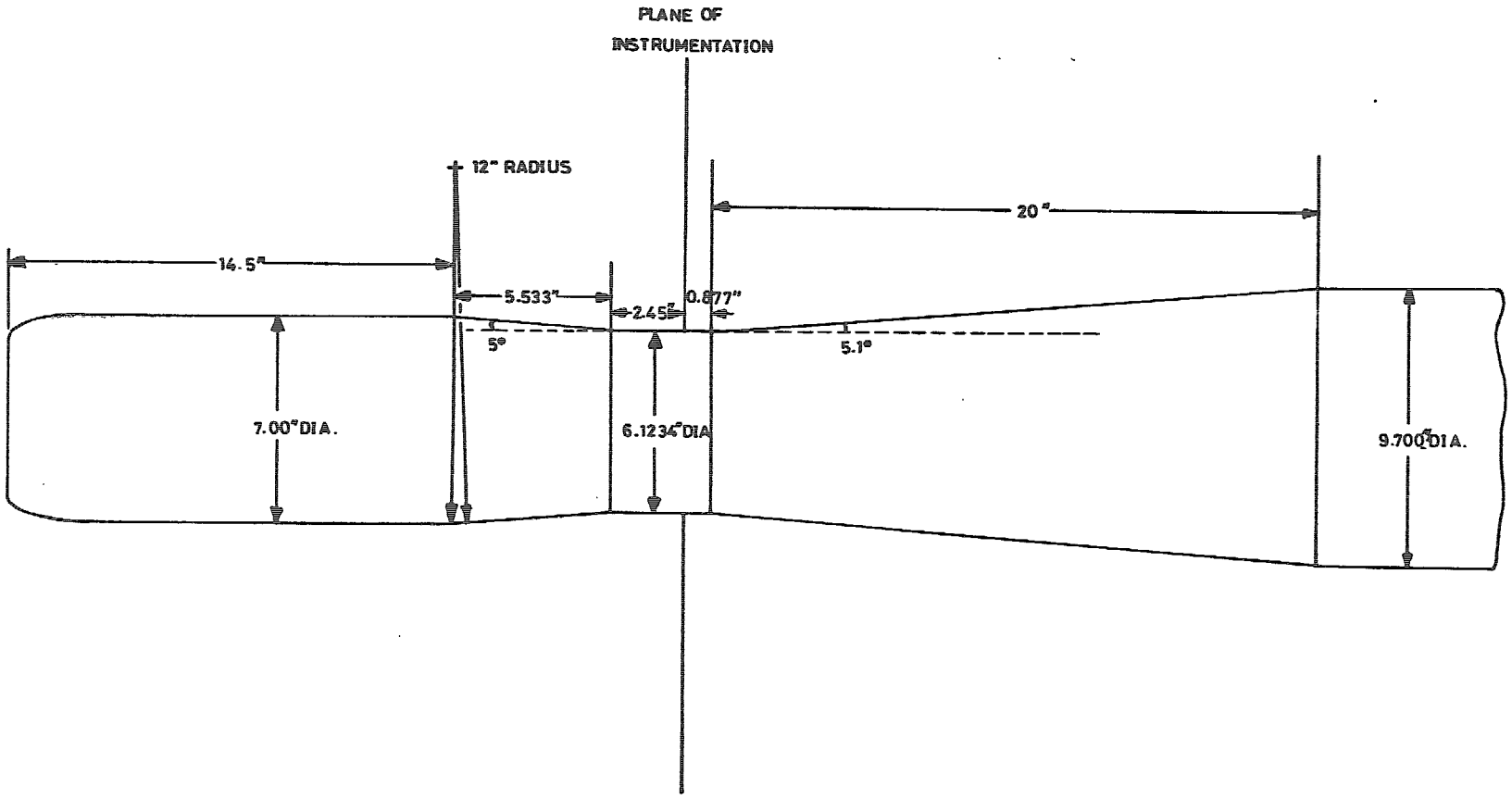

Fig 5 Geometry of model rig

Fig 6

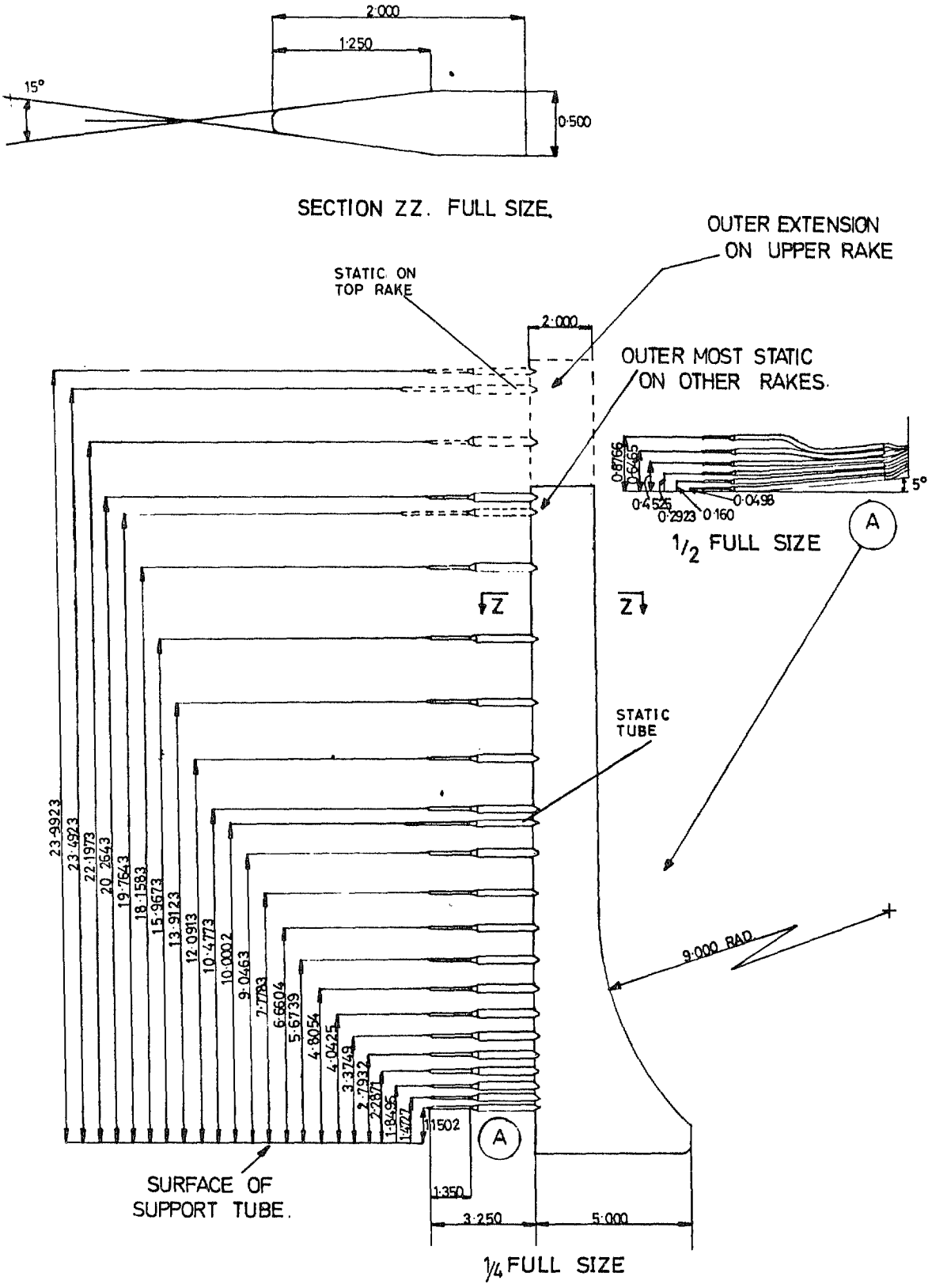

Fig 6 Wake traverse rake assemblies

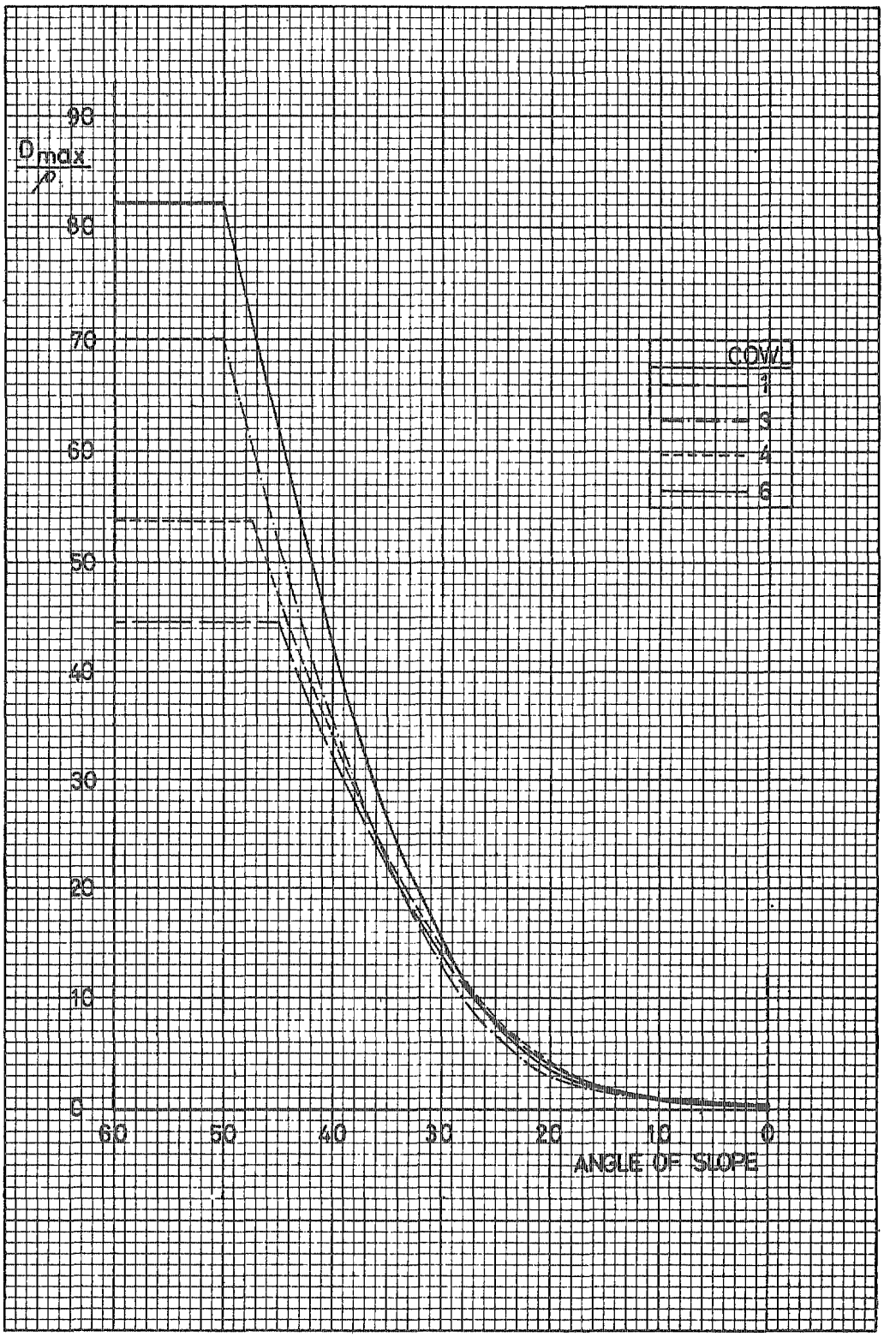

Fig 7 Curvature distributions for cowls 1, 3, 4, 6

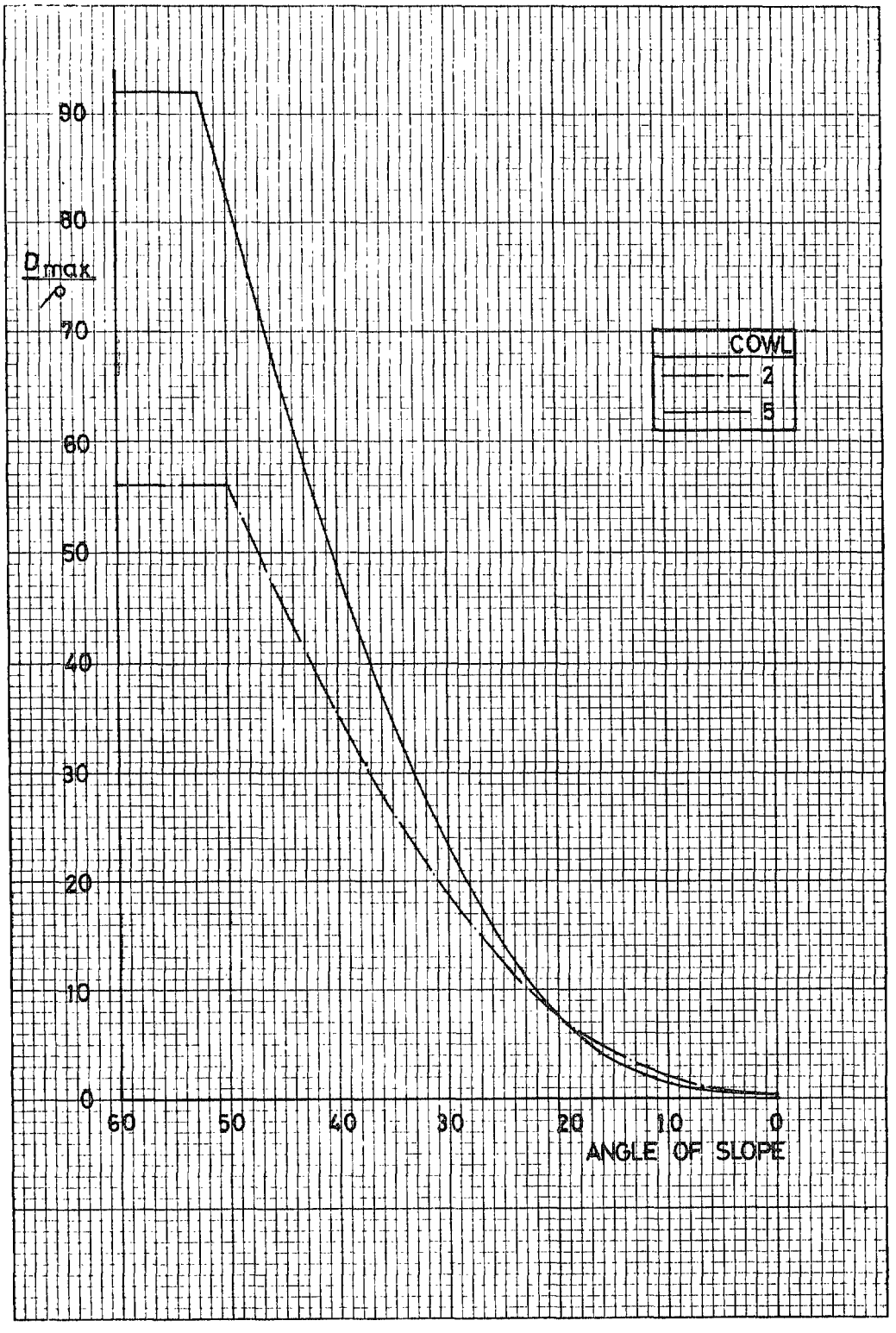

Fig 8 Curvature distributions for cowls 2, 5

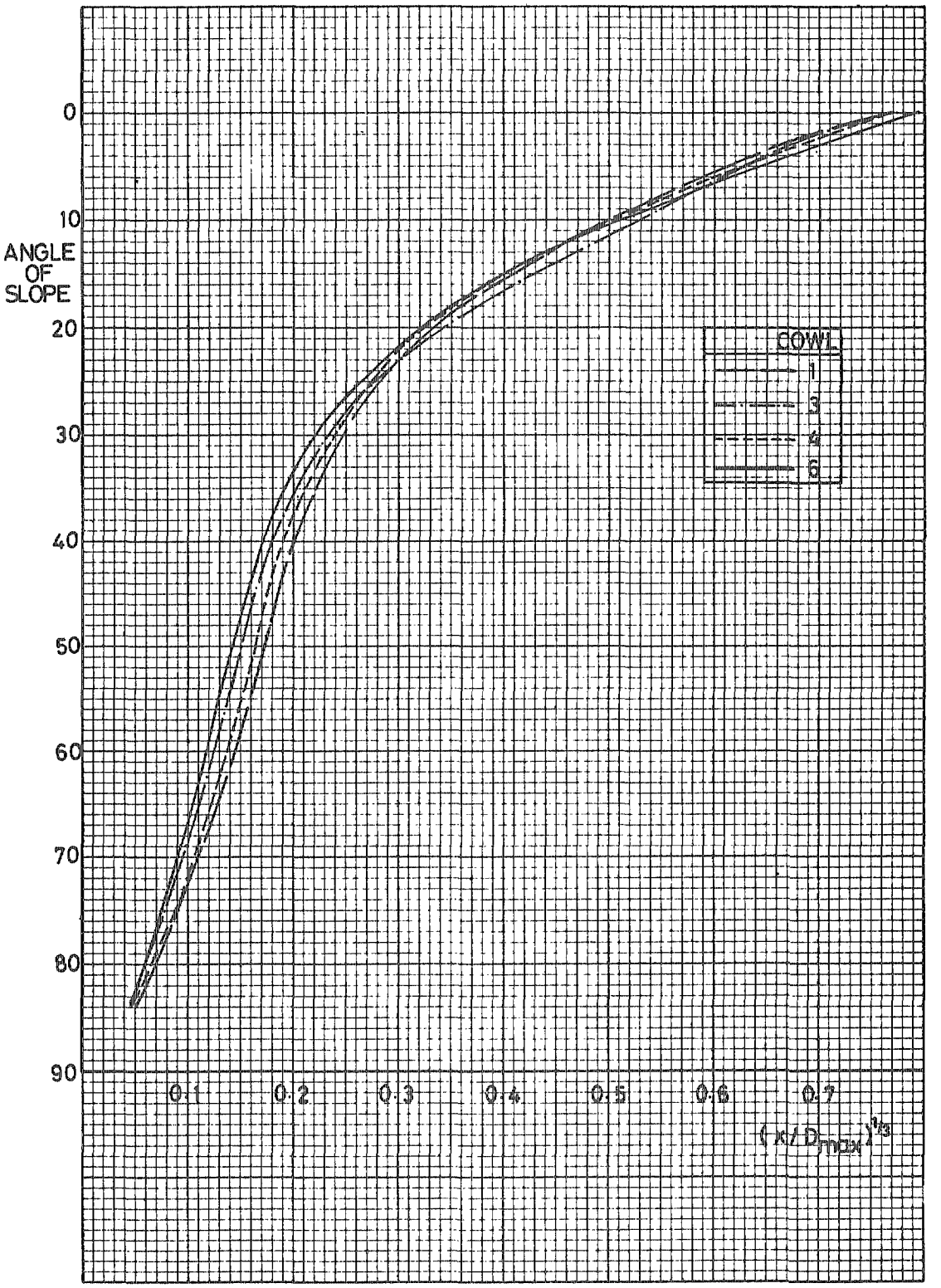

Fig 9 Slope distributions for cowls 1, 3, 4, 6

Fig 10

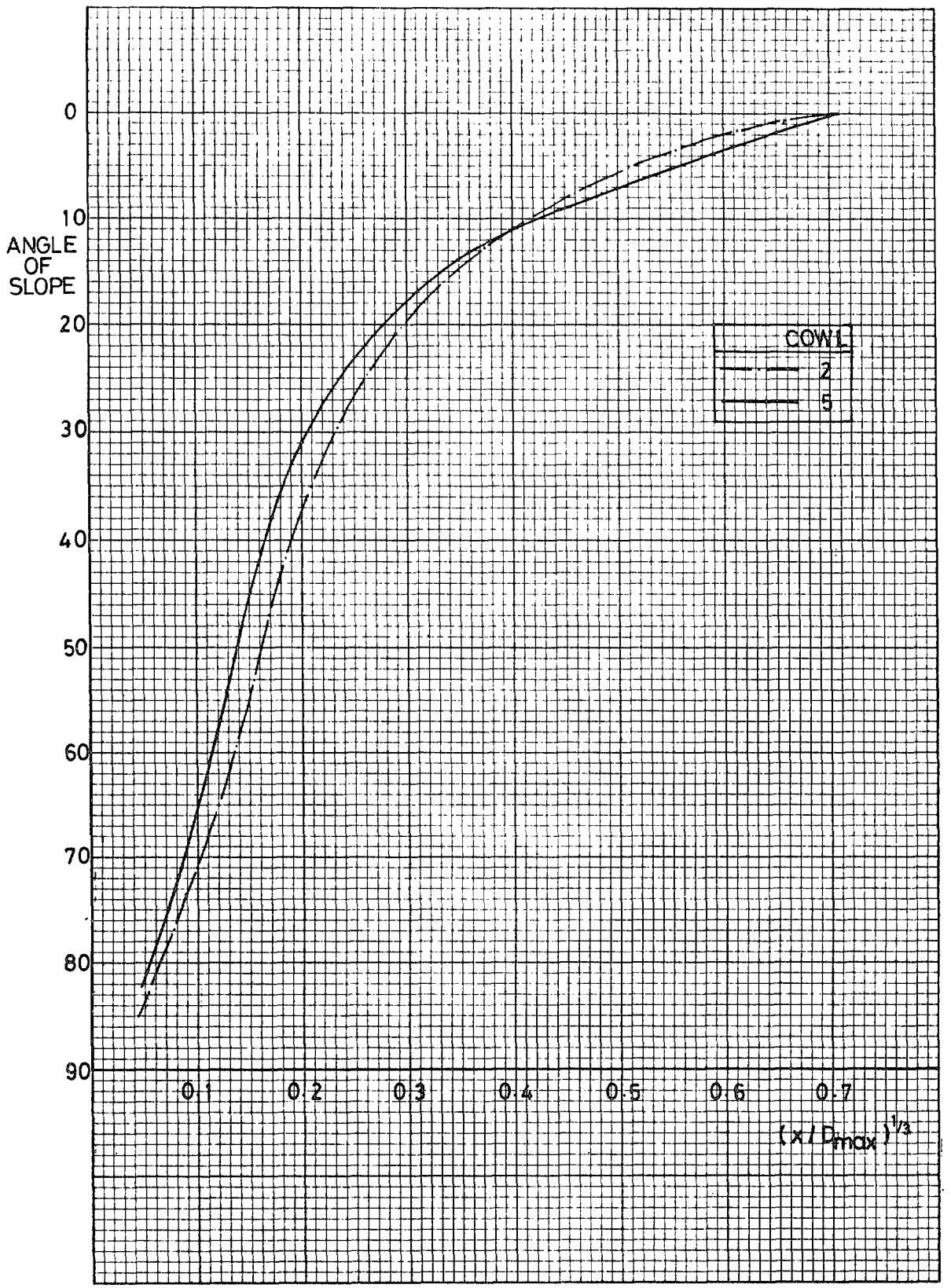

Fig 10 Slope distributions for cowls 2, 5

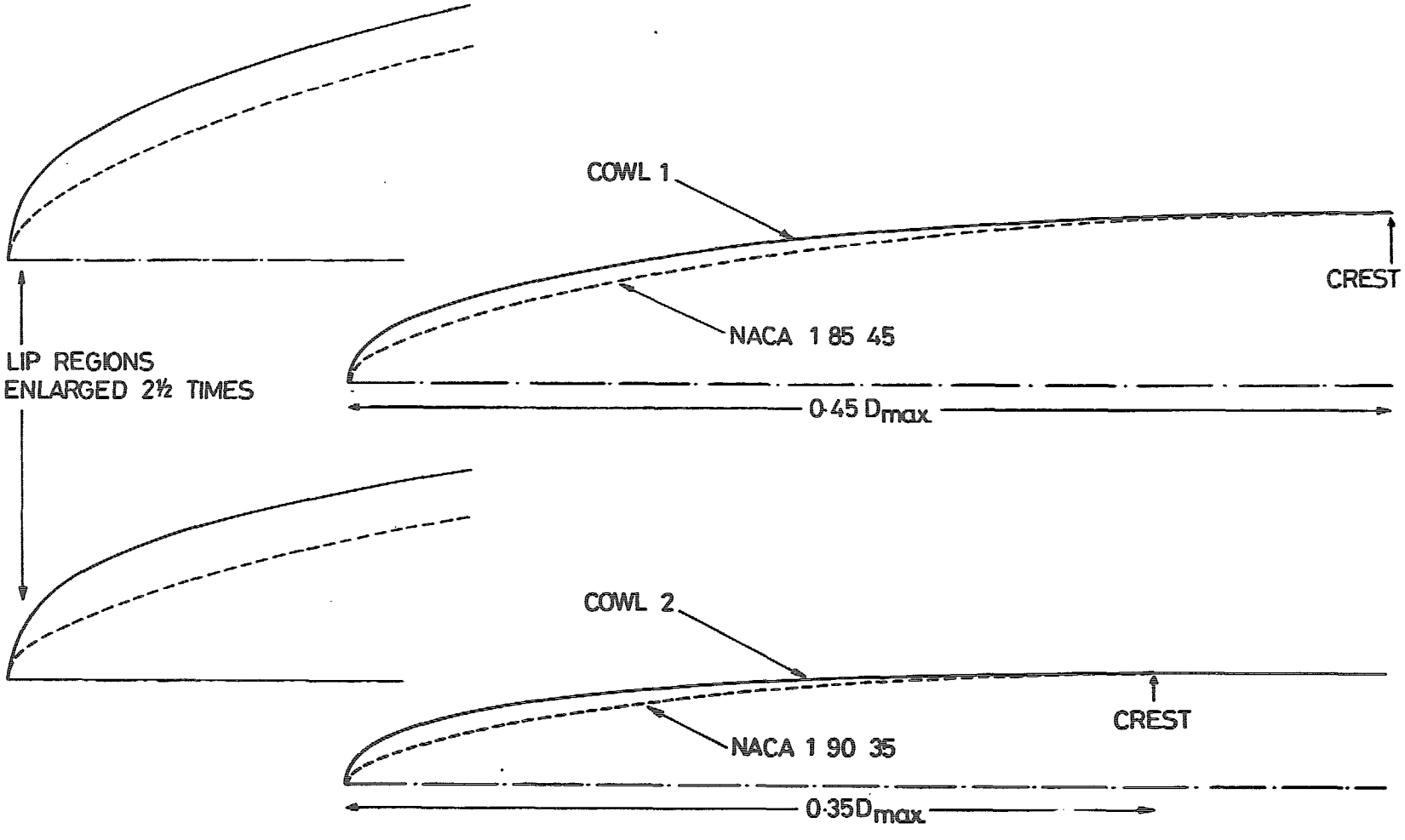

Fig 11 External lip shapes of cowls 1 and 2

Fig 12a

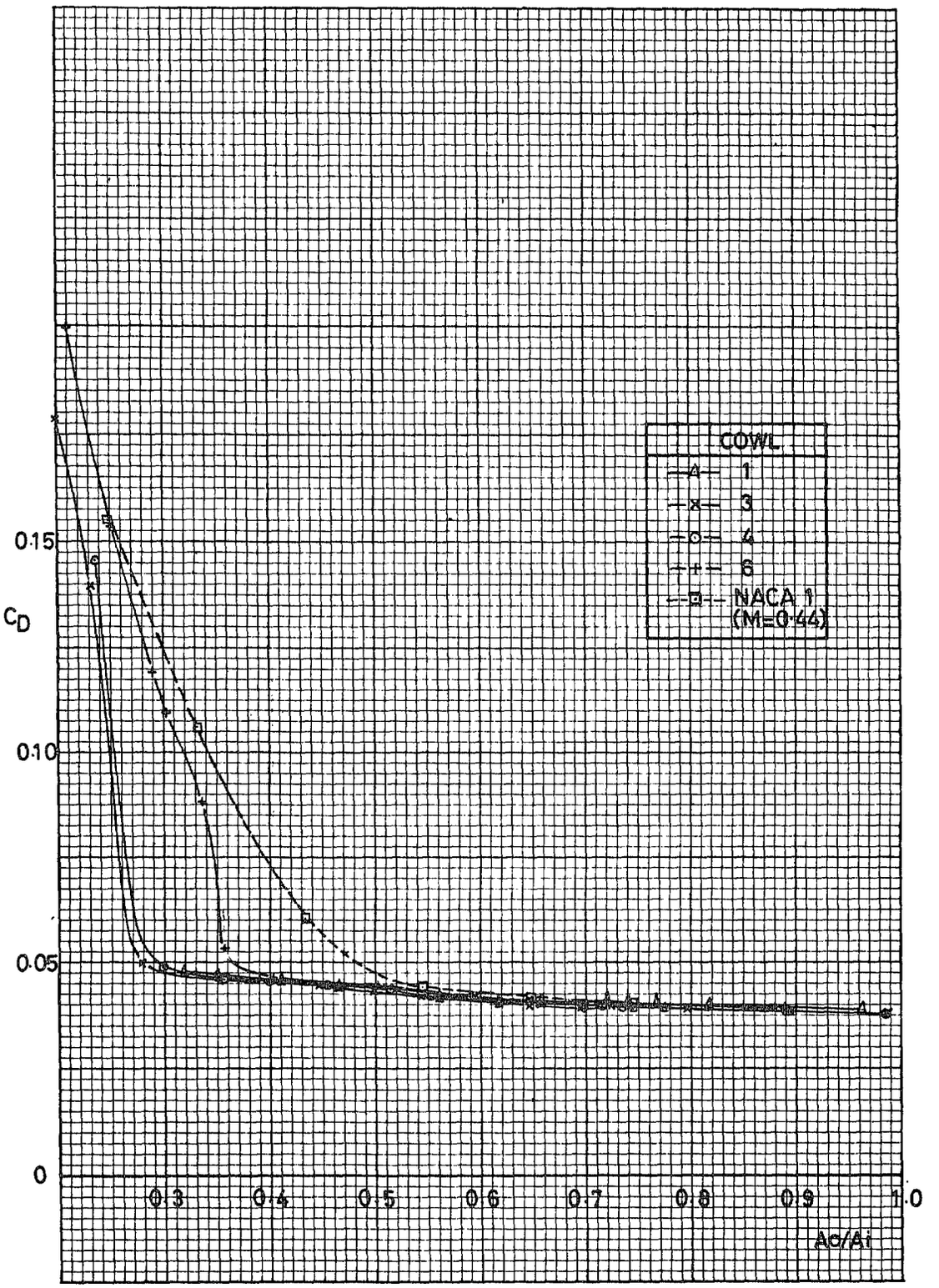

Fig 12a $C_D \sim A_o/A_i$ M = 0.40
85/45 cowls $\alpha = 0°$

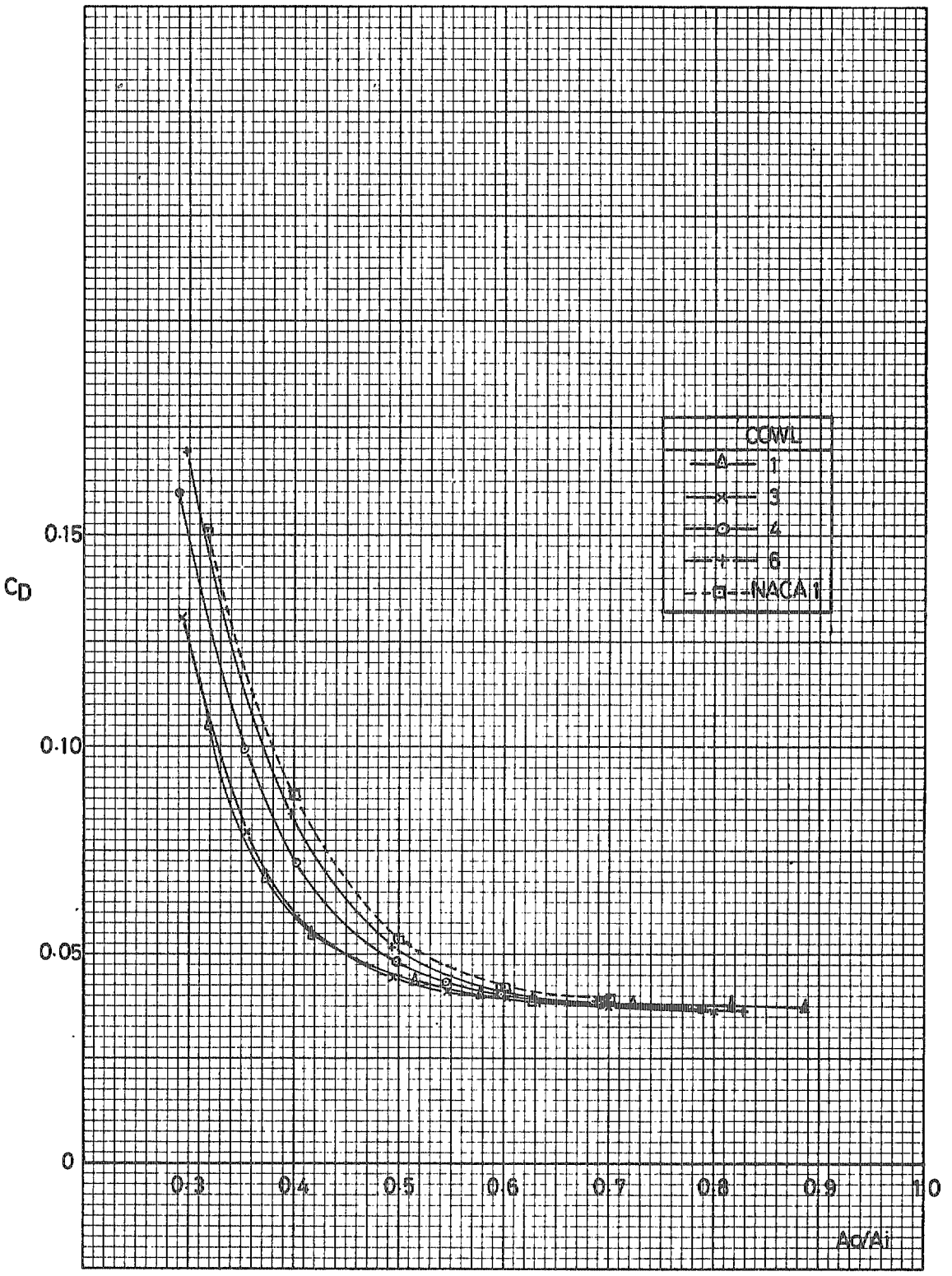

Fig 12b $C_D \sim A_o/A_i$ M = 0.65
85/45 cowls $\alpha = 0°$

Fig 12c

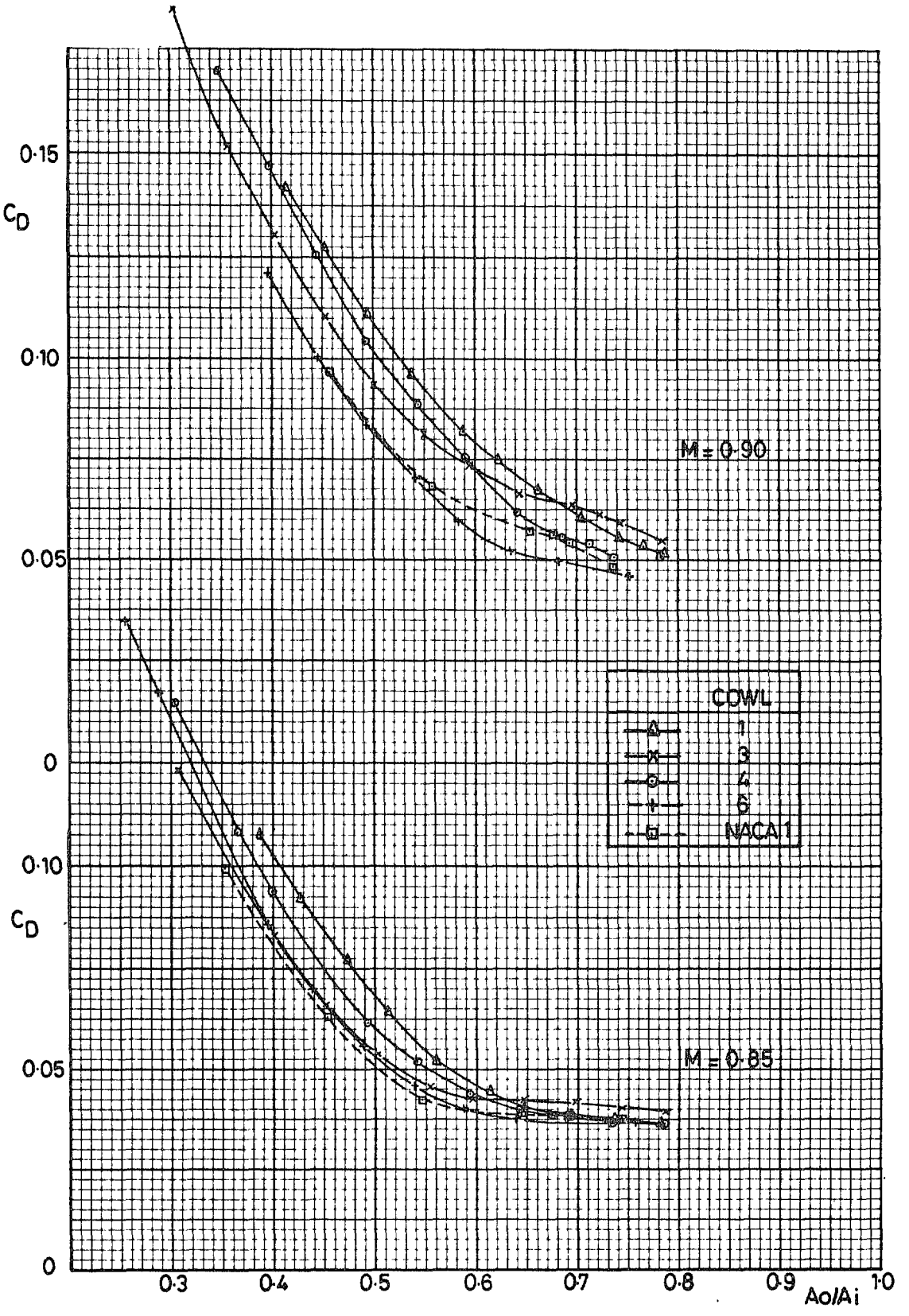

Fig 12c $C_D \sim A_o/A_i$ 85/45 cowls

M = 0.85, 0.90
$\alpha = 0°$

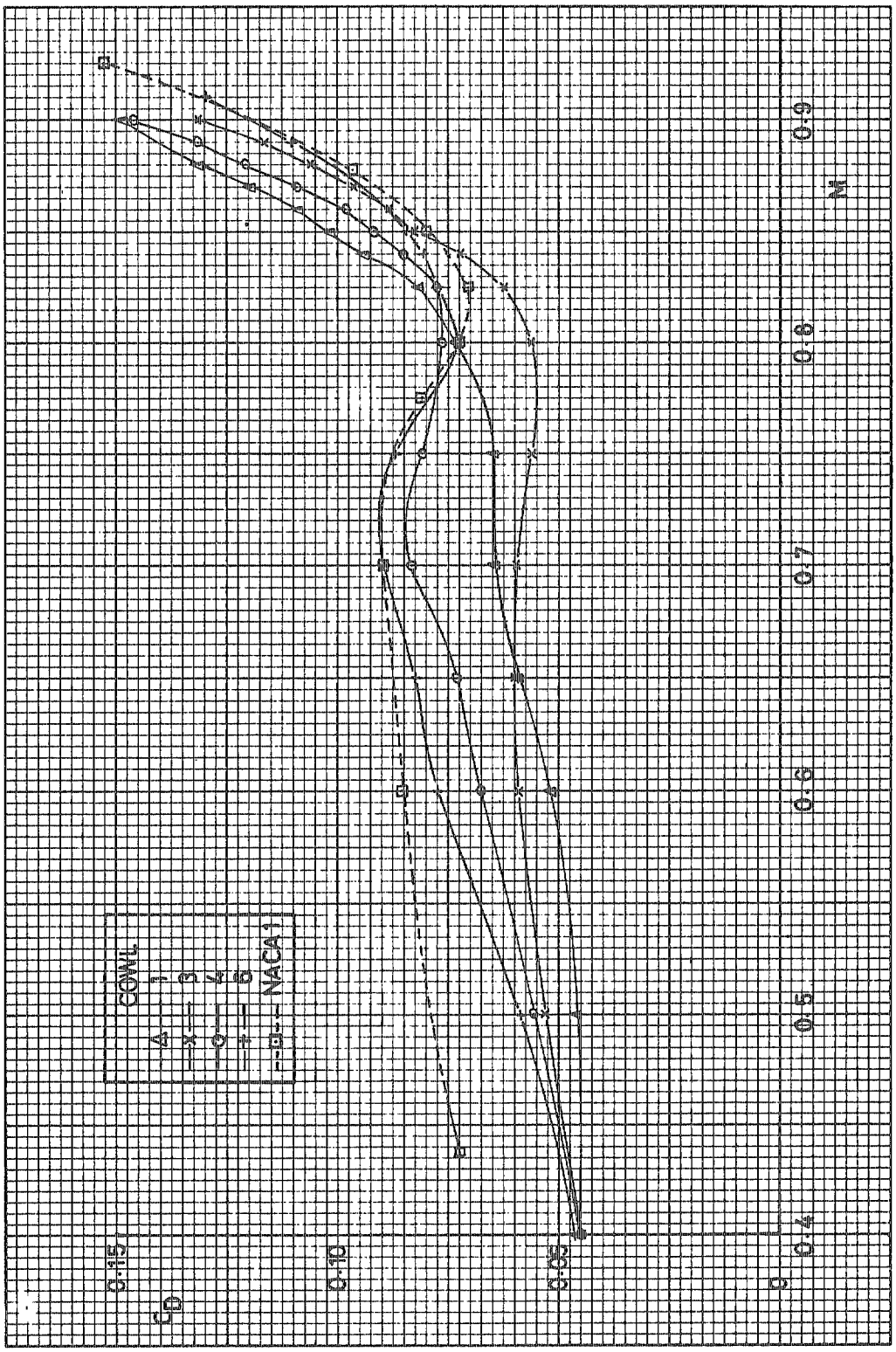

Fig 13a $C_D \sim M$ $A_o/A_i = 0.40$
85/45 cowls $\alpha = 0°$

Fig 13b

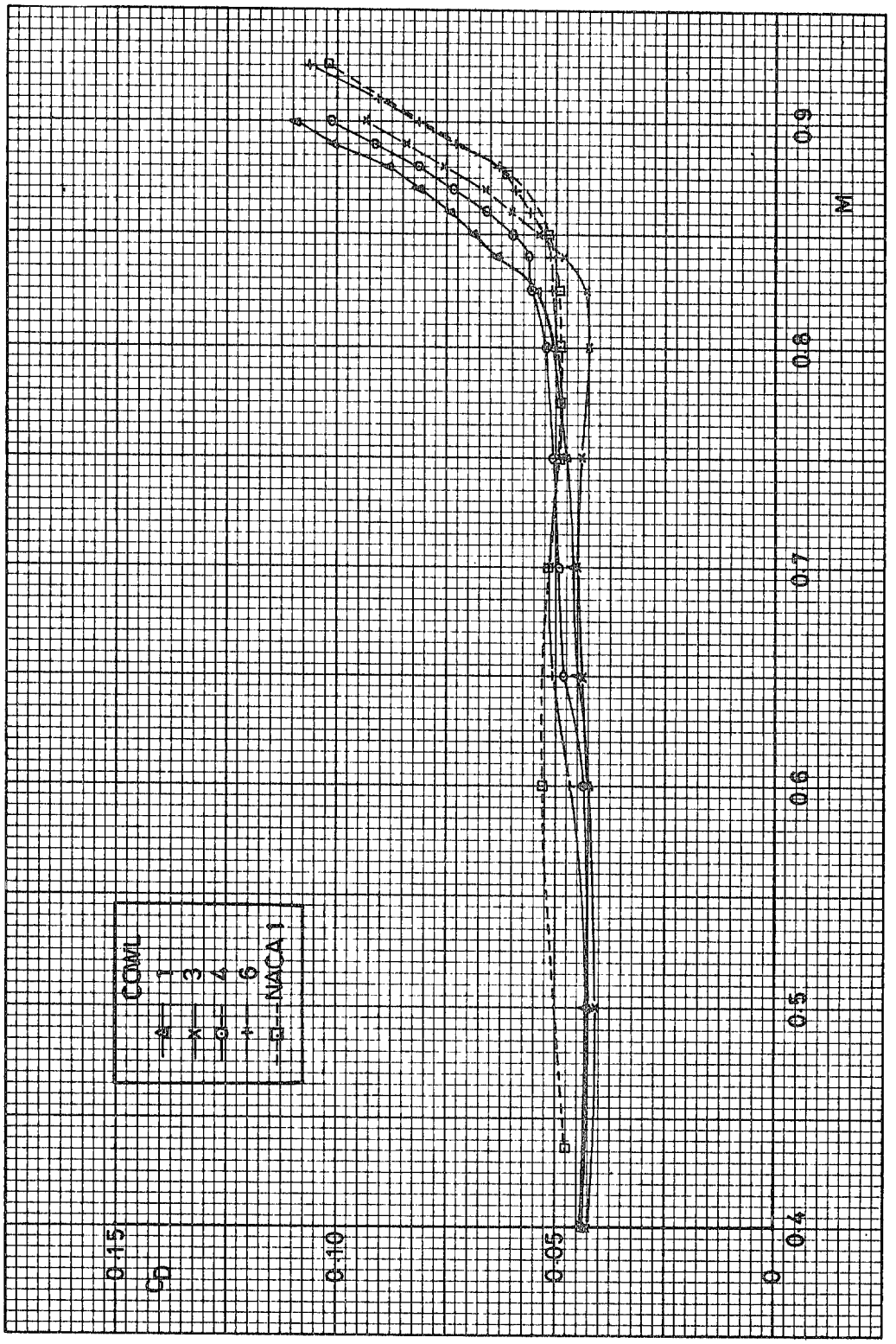

Fig 13b $C_D \sim M$ $A_o/A_i = 0.50$
85/45 cowls $\alpha = 0°$

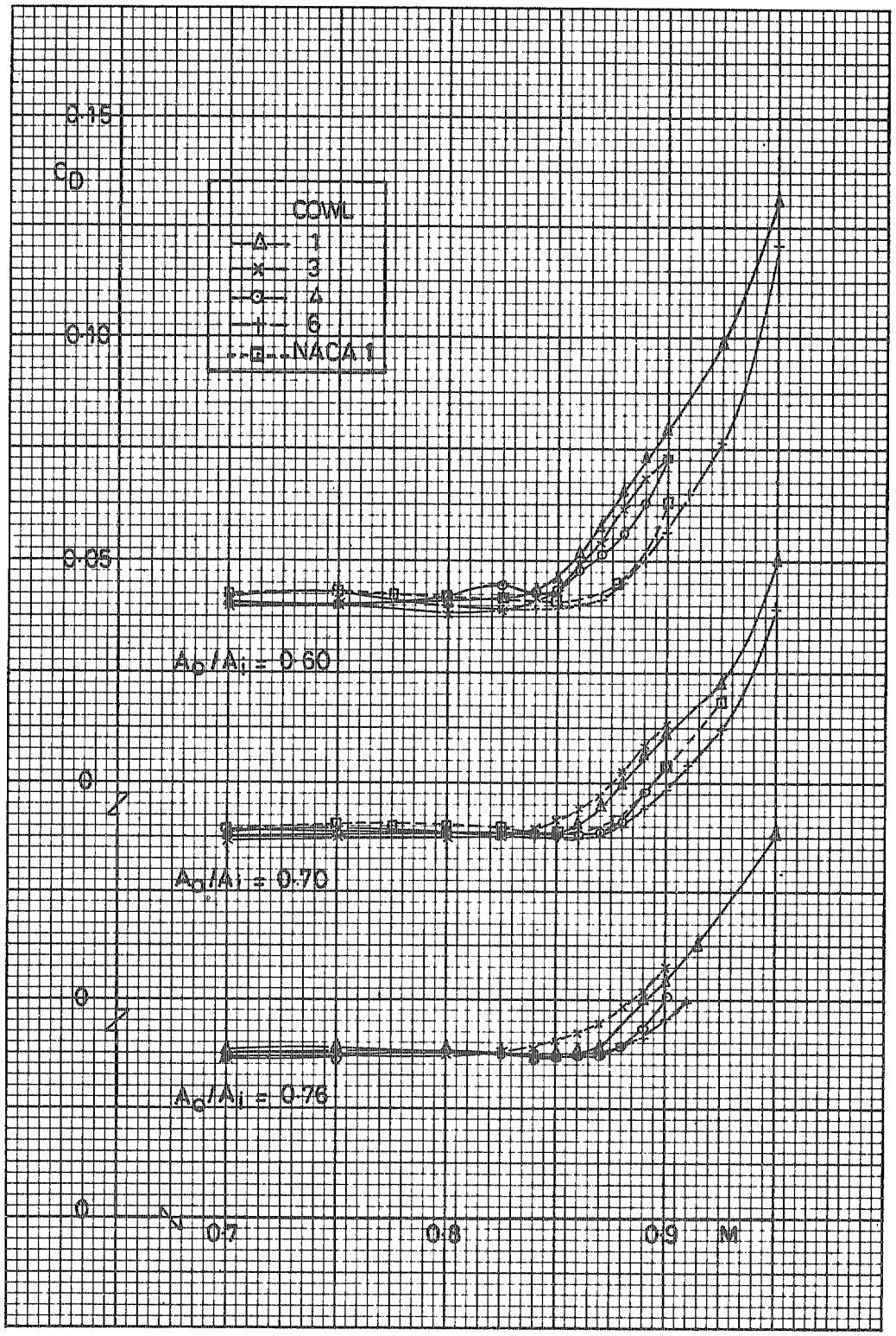

Fig 13c $C_D \sim M$ $A_o/A_i = 0.60, 0.70, 0.76$
85/45 cowls $\alpha = 0°$

Fig 14

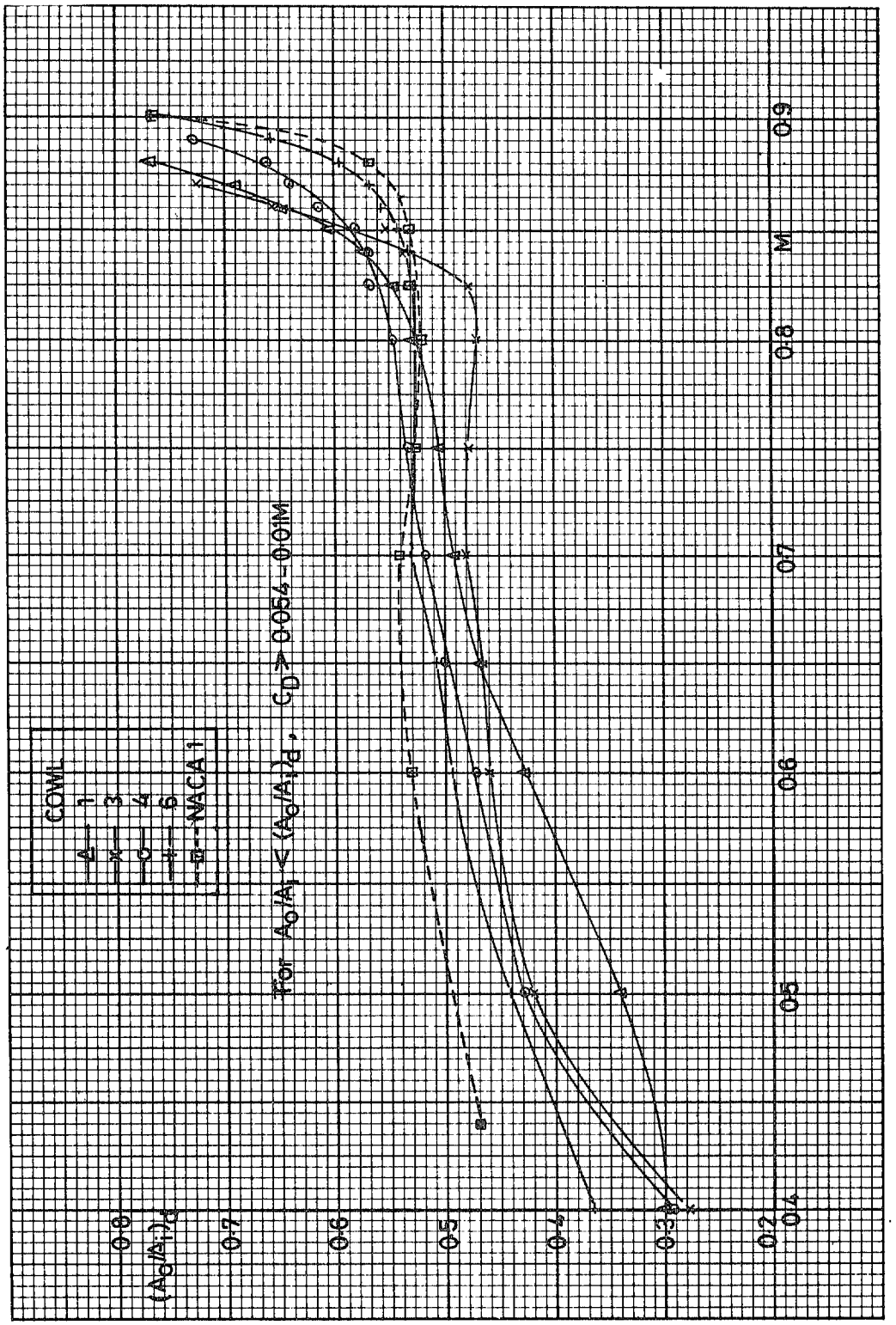

Fig 14 Spillage drag divergence boundary
85/45 cowls

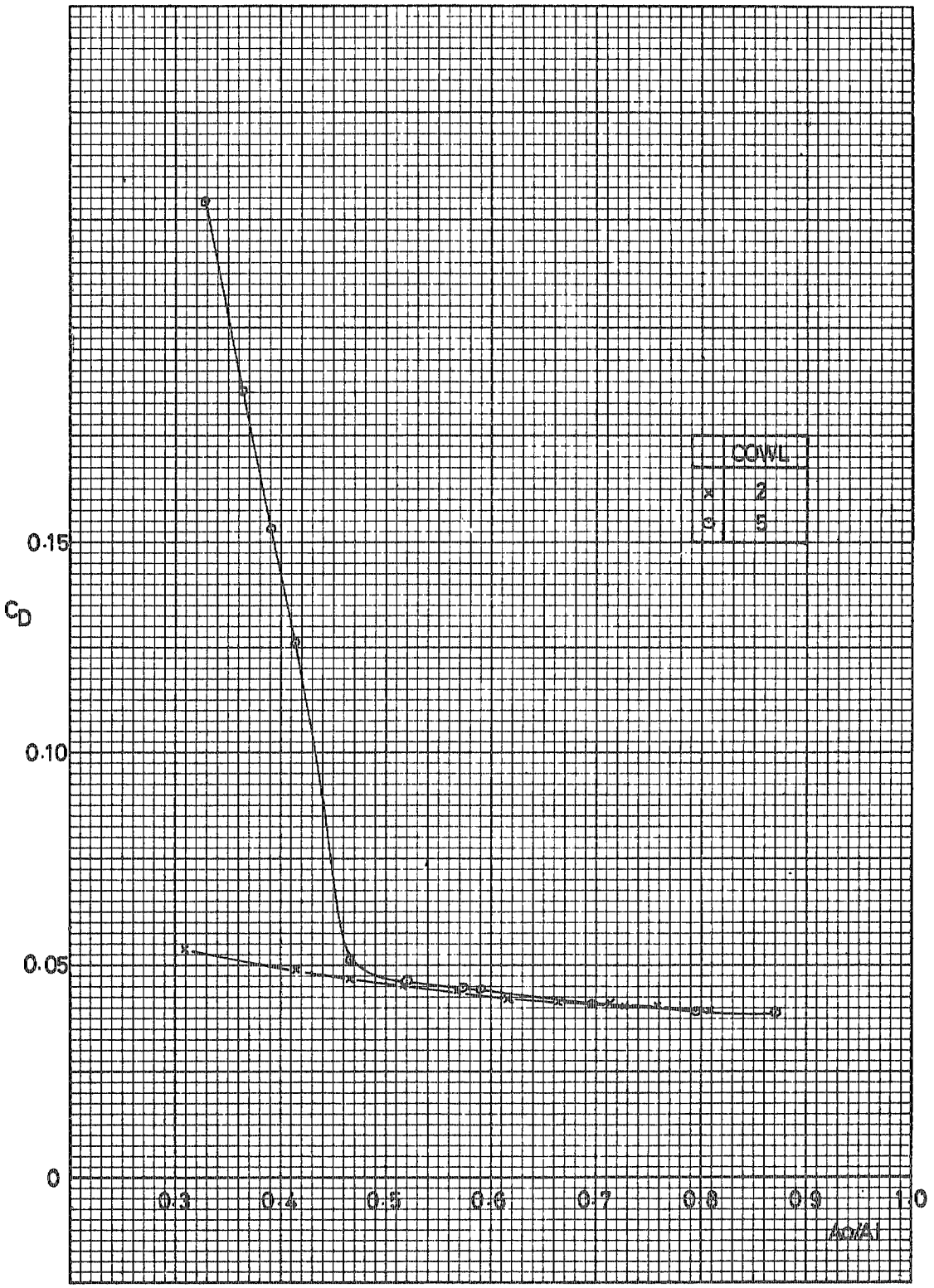

Fig 15a $C_D \sim A_o/A_i$ M = 0.40
90/35 cowls $\alpha = 0°$

Fig 15b

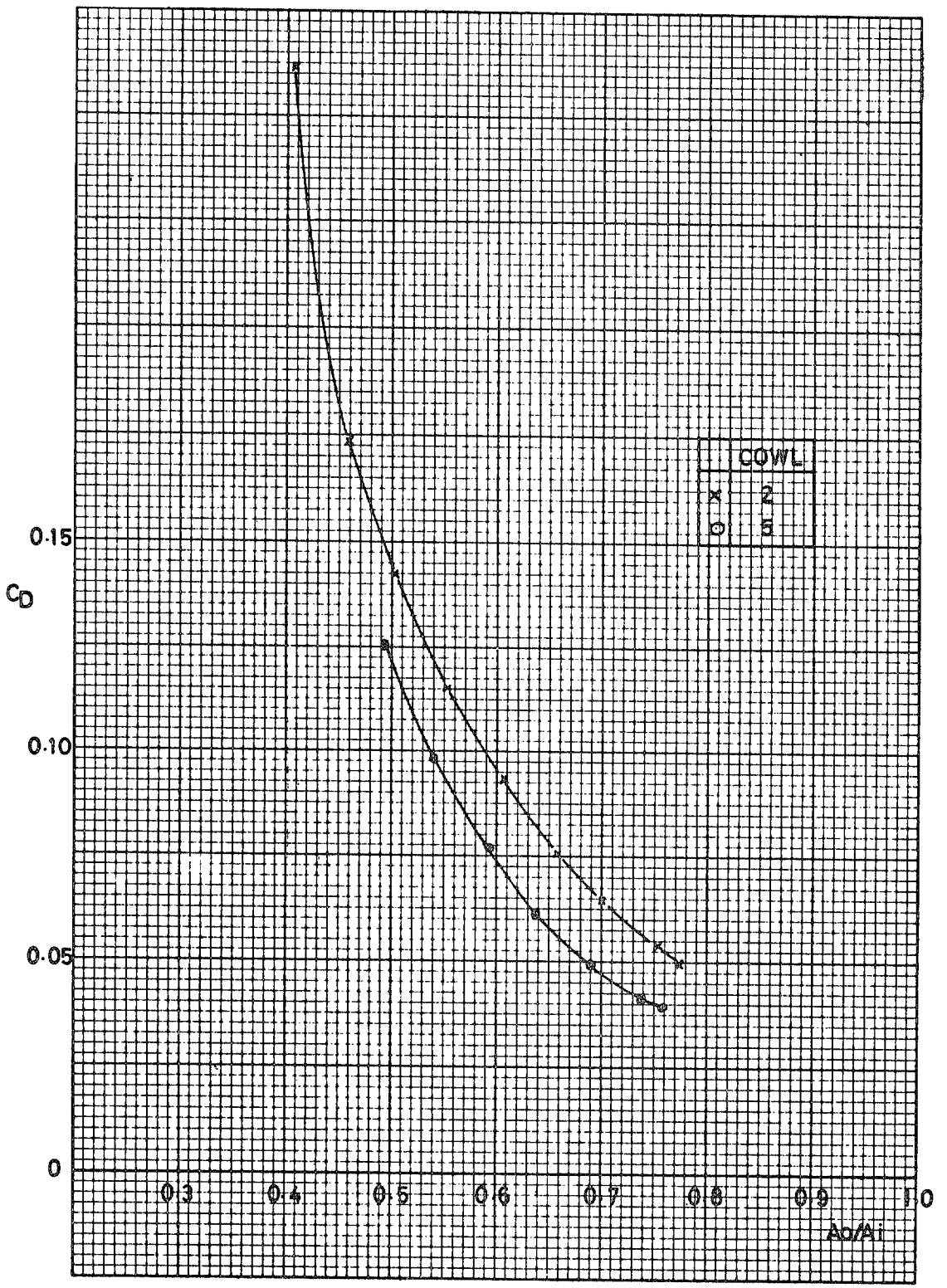

Fig 15b $C_D \sim A_o/A_i$ M = 0.85
90/35 cowls $\alpha = 0^\circ$

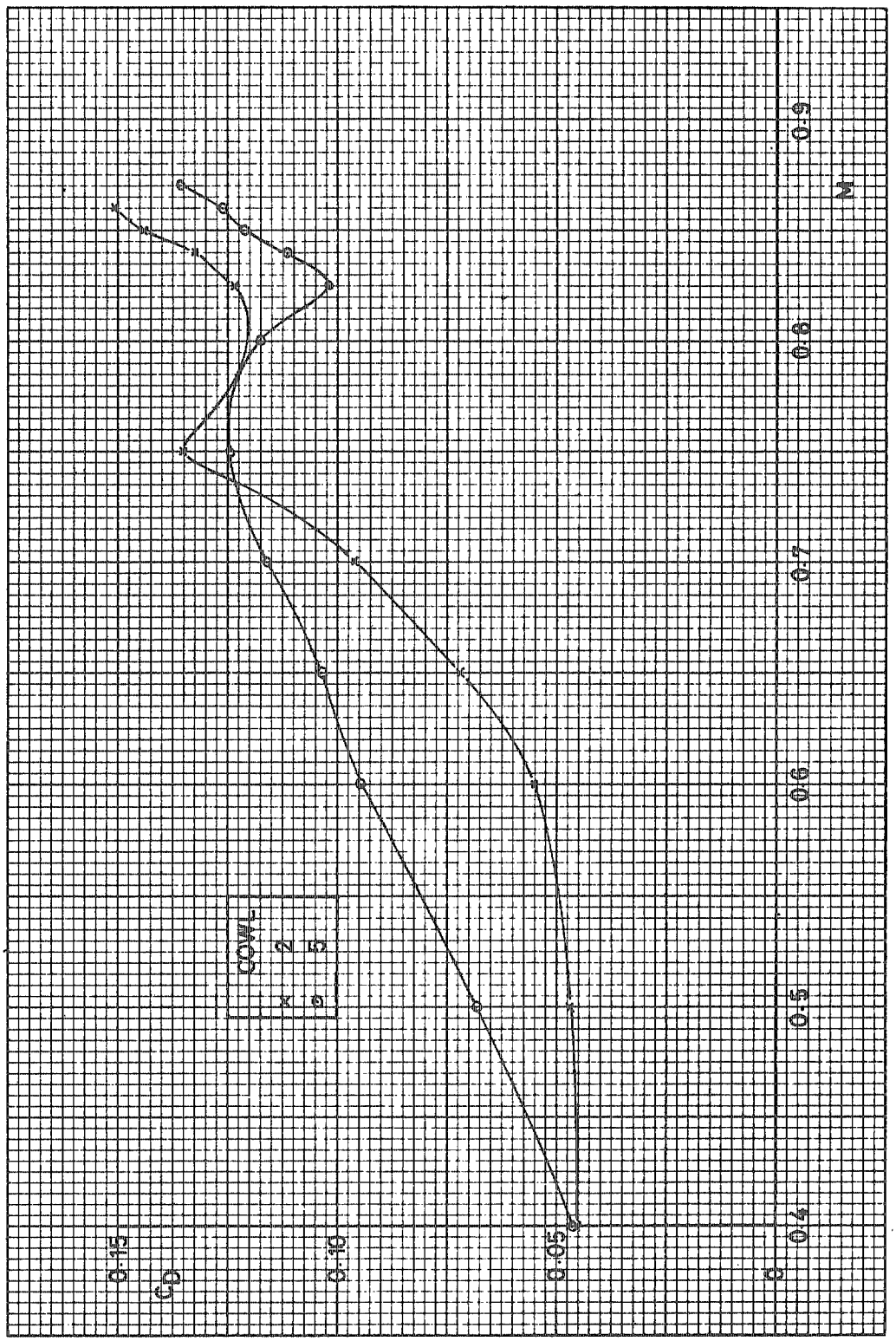

Fig 16a $C_D \sim M$ $A_o/A_i = 0.50$
90/35 cowls $\alpha = 0°$

Fig 16b

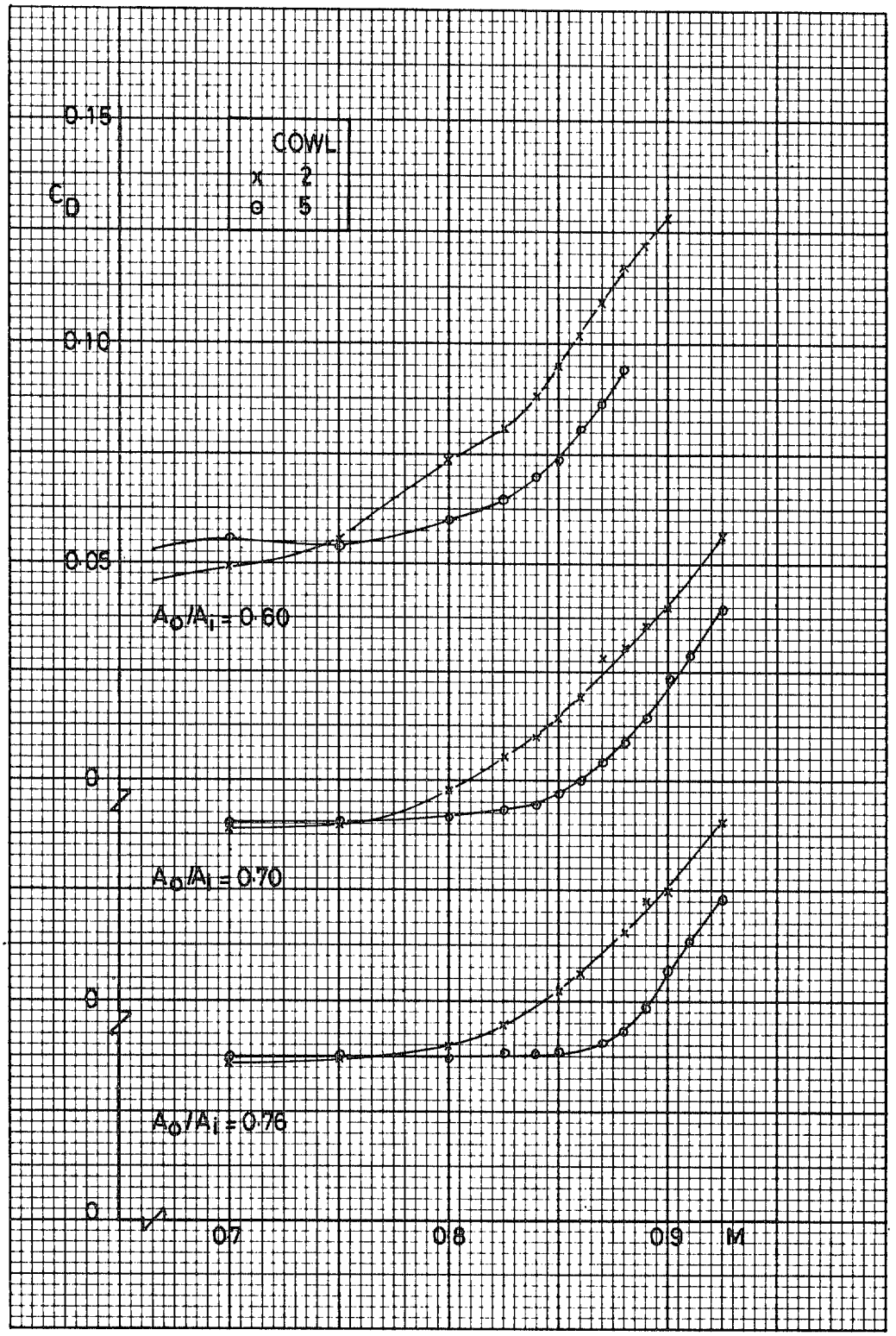

Fig 16b $C_D - M$ $A_o/A_i = 0.6, 0.7, 0.76$
90/35 cowls $\alpha = 0°$

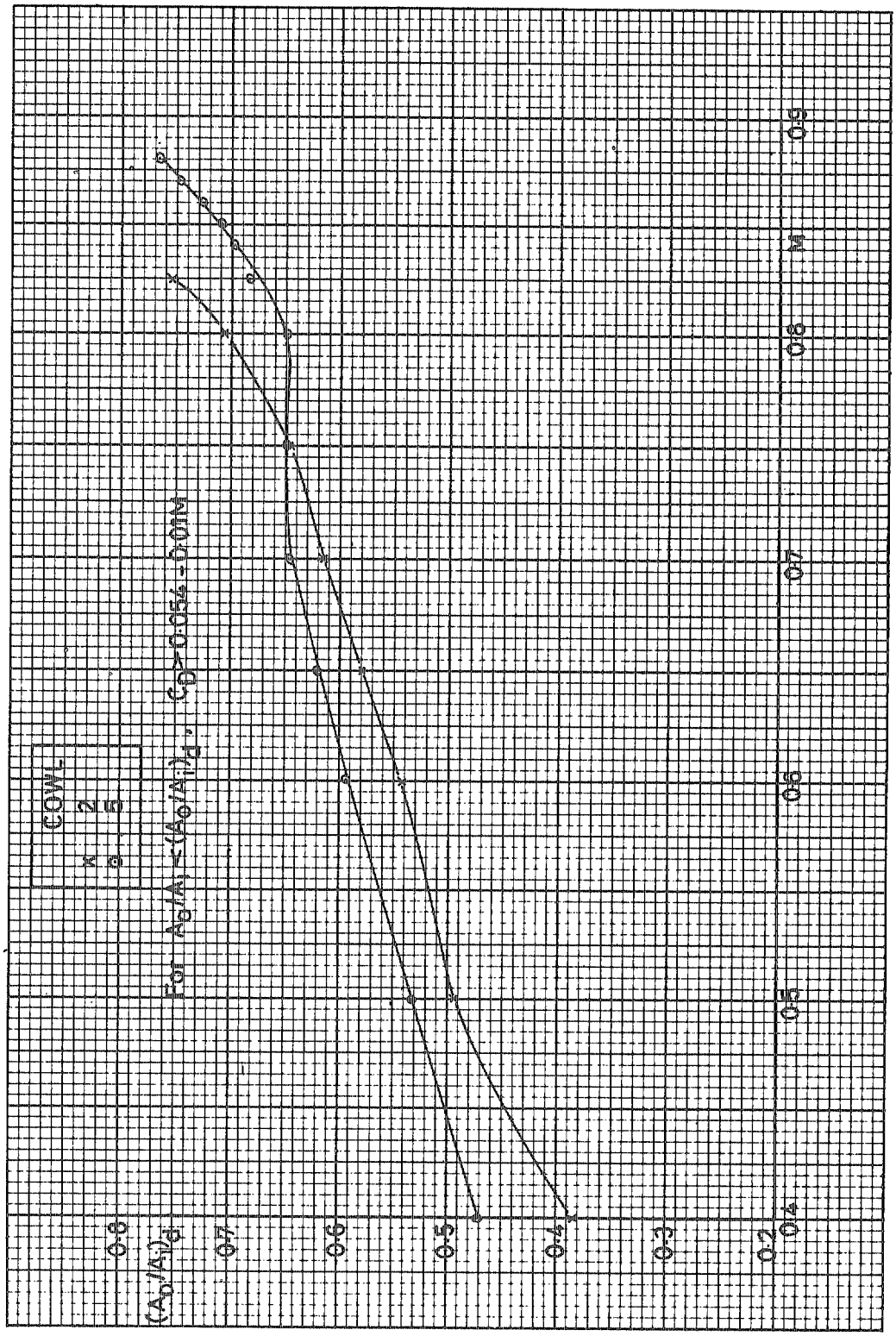

Fig 17 Spillage drag divergence boundary
90/35 cowls

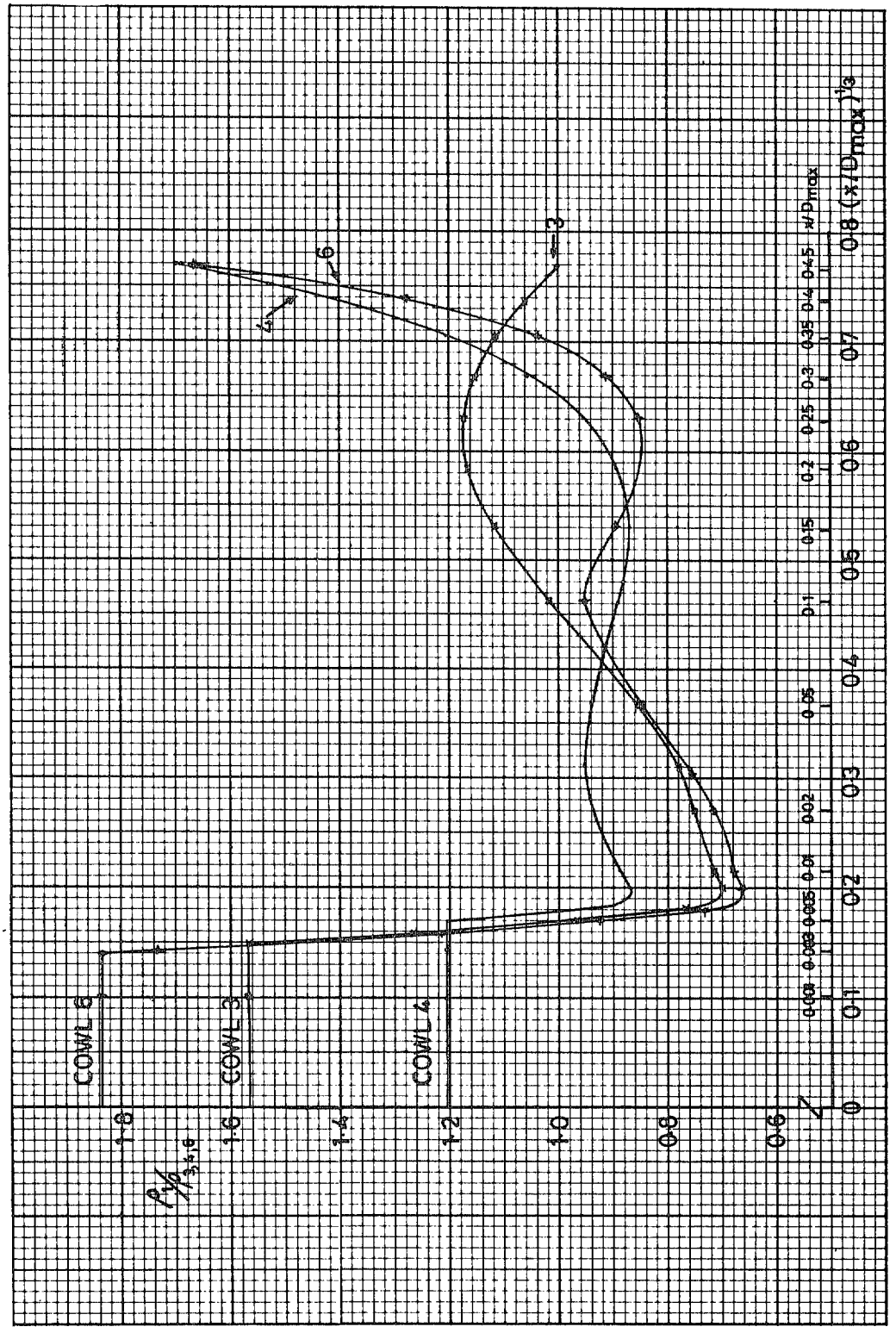

Fig 18 Distribution of curvature for cowls 3, 4, 6
(Cowl 1 geometry used as a basis: 85/45 cowls)

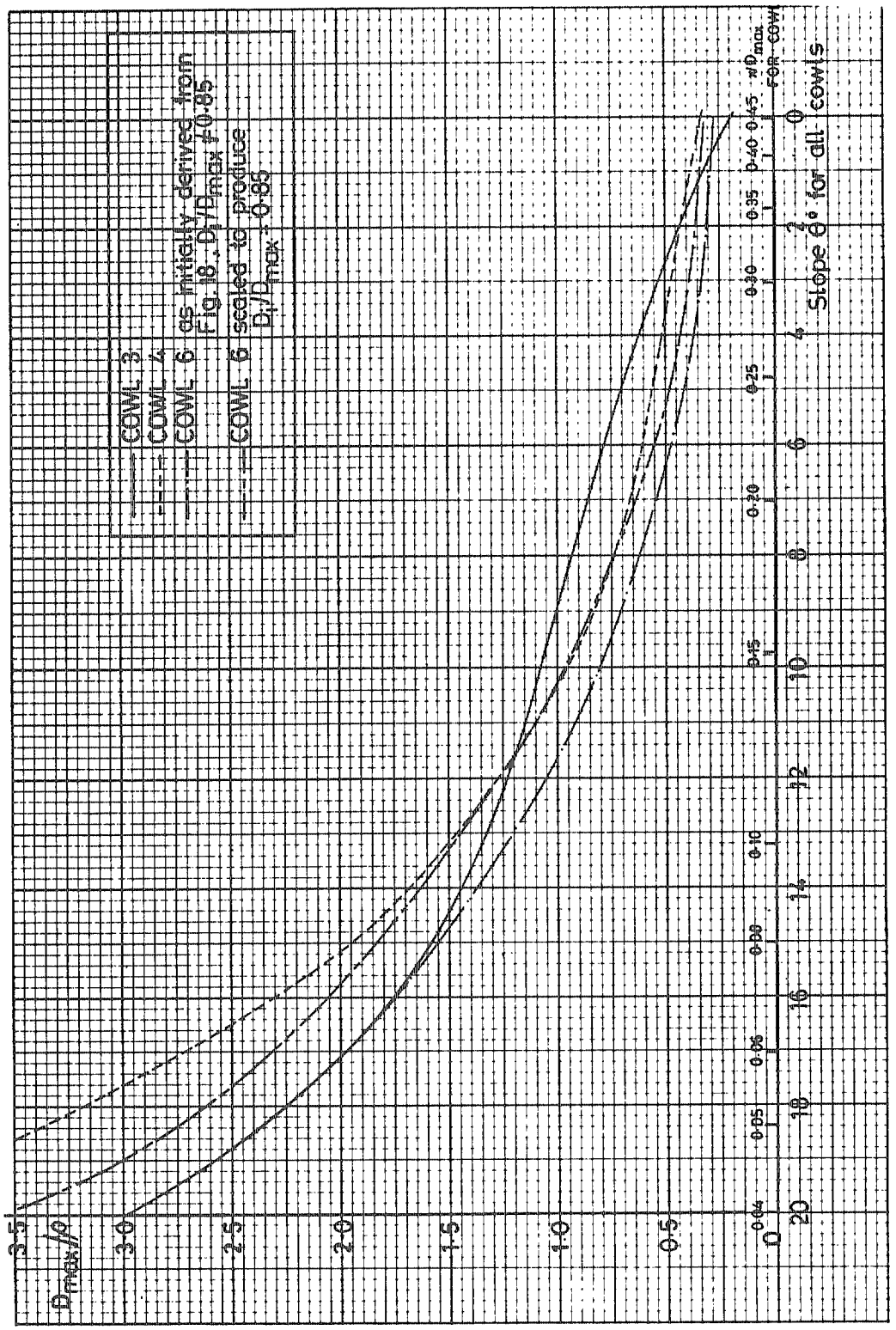

Fig 19 Curvature vs slope for cowls 3, 4, 6 85/45 cowls

Fig 20

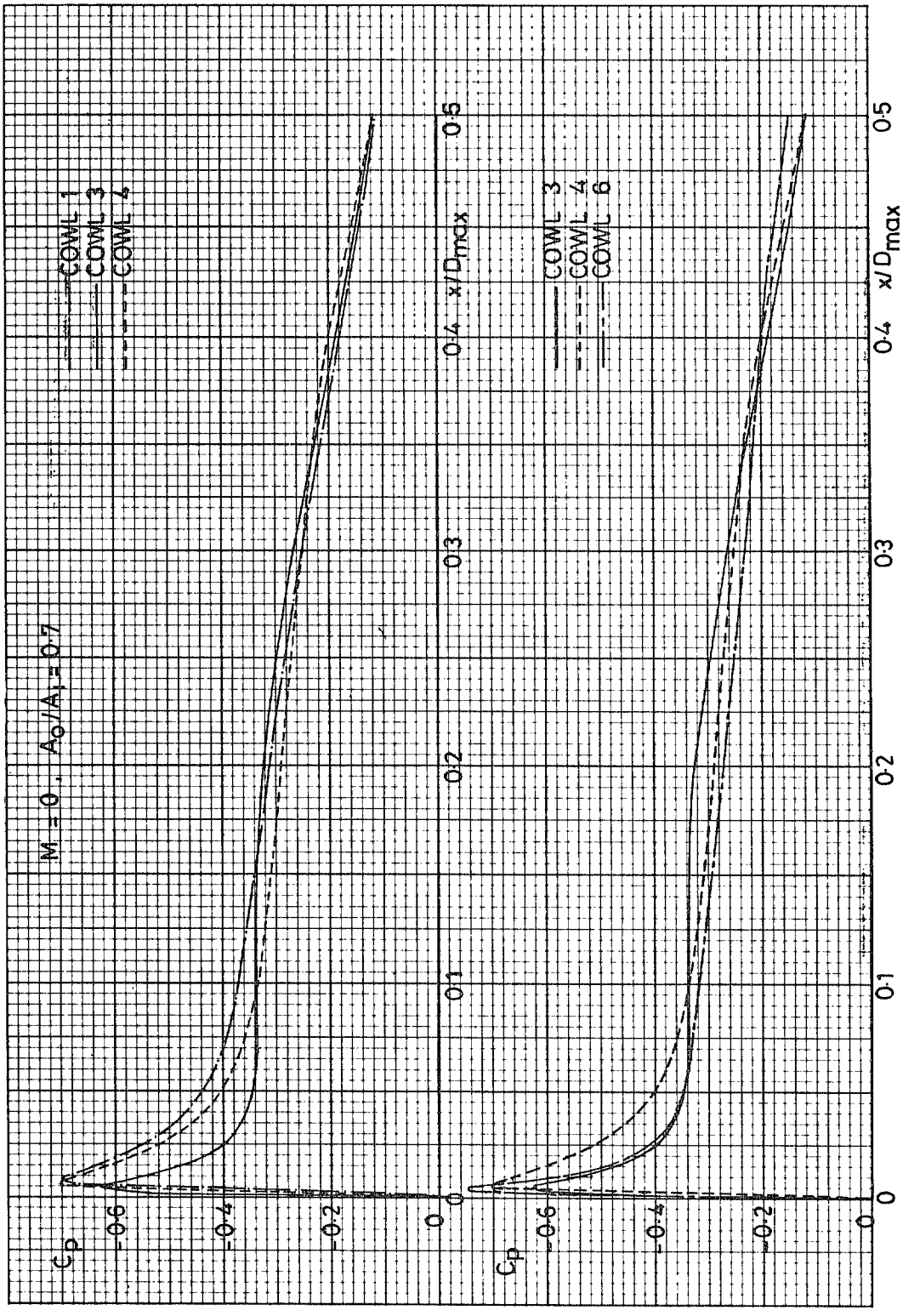

Fig 20 Theoretical incompressible pressure distributions 85/45 cowls

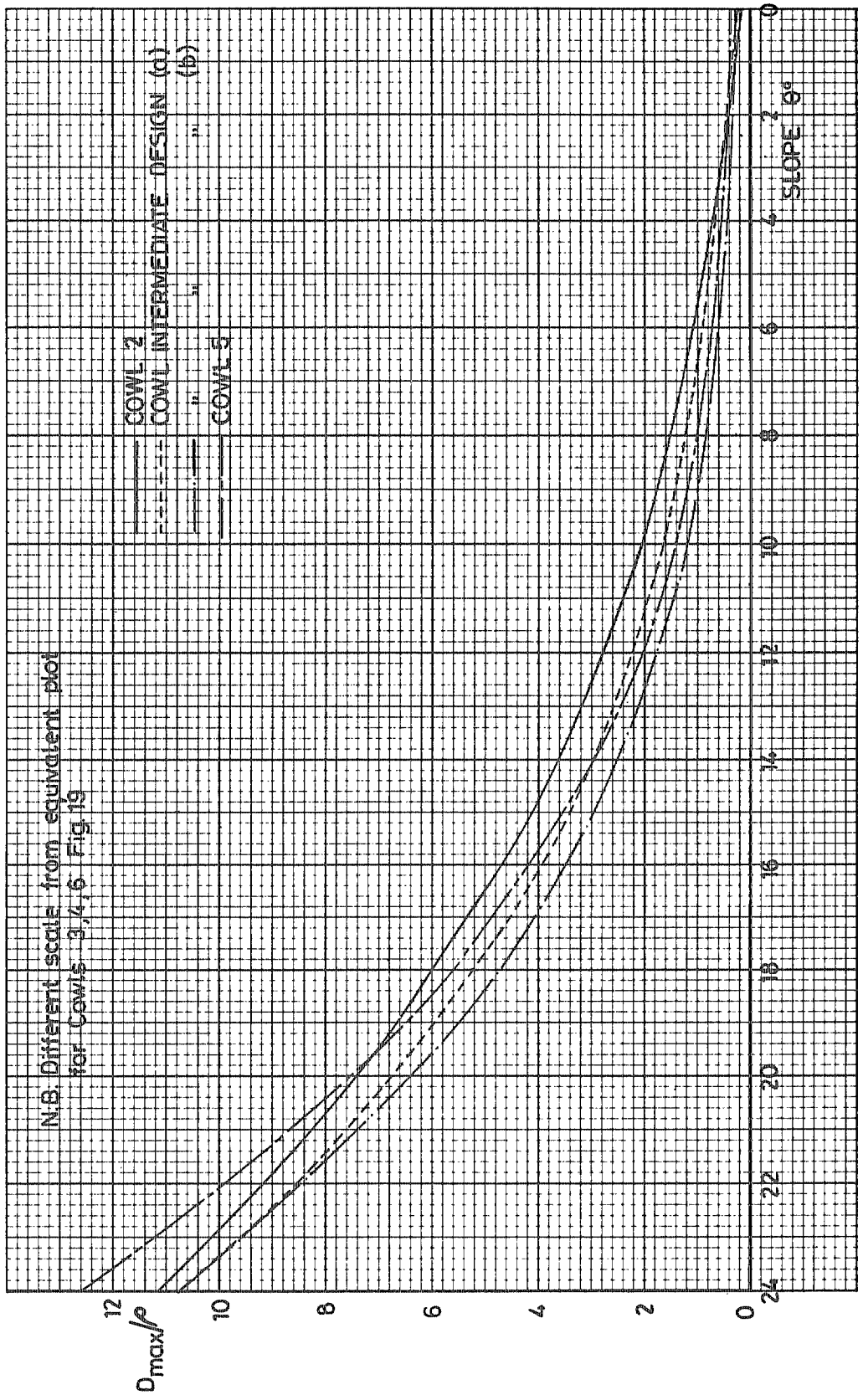

Fig 21 Curvature vs slope for cowls 2, 5 90/35 cowls

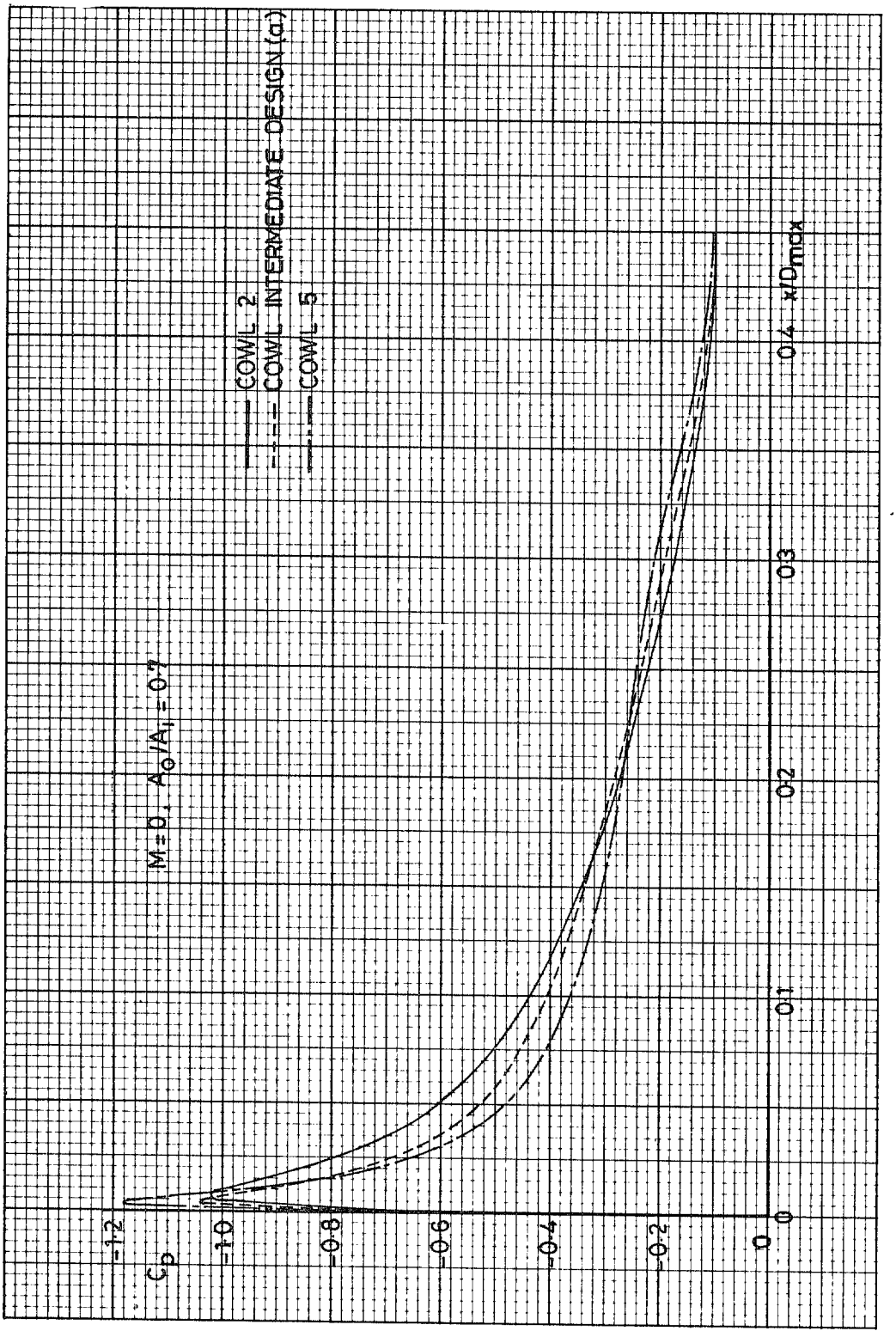

Fig 22 Theoretical incompressible pressure distributions 90/35 cowls

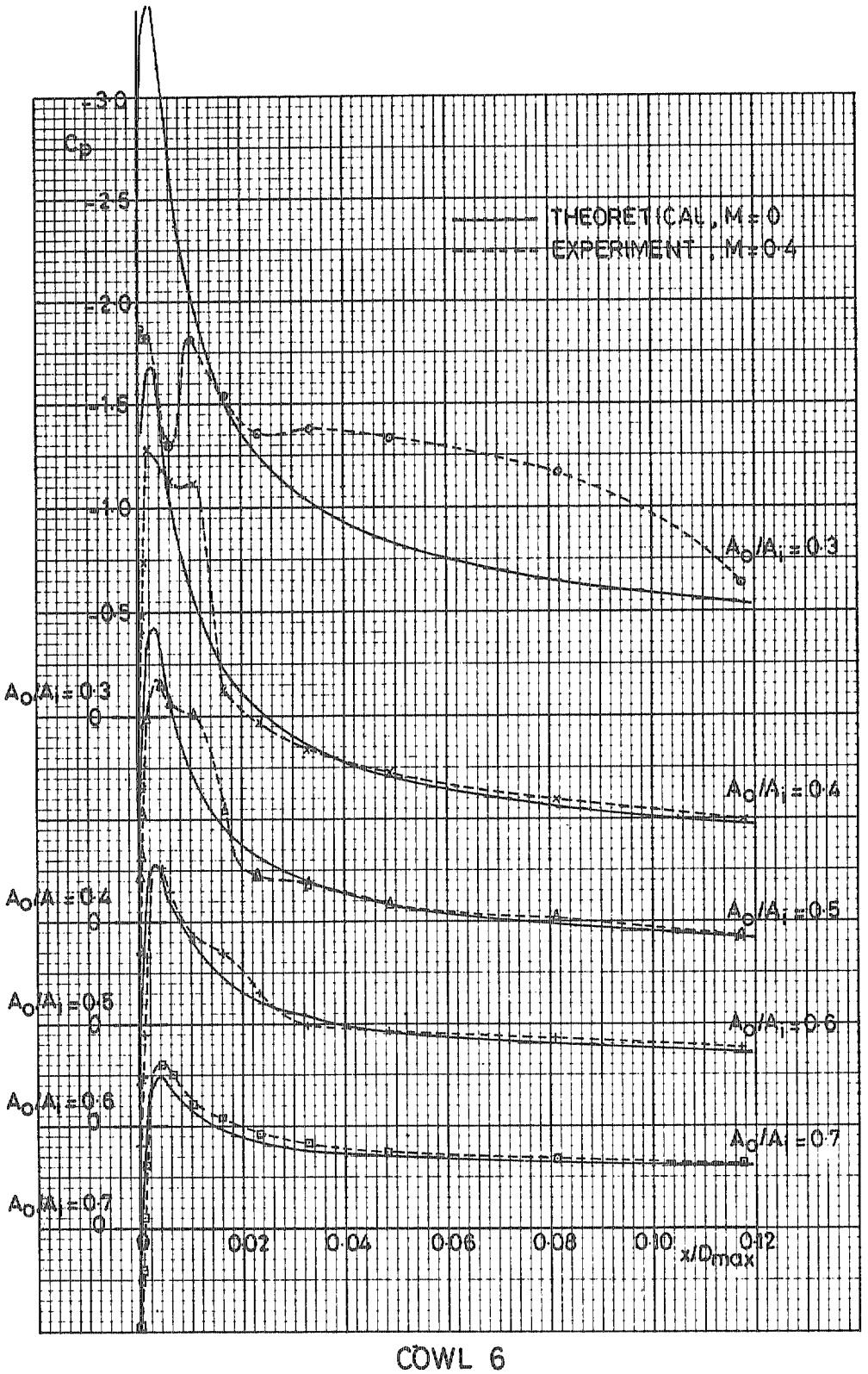

Fig 23 Comparison of theoretical and experimental pressures

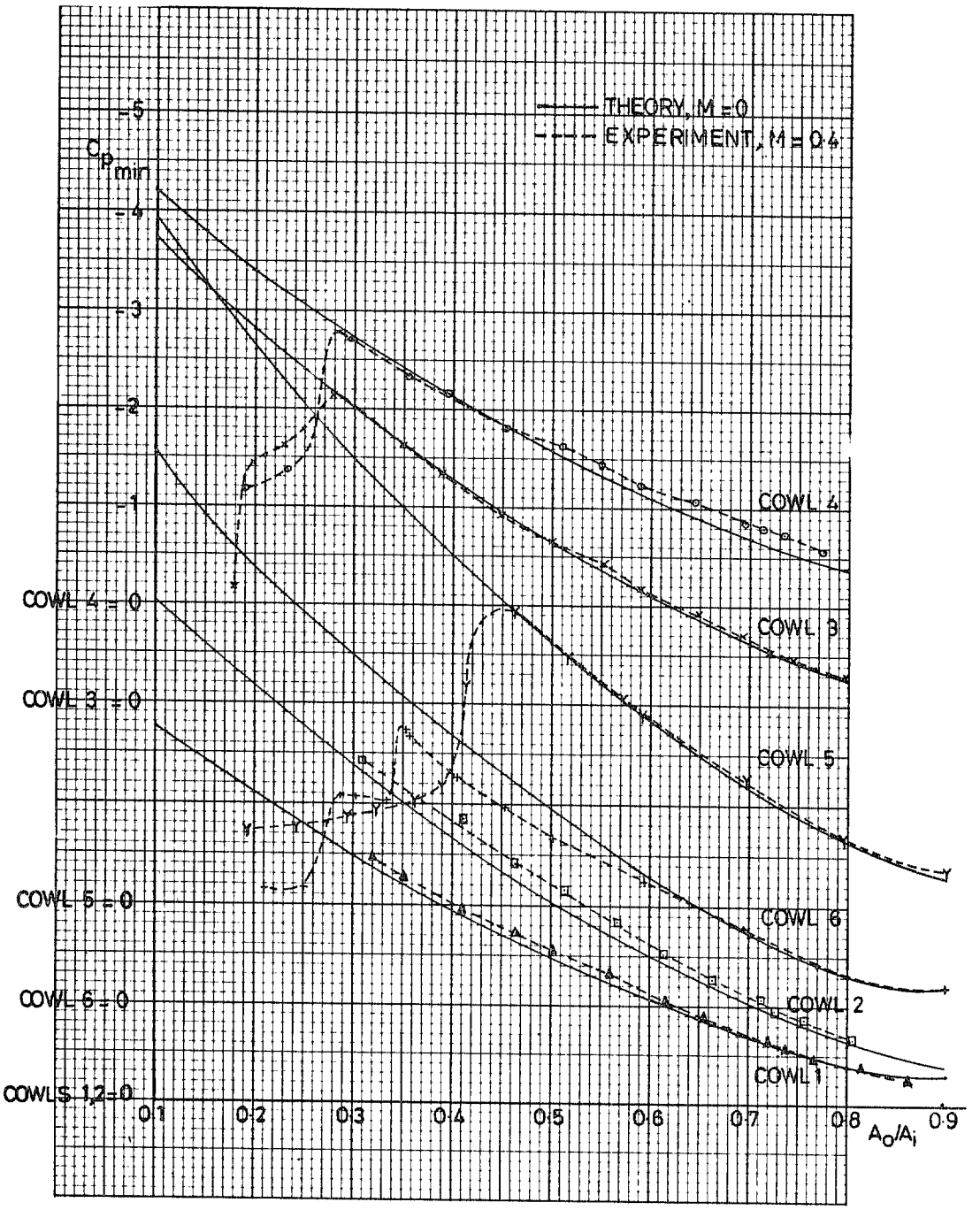

Fig 24 Minimum $C_p \sim A_o/A_i$ for all cowls at low speed

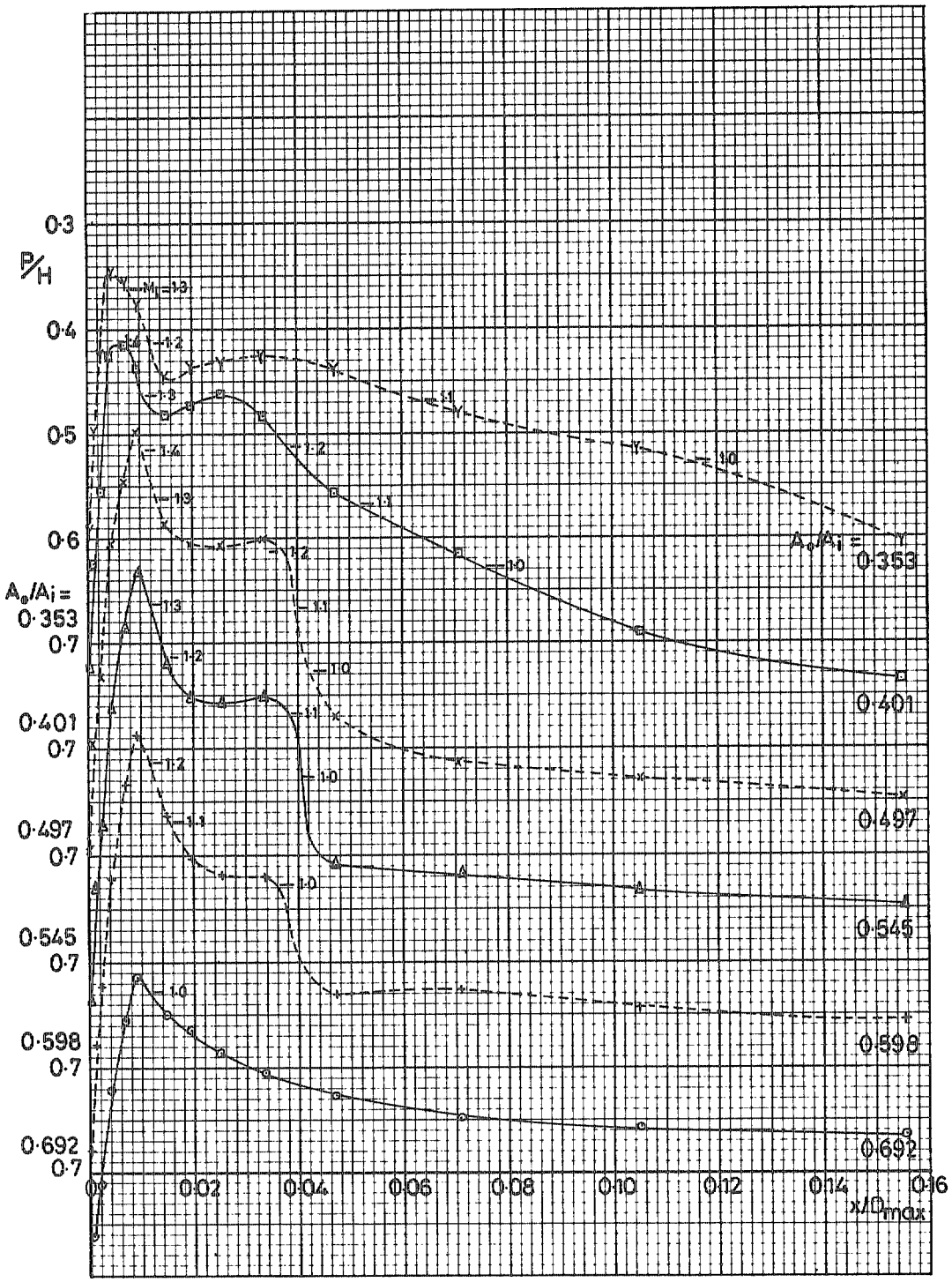

Fig 25 Pressure distributions for cowl 4 at M_o = 0.65

Fig 26

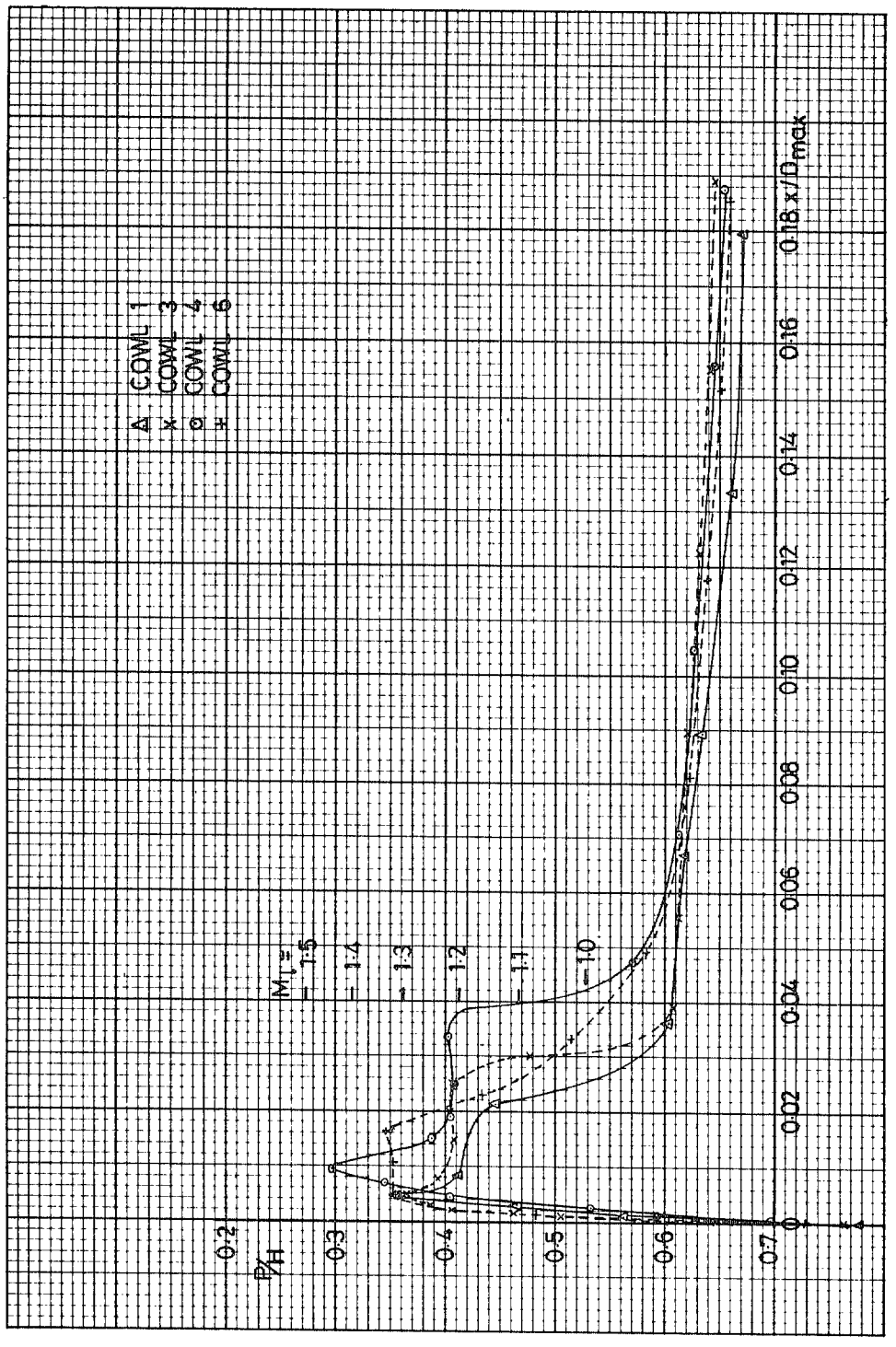

Fig 26 Pressure distributions for A_o/A_i = 0.5 (approx) with M_o = 0.65

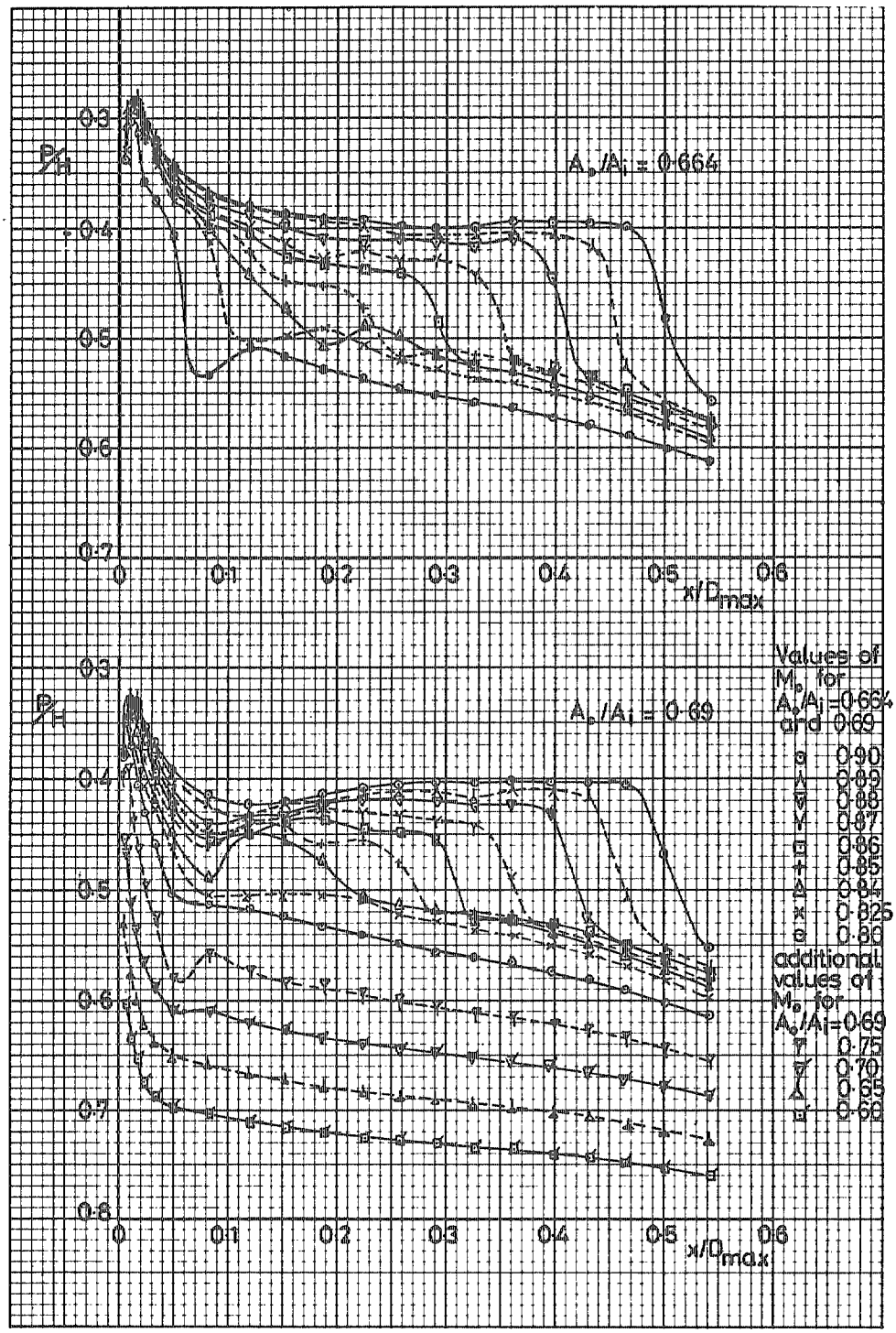

Fig 27 Pressure distributions for cowl 6 at two values of A_o/A_i

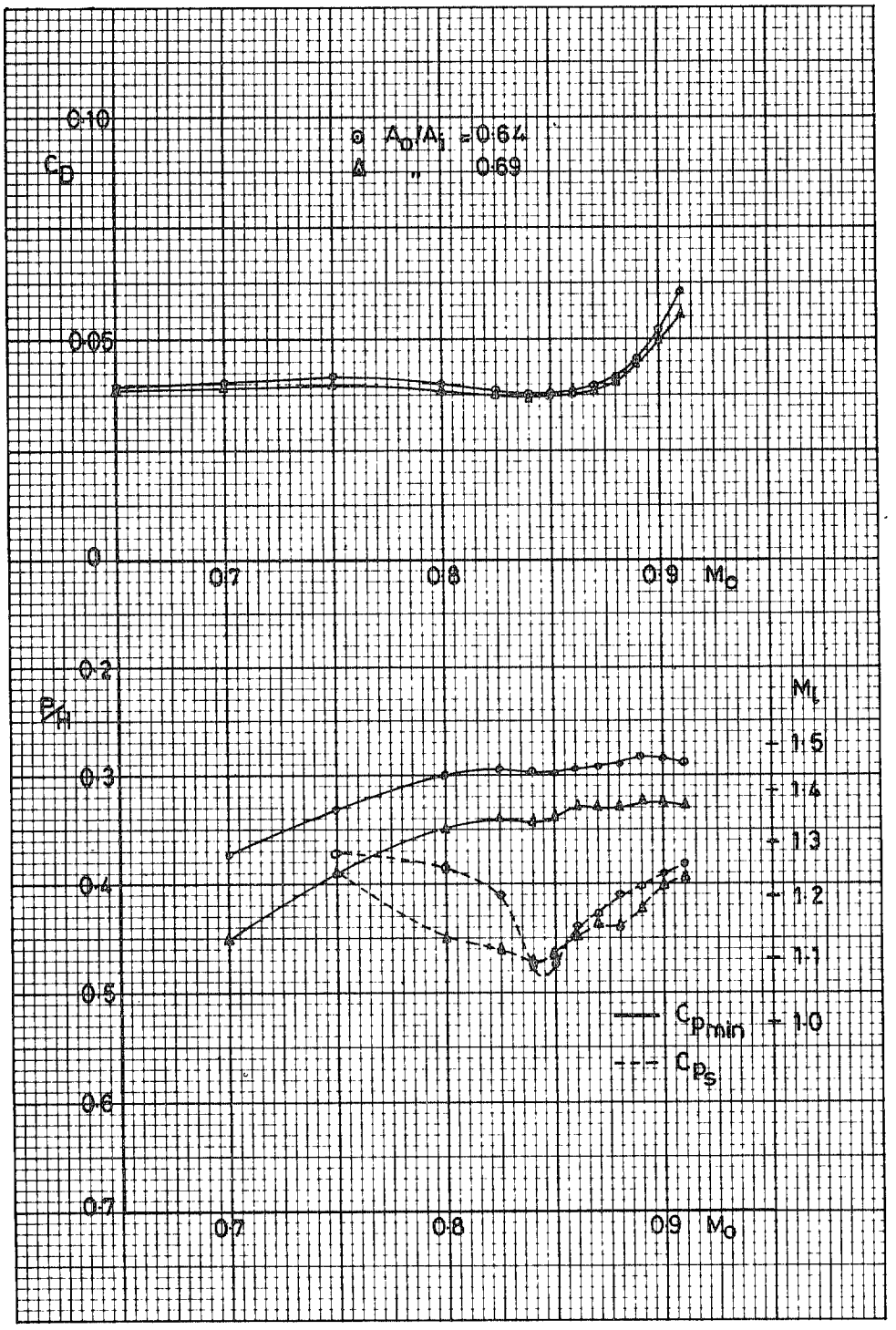

Fig 28 Peak suction, shock strength and drag. Cowl 6

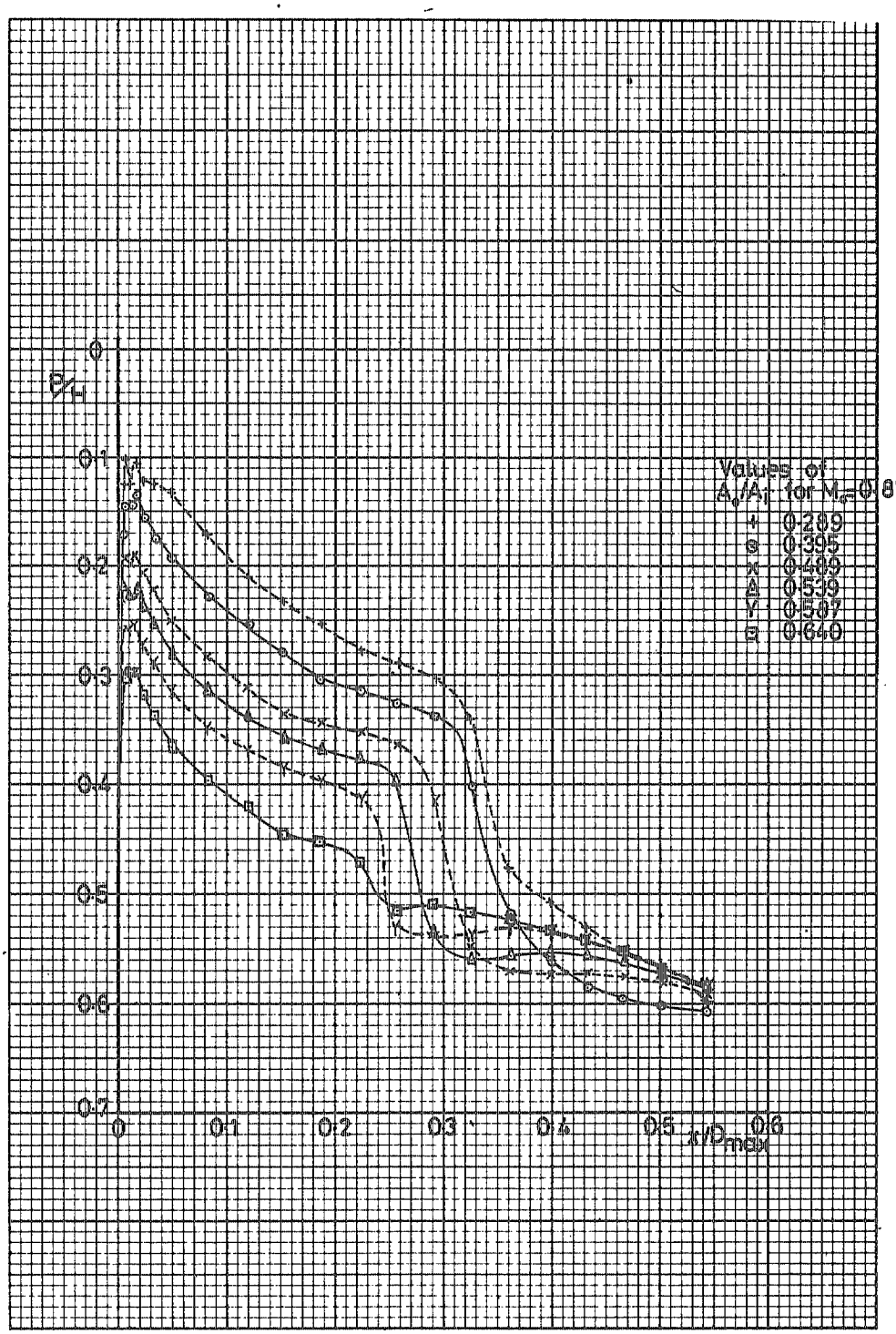

Fig 29 Pressure distributions for cowl 6 at $M_0 = 0.85$

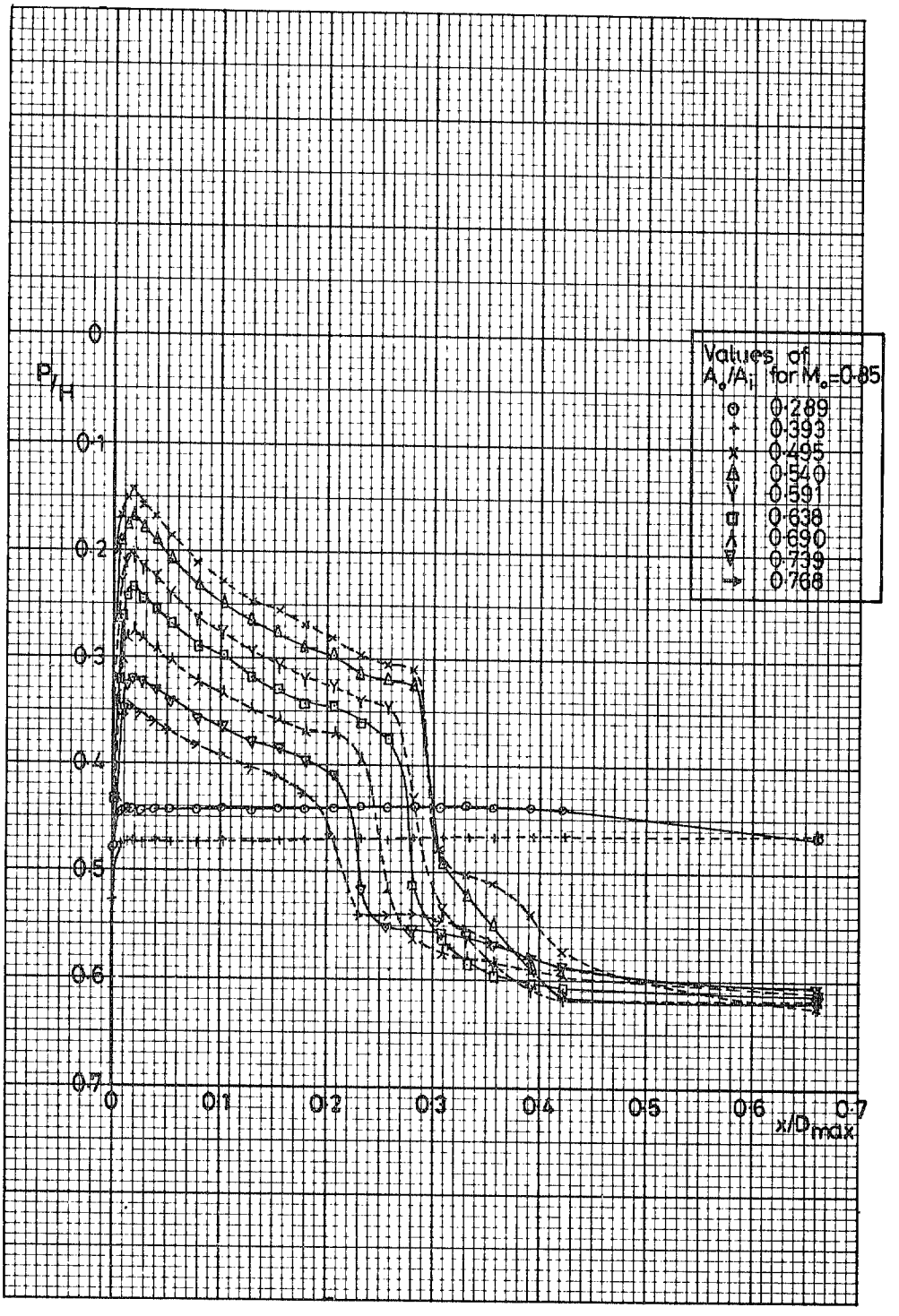

Fig 30 Pressure distributions for cowl 5 at M_o = 0.85

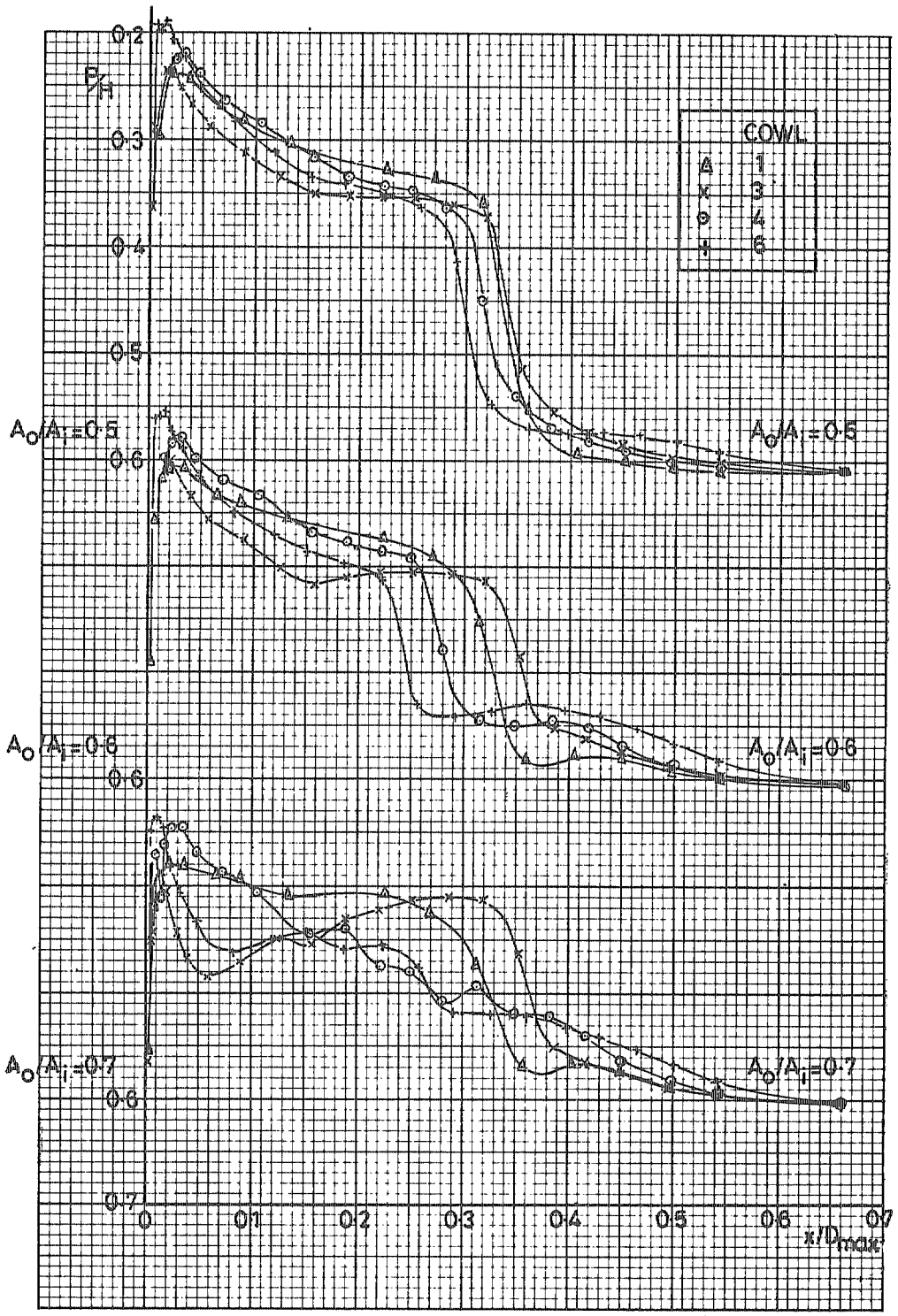

Fig 31 Pressure distributions for 85/45 cowls at $M_o = 0.85$

Fig 32

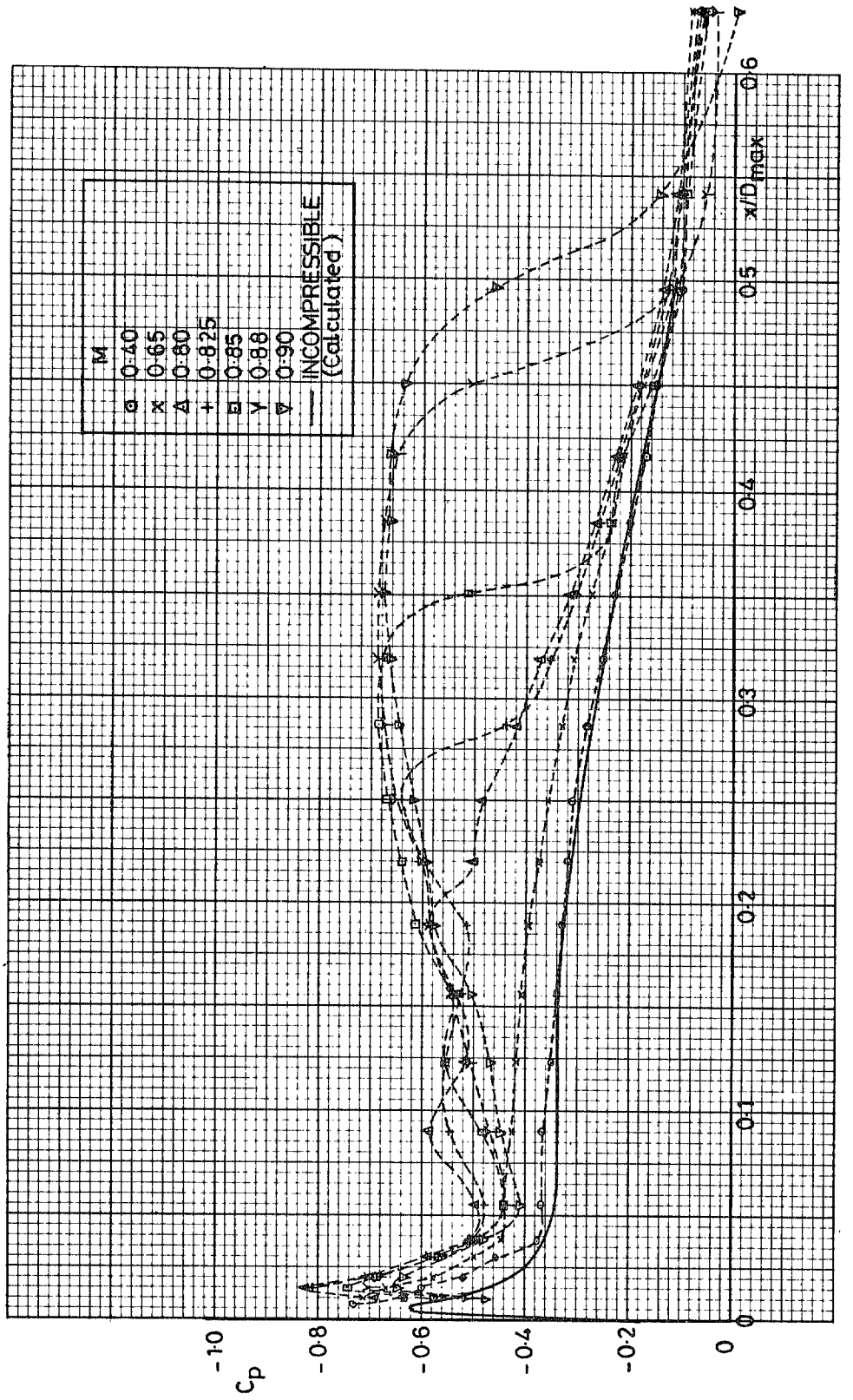

Fig 32 Variation of cowl 3 pressure distribution for Mach number for $A_o/A_i = 0.7$

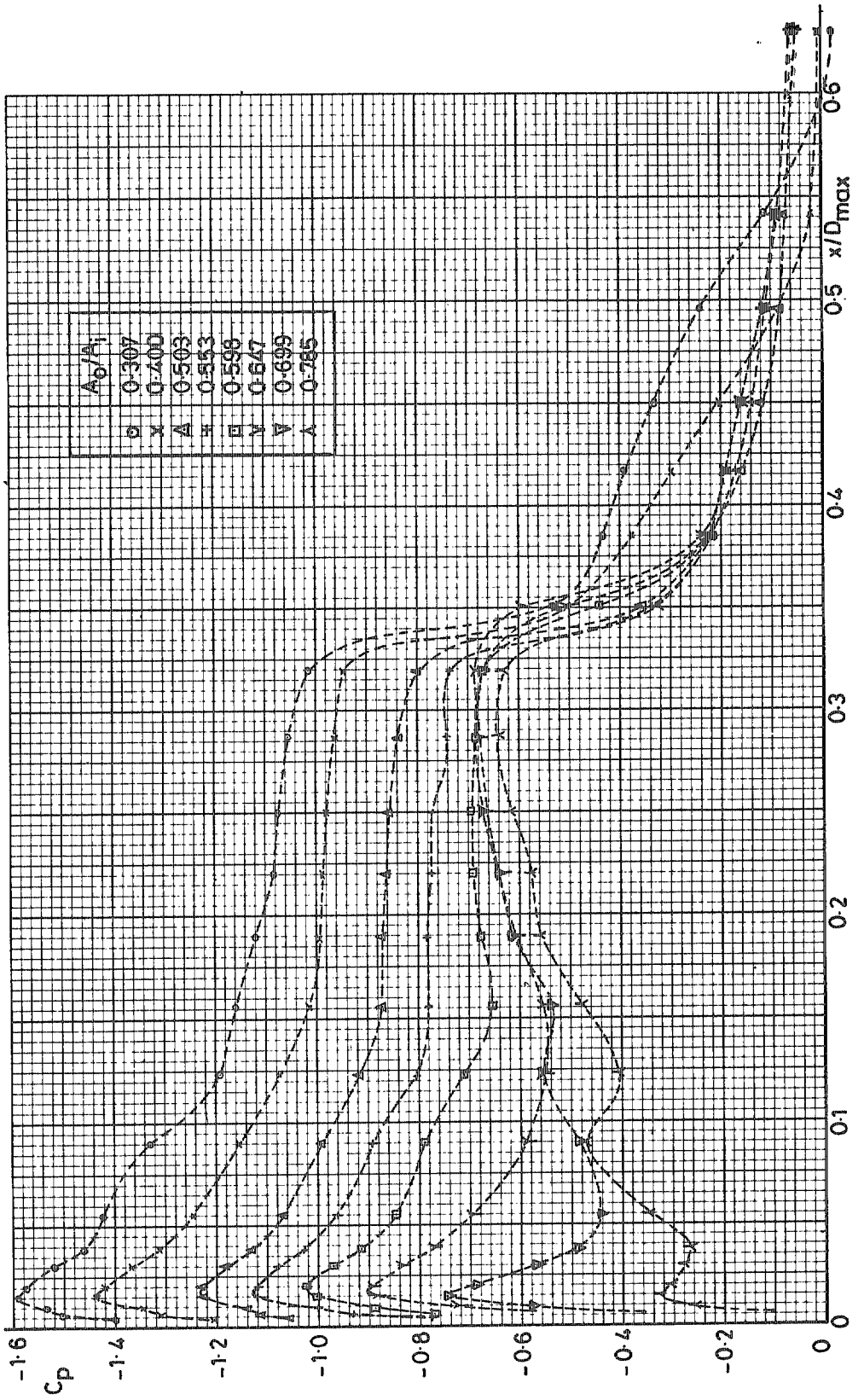

Fig 33 Variation of cowl 3 pressure distribution with flow ratio for $M_o = 0.85$

Fig 34

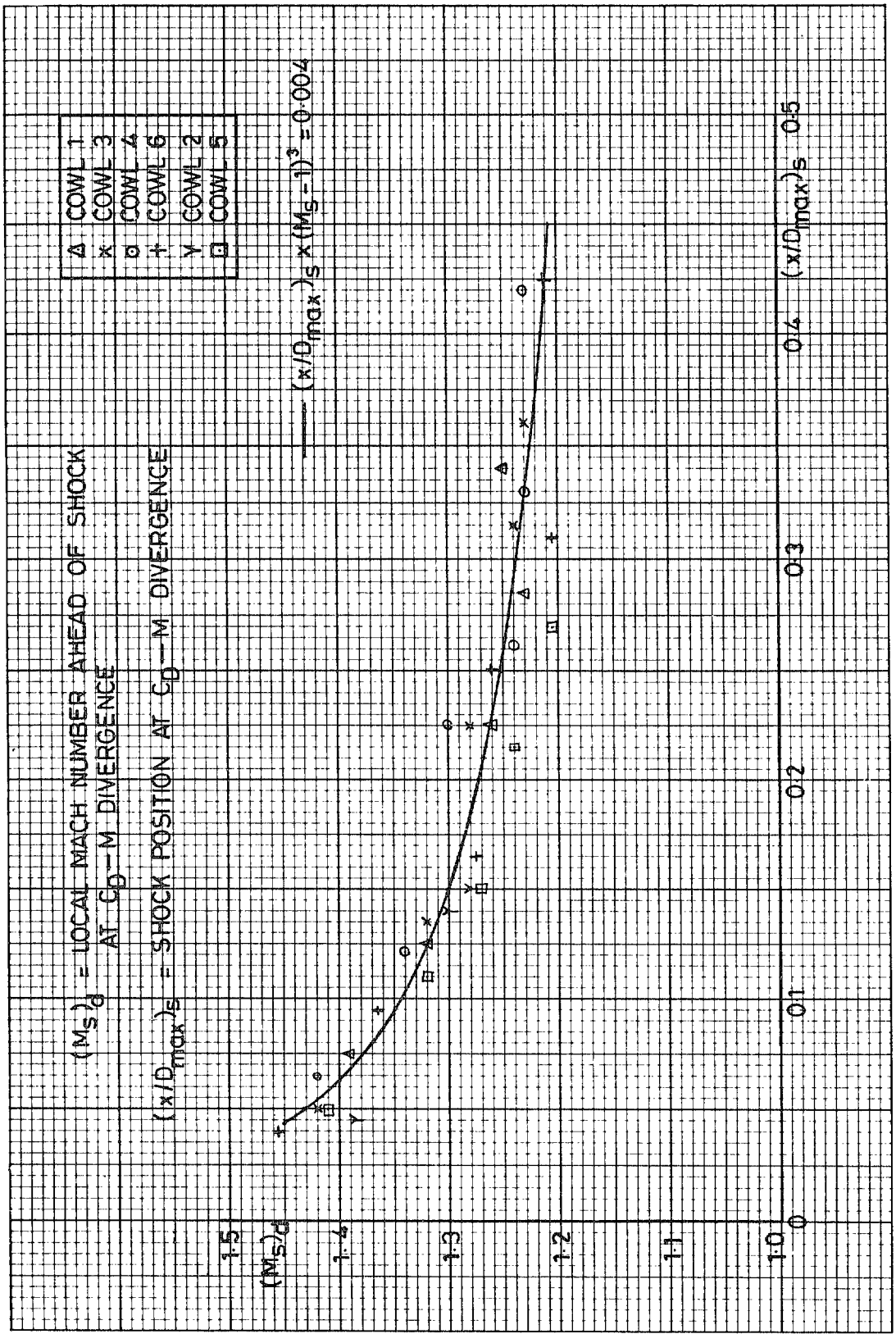

Fig 34 Correlation of drag divergence with shock strength and position

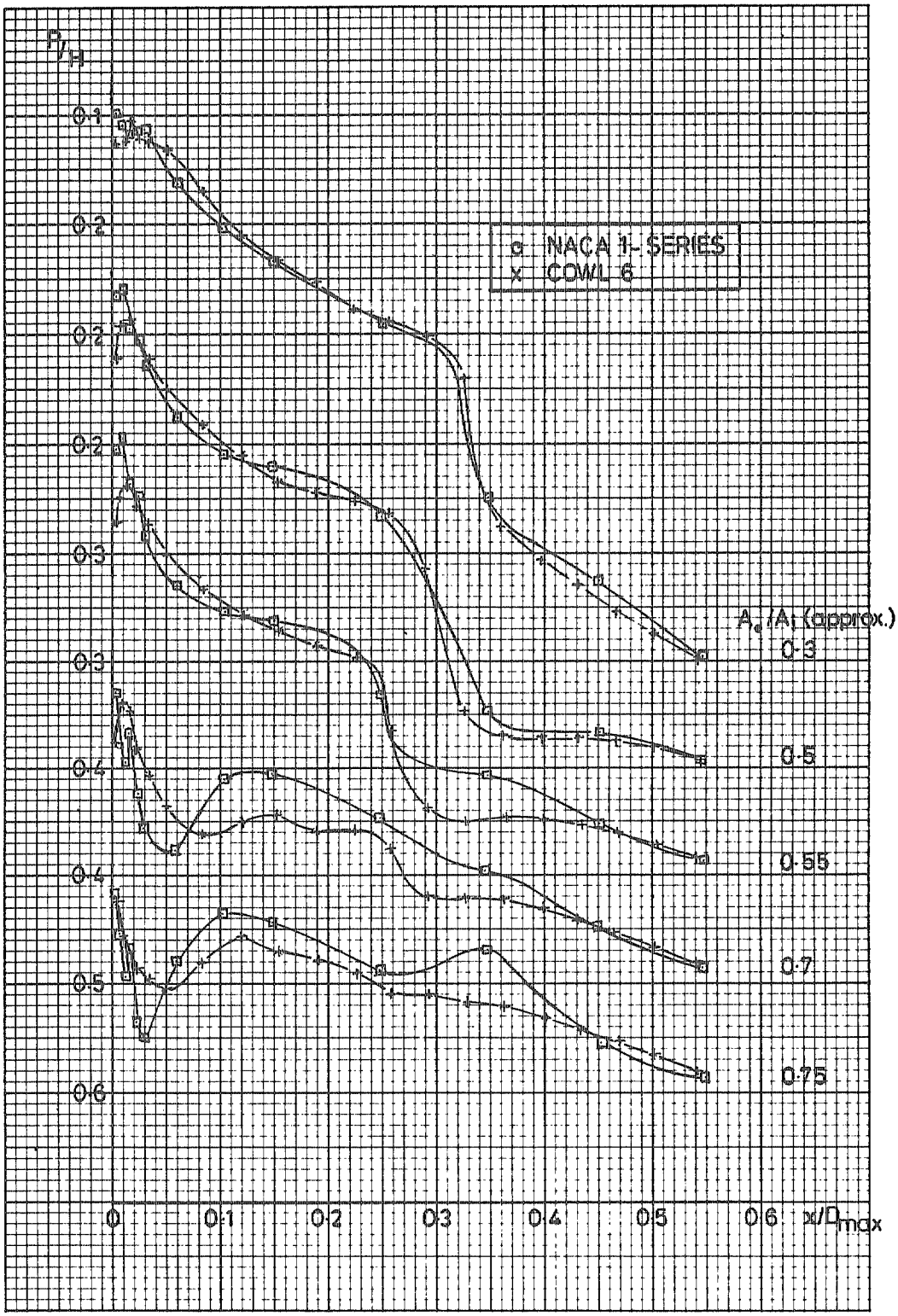

Fig 35a NACA 85/45 cowl and cowl 6 compared at $M_o = 0.85$

Fig 35b

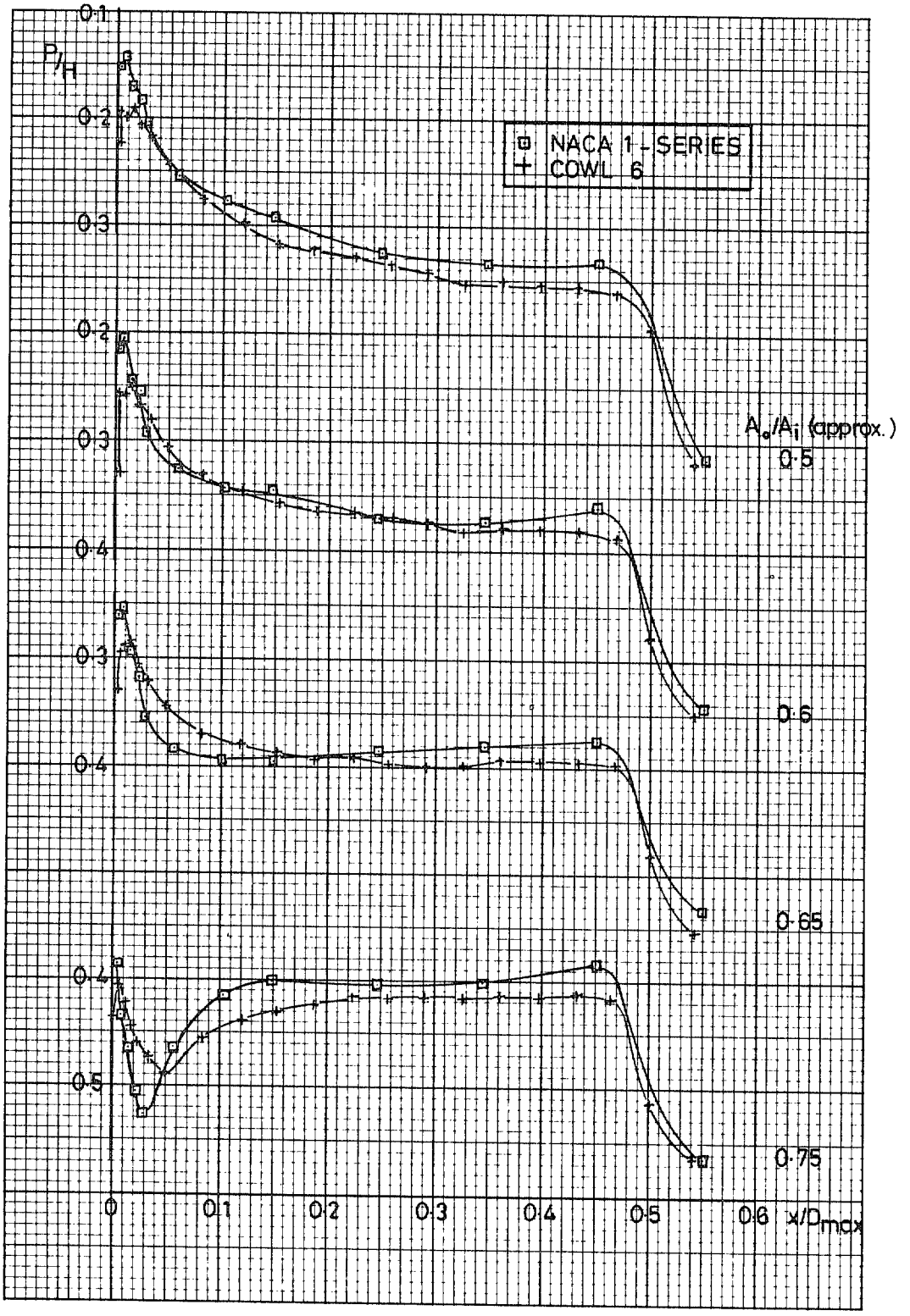

Fig 35b NACA 85/45 cowl and cowl 6 compared at $M_o = 0.90$

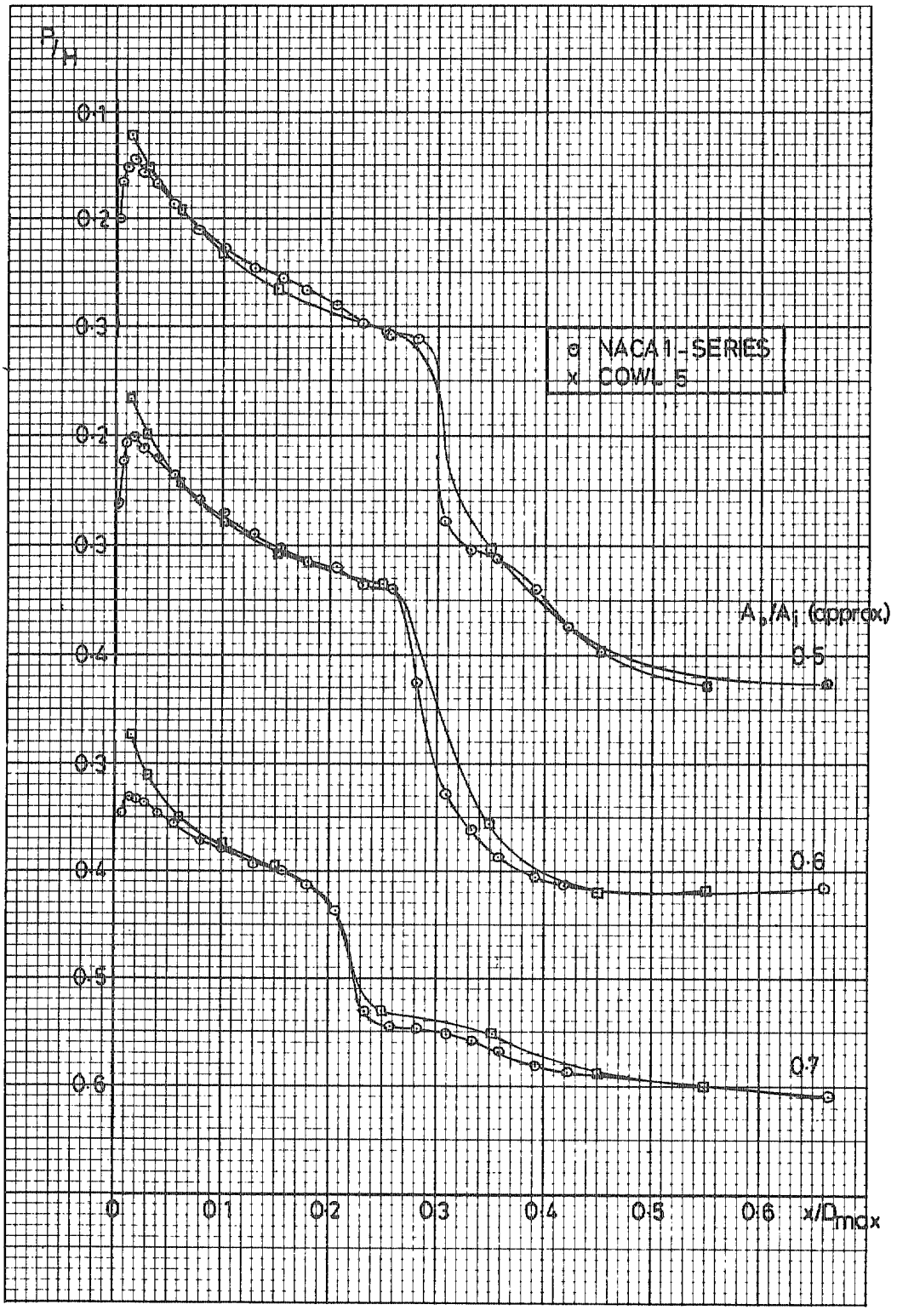

Fig 36a NACA 90/35 cowl and cowl 5 compared at $M_o = 0.85$

Fig 36b

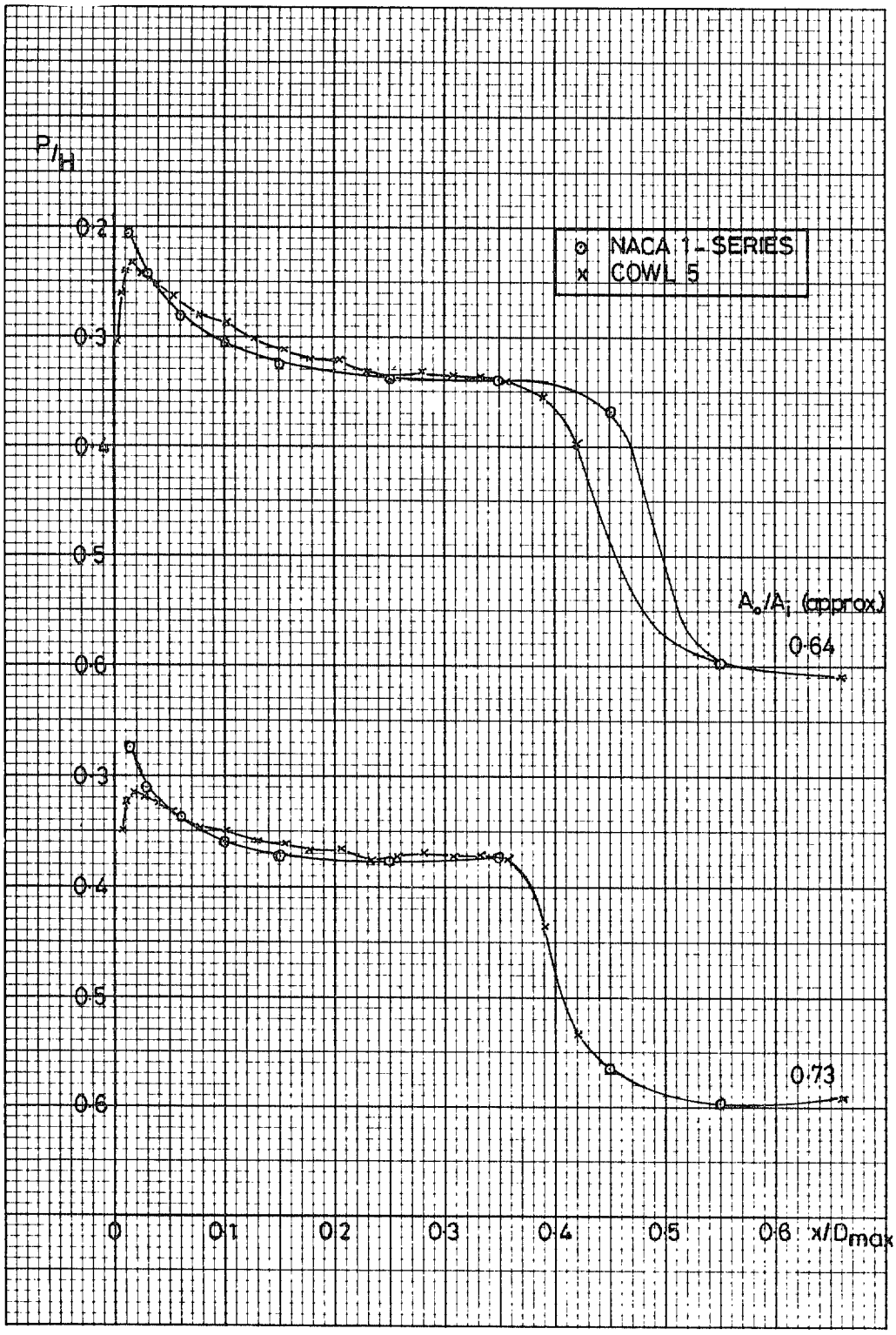

Fig 36b NACA 90/35 cowl and cowl 5 compared at $M_o = 0.90$

Printed in England for Her Majesty's Stationery Office by the Royal Aircraft Establishment, Farnborough. Dd. 596060 K4 3/80.

First published 1980

HER MAJESTY'S STATIONERY OFFICE

Government Bookshops
49 High Holborn, London WC1V 6HB
13a Castle Street, Edinburgh EH2 3AR
41 The Hayes, Cardiff CF1 1JW
Brazennose Street, Manchester M60 8AS
Southey House, Wine Street, Bristol BS1 2BQ
258 Broad Street, Birmingham B1 2HE
80 Chichester Street, Belfast BT1 4JY

Government Publications are also available through booksellers

HMSO

R &M No. 3846
ISBN 011471180